## SYNTHETIC POLYMER MICROGELS FROM PRECIPITATION POLYMERIZATION

By

# SHEILAN SINJARI, B.Sc.

## A Thesis

Submitted to the School of Graduate Studies of McMaster University in Partial Fulfilment of the Requirements

for the Degree

Doctor of Philosophy in Chemistry

McMaster University © Copyright by Sheilan Sinjari, 2025

DOCTOR OF PHILOSOPHY (2025)

McMaster University

(Chemistry & Chemical Biology)

Hamilton, Ontario

TITLE: Synthetic Polymer Microgels from Precipitation Polymerization

AUTHOR: Sheilan Sinjari, B.Sc. (University of Windsor)

SUPERVISOR: Dr. Harald D. H. Stöver

NUMBER OF PAGES: xxiii, 157

#### Abstract

Surfactant-free, micron-sized particles with reproducible diameters, controlled crosslink densities and pH responsiveness are useful in a range of applications, including waste-water treatment, crop protection, and tissue engineering. This thesis focuses on the synthesis of crosslinked polymer microgels by free-radical precipitation copolymerization of maleic anhydride (MAn) with electron rich monomers (*e.g.* styrenes, vinyl ethers) in marginal solvent mixtures. By matching comonomer reactivities, monomer-polymer solubility parameters and degree of crosslinking, the synthesis of narrow-dispersed, functional microgels can be achieved. Here, their properties are explored by optical and electron microscopy, and their mechanical properties by real-time deformability cytometry (RT-DC).

The copolymerization of MAn with 4-methyl styrene (4MS), styrene (Sty), and divinylbenzene (DVB) affords polymer particles that are 3 to 20  $\mu$ m in diameter, depending on reaction solvent composition and crosslinker loading. Hydrolysis of backbone anhydride units yields carboxylic acid groups that render pH-responsiveness to the microgels, where they exhibit reversible swelling as a function of pH. The rapid, alternating polymerization between electron-poor and electron-rich monomers affords high polymer conversions and moderate to high isolated particle yields even in conditions of low total monomer loading. In the presence of 3 to 10 mol% DVB, discrete microgels are formed when the MEK/heptane solvent mixtures have a total Hansen solubility parameter of  $18 \le \delta_t \le 22$  (MPa<sup>1/2</sup>). The mechanical properties of a small series of poly(4MS-co-MAn-co-DVB) particles measured by real-time deformability cytometry

(RT-DC) showed an inverse correlation between Young's modulus and vol% MEK in the reaction solvent.

Replacement of styrenic monomers with alcohol-containing vinyl ethers such as hydroxyethyl vinyl ether (HEVE) resulted in the formation of mono and narrow-disperse microgels with reduced swelling ratios due to lack of hydrophobic association upon collapse of the polymer network at pH < pKa<sub>1</sub> of succinic acid. These microgels also demonstrated an alternative crosslinking reaction attributed to intermolecular ester formation between HEVE hydroxyl groups and MAn units on neighbouring polymer chains, which was shown to eliminate the need for added divinyl crossinkers. In preliminary experiments, vinyl ether-containing microgels showed resistance to protein adsorption compared to poly(4MS-co-MAn-co-DVB) microgels of similar size.

The work presented in this thesis emphasizes the versatility of precipitation polymerization for the development of functional microgels in the 3 to 20  $\mu$ m range, synthesized from readily available styrenic, acrylic, and vinyl ether monomers.

## Acknowledgments

First and foremost, I would like to thank my supervisor, Prof. Harald Stöver, for his endless encouragement, patience, and kindness while guiding me through the rollercoaster of this PhD. It would take another dissertation to properly express my gratitude to him for giving me the opportunity to work with the most creative researchers I have had the pleasure of knowing. With his many food analogies and "crazy" ideas, Dr. Stöver has a talent for getting you excited to learn just about anything. Notably, he taught me the importance of seeing the bigger picture, both in research and in life, without losing my sanity. So, to Dr. Stöver: thank you from the bottom of my heart. I could not have asked for a better mentor and I would not have made it here without you.

I am forever grateful for the guidance I received from Dr. Nick Burke during my first two years at McMaster. Nick: thank you for being *so* patient when answering my never-ending questions, and for helping me navigate our group's research when I started. I don't know how it's possible for one person to know so much, but I'm happy I had the opportunity to learn from someone like you. I would also like to express my thanks to the Stöver group members, past and present, for their continued support over the many, many years. In particular, I want to thank Sam Ros, Alison Stewart, Rachelle Kleinberger and Jing Zhao for their kind guidance and stimulating discussions along the way. To the undergraduate thesis students that I had the pleasure of working with: I am so glad I had the opportunity to mentor and learn from such bright minds. Marta Skreta, Aleksandra Redzic, and Heather Sweny, thank you for your trust and support; working with you has been one of the most enjoyable experiences of graduate school. Many

thanks also to my collaborators at Fraunhofer IZI, Dr. David Smith and Dr. Jesse Freitag, and those at Zellmechanik Dresden, Christoph Herold and Oliver Otto, for introducing me to an exciting area of work.

I would like to thank my past and present committee members, Dr. Shiping Zhu, Dr. Robert Pelton, and Dr. Kalai Saravannamuttu, for their helpful feedback and patience. Additionally, I want to thank the NMR facility, particularly Dr. Bob Berno and Dr. Hilary Jenkins for their guidance with experiments, and for finding time to teach me about NMR every time I asked for help. Of course, I would also like to extend my thanks to the Department of Chemistry and Chemical Biology for a truly unforgettable experience.

To my dear friends, Aden, Jana, Laura, Alison, Christal, MC, Sam and Lucia: words cannot describe how lucky I feel to have had your support over the years. Thank you for sharing laughs, drinks, tears and confusion when things just didn't make sense. Above all, thank you for always being there for me when I needed you.

To Sebastian, who is always willing to listen to my nonsensical chemistry ramblings; thank you for your love and support during the last stretch of this degree. I probably wouldn't have made it to submission without your encouragement.

Finally, to my parents: thank you for your love, support, and for everything you have done for me; absolutely none of this would have been possible without you.

# **Table of Contents**

Abstract	. iii
Acknowledgments	V
Table of Contents	vii
List of abbreviations and symbols	xvi
List of Tablesxv	viii
List of Figuresxv	viii
List of Schemesxx	xiii
CHAPTER 1. Introduction	1
1.1. Microgels and their Applications	1
1.2. Methods of Microgel Synthesis.	2
1.3. Colloidal Stabilization	4
1.3.1. Electrostatic stabilization.	4
Figure 1.1. Schematic representation of electrostatic stabilization of two negatively charged particles in solution. Overlap of the diffuse ion layers at the surface of the particles prevents aggregation. Dashed lines represe the Stern layer.	s ent
Figure 1.2. Representation of DLVO potential showing total interaction energy (V <sub>tot</sub> ) as a sum of van der Waals attraction and EDL forces. The deep, primary minimum represents irreversible aggregation at short distances, while the secondary minimum represents reversible aggregation at intermediate distances	6
1.3.2. Steric Stabilization.	7
Figure 1.3. Schematic representation of steric stabilization for two particles of equal radius bearing polymer chains on their surface. Upon approach, crowding of surface polymer chains results in a decrease in configurational entropy and a net repulsive force that prevents	
aggregation	
1.4. Self-Stabilized Precipitation Polymerization	
1.4.1. Effect of reaction solvent on particle morphology	
1.4.2. Hildebrand and Hansen Solubility Parameters	
1.4.3. Effect of crosslinker concentration	
1.5. Thesis Overview	14
1.6. References.	.17
CHAPTER 2: Tunable Polymer Microgel Particles and their Study using	••
Microscopy and Real-Time Deformability Cytometry	<b>29</b> .
/ LARNIRACT	4()

2.2 INTRODUCTION	30
2.3 EXPERIMENTAL	33
2.3.1 Materials	33
2.3.2. Precipitation Copolymerization of 4MS, Maleic Anhydride and DVB	34
2.3.3. Fluorescent Labelling and Hydrolysis of Microgels	35
2.3.4 Characterization.	35
2.3.4.1. Optical and Confocal Microscopy	35
2.3.4.2. Transmission Electron Microscopy	36
2.3.4.3. Mechanical Properties obtained using RT-DC	36
2.4. RESULTS AND DISCUSSION	37
2.4.1. Effects of Solvency and Cross-linker Loading on Particle Size	37
Scheme 2.1. Mechanism of particle nucleation and growth. Aggrega and de-solvation of oligomers leads to particle nuclei that grow by capturing monomers and oligomers from solution	
Figure 2.1. Fluorescence optical microscope images of representative microgels labelled with fluorescein cadaverine ( $\lambda_{ex}$ =480 nm) formed 70/5, B) 72/5 and C) 72/3, suspended in PBS. Here, the notation '70/represents particles synthesized in 70:30 (v/v) MEK/heptane cosolver mixtures, with 5 mol% effective <i>m</i> - and <i>p</i> -DVB relative to total styre monomers.	e at A) 5' nt nic
Figure 2.2. TEM images of a) 70/5 and b) 73/5 microgels swollen in and embedded in Spurr's epoxy resin. Scale bar is 2 μm. Contrast has increased by 20% for all TEM images. The near vertical lines in B at knife artifacts introduced during microtoming	s been re
Figure 2.3. Deformation of microgels labelled with fluorescein cadavupon manual compression between two glass slides: fluorescence microscope images of 72/3 microgels swollen in PBS: A) before compression, B) compressed between two glass slides, and C) post-compression (after removal of top glass slide). Scale bar = 25 μm	m42
2.4.2. Mechanical Properties of Microgels by RT-DC	43
Scheme 2.2. a) Schematic of an RT-DC microchannel layout. Particle flow from the sample reservoir – focused by a sheath flow – through constriction and measurement zone where the image-based shape and is performed. All flow rates stated are the sum of sample and sheath b) Image of 73/5 microgel captured at the end of the constriction zon. Flow-rate = $0.08 \mu L/s$ .	the alysis flow.
Figure 2.4. Effect of MEK content on properties of hydrolyzed micro in PBS as assessed using RT-DC. a) Scatter plots of Young's Modulu row) and deformation (bottom row) versus microgel cross-sectional and b) contour plot of Young's Modulus versus cross-sectional areas.	is (top areas,

	series of microgels formed using 5 % effective DVB, formed in 70, 72 at 73 vol% MEK (0.08 $\mu$ L/s flow-rate; 15 $\mu$ m channel for 70/5; 20 $\mu$ m channel for 72/5 and 73/5)	
	Figure 2.5. Effect of cross-linker levels on microgel properties assessed using RT-DC. a) Scatter plots of Young's Modulus (top row) and deformation (bottom row) versus microgel cross-sectional areas, and b) contour plot of Young's Modulus versus cross-sectional areas, for a serie of microgels formed using 3 to 6 mol% DVB, in presence of 72 vol% MEK (0.08μL/s flow rate; 30μm channel for 72/3; 15μm channel for 72/72/5 and 72/6)	/4,
	Figure 2.6. a) Young's modulus (top) and Deformation (bottom) scatter plots for 72/4 microgels as function of flow rate, and b) contour plot of Young's modulus of 72/4 microgels, showing shear-stiffening with increasing flow rate.	49
2.5 CONO	CLUSIONS	
	RENCES	
	NDIX	
	Table A2.1. Particle diameters for hydrolyzed microgels formed using 3-6% DVB and 70-73% MEK suspended in PBS. Diameters were obtained using optical microscopy (Nikon Eclipse LV100ND upright optical microscope equipped with NIS-Elements Microscope imaging software). Number of particles analyzed ranged from 100-3000 for each microgel type, which were synthesized and analyzed in triplicate	
	Figure A2.1. Microgel homogeneity as assessed by confocal microscopy (Nikon A1 Confocal Eclipse Ti microscope): equatorial sections of 70/5 microgels swollen in water and corresponding line profile. Scale bar is 25µm.	
	Figure A2.2: Young's moduli of microgels as a function of %DVB and vol% MEK (flow rate = $0.08~\mu L/s$ )	
	Figure A2.3: Young's moduli of microgels as a function of flow-rate, showing strain-stiffening	59
	: Lightly Crosslinked Microgels by Precipitation Polymerization of dride and Styrenic Monomers	60
	TRACT	
	ODUCTION	
	Scheme 3.1. Microgel synthesis and hydrolysis to polyanionic microgel particles. Fluorescence microscope images of a) poly(Sty-co-MAn-co-DVB) and b) poly(4MS-co-MAn-co-DVB) microgels functionalized with a rhodamine label, hydrolyzed and swolle in phosphate buffered saline (PBS). Microspheres were made in 70/30 MEK/heptane using 5 mol% DVB-55 crosslinker. Magnification is 20x.	n

NA = 0.45	64
3.3. EXPERIMENTAL	65
3.3.1. Materials	65
3.3.2. Synthesis of Microspheres by Precipitation Copolymerization	65
3.3.3. Fluorescent Labelling and Anhydride Hydrolysis of Microspheres	66
3.3.4. Optical and Fluorescence Microscopy	67
3.3.5. Scanning Electron Microscopy (SEM)	67
3.3.6. Synthesis and stability of 1,4-butanediol diacrylate (BDDA) crosslin	ked
microspheres	
3.4. RESULTS AND DISCUSSION	
3.4.1. Precipitation copolymerization of styrenic monomers, MAn and DV	
3.4.1.2. Properties of poly(4MS-co-MAn-co-DVB) microspheres	
Figure 3.1. Optical microscope images of poly(4MS-co-MAn-co-D microspheres swollen in THF, reflecting the impact of crosslinker of and solvent composition on morphology and diameter. Microsphere crosslinked with 3 mol% DVB (top row) and 5 mol% DVB (botton made in MEK/heptane mixtures of a) 60/40 b) 65/35 and c) 70/30. bars are 20 μm.	content es are n row), Scale
3.4.1.3 pH-dependent swelling of hydrolyzed poly(4MS-co-MAn-co-DVB	<u>.</u> )
microspheres	71
Table 3.1. Average microgel diameter and swelling as a function of DVB% loading and pH	
3.4.1.4. Precipitation polymerization with mixtures of 4MS and Sty	72
Figure 3.2. Average diameters for THF-swollen microspheres as a function of 4MS:Sty comonomer ratios for particles made in MEK/heptane solvent mixtures containing 65, 70 and 75 vol% ME mol% DVB. Each data point represents the average particle diamet two replicate experiments, where n≥ 100 diameters were measured replicate	er from per
3.4.1.5. Properties of poly(Sty-co-MAn-co-DVB) microspheres	74
Figure 3.3. Particle diameter of THF-swollen Sty/MAn/DVB particle function of DVB mole % and vol% MEK. Data points represent an average of 100-5000 measurements	
Figure 3.4. SEM micrographs of Sty-MAn-DVB particles crosslink 5 mol% DVB, showing morphology transitions from hard spheres swellable microgels, as a function of vol% MEK. Microspheres we made in MEK vol% of a) 60, b) 70 and c) 75. Accelerating voltage 20kV	to ere is
3.4.1.6. Precipitation polymerization of 4MS, MAn and	10
1 4-butanediol-diacrylate (BDDA)	77

3.4.2 Properties of poly(4MS-co-MAn-co-BDDA) particles	77
Figure 3.5. Optical microscope images of BDDA crosslinked microspheres suspended in THF. Microspheres were made in 6 (bottom row) and 70 vol% MEK (top row), crosslinked with (15, 8 and 10 mol% BDDA. Scale bars are 20µm	left to right)
3.5. CONCLUSIONS	79
3.6. REFERENCES.	81
3.7. APPENDIX	
Figure A3.1 Average particle diameters of poly(4MS-co-MAn microgels swollen in neat MEK as a function of DVB mol% a vol% as determined by optical microscopy. Microspheres synt 50 vol% MEK with $\geq 5$ mol% DVB, as well as those made in 6 MEK with 10 mol% DVB are too small to resolve by optical not thus diameters are not reported. It is important to note that both 18.6 MPa1/2) and MEK ( $\delta = 19.1$ MPa1/2) are considered good for the poly(styrene-alt-maleic anhydride) copolymer ( $\delta = 19.0$ which can be used as a linear model for the microspheres preserved when selecting a solvent that will swell the polymer network.	nd MEK hesized in $60\text{vol}\%$ nicroscopy, h THF ( $\delta$ = od solvents $6$ MPa1/2), ented in this vork87
Figure A3.2 Optical microscope images of microspheres made mol fraction of (a) 0.1, (b) 0.5 and (d) 0.9. Microspheres were solvent mixtures of 65 vol% MEK at 5 mol% DVB loading. So 20 μm	made in cale bars are
Table A3.1. Partial and total Hansen solubility parameters for MEK/heptane solvent mixtures. Estimated by $\delta = \varphi a \delta a + \varphi b \alpha \phi$ is the volume fraction, and solvents (e.g. MEK and heptane represented by subscripts a and b	) are
Figure A3.3 Scanning electron micrographs of poly(4MS-co-MAn-co-DVB) microspheres crosslinked with 5 made in a) 40 and b) 60 vol% MEK. Accelerating voltage is 20	mol% DVB
Figure A3.4. Average diameter of 5 mol% BDDA-crosslinked over time at pH 2, 7.4 and 9, heated to 37°C. Error bars are a s deviation of diameters measured by brightfield microscopy and using Nikon NIS elements imaging software	tandard d analyzed
CHAPTER 4: Microgels formed by precipitation copolymerization of vi	
4.1. ABSTRACT	
4.2. INTRODUCTION	92
Scheme 4.1. Precipitation polymerization of HEVE and MAn with 0 - 10 mol% BDVE as a crosslinker. Hydrolysis with aqu yields crosslinked microgels that swell in aqueous solutions of	eous base
4.3 EXPERIMENTAL	-
Dan Dimini in II.	

4.3.1. Materials	96
4.3.2. Precipitation copolymerization of vinyl ethers and maleic anhydride	96
4.3.3. Microgel isolation and purification	97
4.3.4. Fluorescent labeling and anhydride hydrolysis	98
4.3.5. Confocal microscopy - FITC-BSA protein binding	99
4.3.6. Hydrolytic stability of poly(HEVE-co-MAn) microgels	99
4.4 DISCUSSION	100
4.4.1. Effects of polymerization solvent on microgel formation and morpho 101	logy
4.4.1.1. Precipitation Polymerization in MEK/heptane and MEK/aceton cosolvent mixtures	
Figure 4.1. Poly(HEVE-co-MAn-co-BDVE) microgels made with 2 wt% BDVE crosslinker, formed in a) 95%, b) 97% and c) 100% v/v as the polymerization solvent. Microgels were labelled with TAMRA-cadaverine at a targeted labeling of 0.1 mol% with respect anhydride groups and re-suspended in deionized water prior to imag 103	MEK to ging
4.4.1.2. Polymerization in MEK/ACN mixtures	103
Figure 4.2. Optical images of HEVE-MAn microgels crosslinked w % BDVE, prepared with MEK:ACN ratios in the polymerization microgels of 95:5, 90:10, and 80:20 (left to right). Anhydride-form microgels row) are suspended in DMF and succinic acid-form (bottom row) in (150mM NaCl) at pH 7	ixture (top n saline
4.4.2. Effect of Crosslinker Loading on HEVE-MAn Polymerizations - Self-cross-linking reactions	
Figure 4.3. Brightfield (a) and fluorescence (b) images of poly(HEVE-co-MAn) microgels suspended in (a) THF and (b) phos buffered saline (PBS, pH = 7.4). For (b), 0.1 mol% of anhydride growere labelled with TAMRA-cadaverine before hydrolysis of remain anhydrides. Scale bars = $25 \mu m$ .	oups ning
Figure 4.4. 1H NMR spectrum of HEVE and MAn showing acetal formation with time during heating at 50°C in DMSO-d6. Monomer loading was 10 wt%, with 2 wt% AIBN relative to total monomer content. Anisole was used as an internal standard. Offset is 0.05 ppr	
Figure 4.5. Overlaid full 1H NMR spectra of HEVE and MAn show changes with time during heating to 50°C. Anisole was used as an instandard	
Figure 4.6. 1H NMR spectrum of HEVE and MAn after 24 hours of heating at 50°C in DMSO-d6. Monomer loading is 10 wt%, with 2 AIBN relative to total monomer content and anisole as an internal	

	standard. Reactions outlined in red depict the possible ring opening of MAn with HEVE, followed by hydrolysis of the vinyl ether group to yield acetaldehyde and the maleic acid half ester
	Figure 4.7. Stacked 1D spectra of diethylene glycol monovinyl ether (DEVE) and MAn after heating at 50°C in DMSO-d6 (0 min to 150 min). Monomer loading was 10 wt%, with 2wt% AIBN relative to total monomer content, with anisole as an internal standard
	monovinyl ether (DEVE) and MAn after 24 hours of heating at 50°C in DMSO-d6. Monomer loading was 10 wt%, with 2wt% AIBN relative to total monomer content, with anisole used as an internal standard114
443 1	poly(HEVE-co-MAn) Microgel Degradation via Hydrolysis
т.т.Э. ј	Figure 4.9. Brightfield images of 100/0 microgels suspended in pH 4 (top row), pH 7 (middle row) and pH 12 (bottom row) solutions and heated to 70°C for 24 to 48 hours. Microgels heated in pH 12 solution were completely degraded after 24 hours.
4.4.4. (	Comparison of protein binding to vinyl ether and styrenic microgels117 Figure 4. Confocal images of A) 70/6 poly(4MS-co-succinic acid-co-DVB) and B) 100/5 poly(HEVE-co-succinic acid) microgels after incubation with 0.01wt% FITC-BSA. Microgels were washed with PBS with two centrifugation cycles and allowed to settle prior to imaging.  Microgels are labelled with 0.1 mol% TAMRA-cadaverine. Scale bars are 50µm
4.5. CONO	CLUSIONS119
4.6. REFE	RENCES
4.7. APPE	NDIX126
	Table A4.1. p(HEVE-co-MAn) particle diameters and isolated yields. Polymerizations were carried out in neat MEK at 4 wt% total monomer loading and varying mol% BDVE. Microgels were swollen in water at pH 9 and imaged on a Nikon LV100 upright microscope in transmission mode to obtain diameters using NIS elements software, with n = 700-2000 measurements taken across 3 or more representative optical images per sample
	Figure A4.1. Volume swelling as a function of mol% BDVE for microgels polymerized in neat MEK at 4% monomer loading. The microgels were hydrolyzed and swelling ratios were calculated as microgel diameter at pH $^{7}$ / diameter at pH $^{2}$ , assuming a fully collapsed microgel state at pH $^{2}$ $^{127}$
	Figure A4.2. Representative brightfield images of poly(DEVE-co-MAn-co-BDVE) microgels suspended THF. Microgels were synthesized with 2.5 mol% (top row) or 5 mol% (bottom row)

	represented by the first number in the inset (e.g. 88/2.5 corresponds microgels formed in 88 vol% MEK in the MEK/heptane mixture). Hydrolysis of the anhydride groups lead to complete (88/2.5, 88/5) partial dissolution (90/2.5, 90/5, 95/2.5, 95/5) of the particles. All bars = 25 µm	or scale
Chapter 5: P	Properties of Disulfide Crosslinked microgels formed by precipitat	
	ion	
	TRACT	
	RODUCTION	
5.3. EXPI	ERIMENTAL	131
	Materials	
	Synthesis of Bis(2-acryloyl)oxyethyl disulfide (BAOD)	
5.3.4	Microgel Degradation with tris(2-carboxyethyl phosphine) (TCEP)	134
5.3.5.	Microgel degradation with tris(hydroxypropyl phosphine) (THPP)	134
	CUSSION	
5.4.1.	Microgel synthesis and characterization	135
	morphology with varying vol% MEK in the polymerization solvent mol% BAOD. Insets are representative fluorescence images of microsuspended in water (pH 7.8) following rhodamine labeling and substructions anhydride hydrolysis. All scale bars are 50 µm	rogels sequent 136
	crogel degradation with tris(2-carboxyethyl phosphine) hydrochloride	
	Figure 5.2. Fluorescence images of 70/10 microgels at t=0, 0.5, 10, min, following TCEP addition. [TCEP]:[disulfide] is estimated to b ~100:1 (Table A5.1 and Figure A5.5). Scale bars are 50µm	e
5.4.3. Red	duction with tris(hydroxypropyl phosphine) (THPP)	
	Reacting microgels with THPP in a < 1:1 mole ratio allows for the measurement of swelling over time (Fig. 5.4). For the same 70/10 microgel suspension, maximum particle diameters are reached with mins following mixing of microgels with THPP	in 15
	Figure 5.4. Fluorescence images depicting changes in 70/10 (TOP) 65/10 (BOTTOM) BAOD microgel diameters with time following with 0.1 eq'v of THPP. Scale bars = 50μm	mixing
5.5. CON	CLUSIONS	
5.6. REFI	ERENCES	141
5.7. APPI	ENDIX	143

Figure A5.1. Isolated particle yields for BAOD-crosslinked microgels at

different mol% BAOD loading, made polymerization mixture	
Figure A5.2. Microgel diameters as a standard deviations of particle diameter particle diameter measurements using	function of pH. Scale bars are er taken from an average of > 1000
Figure A5.3. 1H NMR of BAOD in C	DCl3. ca. 93% yield145
Table A.5.1. Estimated mol% disulfid 146	e in microgels from {1H}31P NMR
Figure A5.4. 31P NMR of THPP stand THPP = -30.24	11
Figure A5.5. 31P NMR of 70/10 micr %BAOD = 2.33	•
Figure A5.6. 31P NMR of 65/10 micr % BAOD = 2.25%	<u> </u>
Figure A5.7. 31P NMR of 60/10 micr %BAOD = 2.04	C
Chapter 6. Summary and Recommendations for I	<b>Suture Work151</b>
6.1. Thesis Conclusions	151
6.2. Chapter 2	151
6.3 Chapter 3	153
6.4. Chapter 4	154
6.5. Chapter 5	157

# List of abbreviations and symbols

4MS 4-methylstyrene

ACN Acetonitrile

AIBN Azobisisobutyronitrile

BAOD bis(2-acryloyloxyethyldisulfide)

BDDA 1,4-butanediol diacrylate

BDVE 1,4-butanediol divinyl ether

BHEDS 2-hydroxyethyl disulfide

BSA Bovine serum albumin

CED Cohesive energy density

CLSM Confocal laser scanning microscopy

DCM Dichloromethane

DEVE Diethylene glycol vinyl ether

DMF N,N-dimethylformamide

DVB Divinylbenzene-55

FITC Fluorescein isothiocyanate

FITC-BSA Albumin–fluorescein isothiocyanate conjugate

GSH Glutathione

HEVE 2-hydroxyethyl vinyl ether

HSP Hansen solubility parameter

MAn Maleic anhydride

MEK Methyl ethyl ketone

NA Numerical aperture

NMR Nuclear magnetic resonance

PBS Phosphate buffered saline

PEG Polyethylene glycol

RT-DC Real-time deformability cytometry

SEM Scanning electron microscopy

Sty Styrene

TAMRA Tetramethylrhodamine carboxamide

TCEP Tris(2-carboxyethyl)phosphine

TEM Transmission electron microscopy

THF Tetrahydrofuran

THPP Tris(hydroxypropyl) phosphine

δ Hildebrand solubility parameter

ΔH Enthalpy

 $\Delta S$  Entropy

 $\Delta G$  Gibbs free energy

# **List of Tables**

<b>Table A2.1.</b> Particle diameters for hydrolyzed microgels formed using 3-6% DVB and 70-73% MEK suspended in PBS. Diameters were obtained using optical microscopy (Nikon Eclipse LV100ND upright optical microscope equipped with NIS-Elements Microscope imaging software). Number of particles analyzed ranged from 100-3000 for each microgel type, which were synthesized and analyzed in triplicate
Table 3.1. Average microgel diameter and swelling as a function of DVB% loading and pH
<b>Table A3.1</b> . Partial and total Hansen solubility parameters for MEK/heptane solvent mixtures. Estimated by $\delta = \phi_a \ \delta_a + \phi_b \ \delta_b$ ; where $\phi$ is the volume fraction and solvents (MEK and heptane) are represented by subscripts a and b
<b>Table A4.1.</b> poly(HEVE-co-MAn) particle diameters and isolated yields. Polymerizations were carried out in neat MEK at 4 wt% total monomer loading and varying mol% BDVE. Microgels were swollen in water at pH 9 and imaged on a Nikon LV100 upright microscope in transmission mode to obtain diameters using NIS elements software, with n = 700-2000 measurements taken across 3 or more representative optical images per sample
<b>Table A.5.1.</b> Estimated mol% disulfide in microgels from {1H}31P NMR 146
List of Figures
<b>Figure 1.1.</b> Schematic representation of electrostatic stabilization of two negatively charged particles in solution. Overlap of the diffuse ion layers at the surface of the particles prevents aggregation. Dashed lines represent the Stern layer
<b>Figure 1.2.</b> Representation of DLVO potential showing total interaction energy (V <sub>tot</sub> ) as a sum of van der Waals attraction and EDL forces. The deep, primary minimum represents irreversible aggregation at short distances, while the secondary minimum represents reversible aggregation at intermediate distances
<b>Figure 1.3.</b> Schematic representation of steric stabilization for two particles of equal radius bearing polymer chains on their surface. Upon approach, crowding of surface polymer chains results in a decrease in configurational entropy and a net repulsive force that prevents aggregation
<b>Figure 2.1.</b> Fluorescence optical microscope images of representative microgels labelled with fluorescein cadaverine (λex=480 nm) formed at A) 70/5, B) 72/5 and C) 72/3, suspended in PBS. Here, the notation '70/5' represents particles synthesized in 70:30 (v/v) MEK/heptane cosolvent mixtures, with 5 mol% effective m- and p-DVB relative to total styrenic monomers
<b>Figure 2.2.</b> TEM images of a) $70/5$ and b) $73/5$ microgels swollen in THF and embedded in Spurr's epoxy resin. Scale bar is 2 $\mu$ m. Contrast has been increased by 20% for all TEM images. The near vertical lines in B are knife artifacts introduced during

microtoming41
<b>Figure 2.3.</b> Deformation of microgels labelled with fluorescein cadaverine upon manual compression between two glass slides: fluorescence microscope images of 72/3 microgels swollen in PBS: A) before compression, B) compressed between two glass slides, and C) post-compression (after removal of top glass slide). Scale bar = 25 $\mu$ m
<b>Figure 2.4.</b> Effect of MEK content on properties of hydrolyzed microgels in PBS as assessed using RT-DC. a) Scatter plots of Young's Modulus (top row) and deformation (bottom row) versus microgel cross-sectional areas, and b) contour plot of Young's Modulus versus cross-sectional areas, for a series of microgels formed using 5 % effective DVB, formed in 70, 72 and 73 vol% MEK (0.08 $\mu$ L/s flow-rate; 15 $\mu$ m channel for 70/5; 20 $\mu$ m channel for 72/5 and 73/5)
<b>Figure 2.5.</b> Effect of cross-linker levels on microgel properties assessed using RT-DC. a) Scatter plots of Young's Modulus (top row) and deformation (bottom row) versus microgel cross-sectional areas, and b) contour plot of Young's Modulus versus cross-sectional areas, for a series of microgels formed using 3 to 6 mol% DVB, in presence of 72 vol% MEK ( $0.08\mu L/s$ flow rate; $30\mu$ m channel for $72/3$ ; $15\mu$ m channel for $72/4$ , $72/5$ and $72/6$ )
<b>Figure 2.6.</b> a) Young's modulus (top) and Deformation (bottom) scatter plots for 72/4 microgels as function of flow rate, and b) contour plot of Young's modulus of 72/4 microgels, showing shear-stiffening with increasing flow rate
<b>Figure A2.1.</b> Microgel homogeneity as assessed by confocal microscopy (Nikon A1 Confocal Eclipse Ti microscope): equatorial sections of 70/5 microgels swollen in water and corresponding line profile. Scale bar is 25μm
Figure A2.2. Young's moduli of microgels as a function of %DVB and vol% MEK (flow rate = $0.08~\mu L/s$ )
Figure A2.3: Young's moduli of microgels as a function of flow-rate, showing strain-stiffening
<b>Figure 3.1.</b> Optical microscope images of poly(4MS-co-MAn-co-DVB) microspheres swollen in THF, reflecting the impact of crosslinker content and solvent composition on morphology and diameter. Microspheres are crosslinked with 3 mol% DVB (top row) and 5 mol% DVB (bottom row), made in MEK/heptane mixtures of a) 60/40 b) 65/35 and c) 70/30. Scale bars are 20 µm
<b>Figure 3.2.</b> Average diameters for THF-swollen microspheres as a function of 4MS:Sty comonomer ratios for particles made in MEK/heptane solvent mixtures containing 65, 70 and 75 vol% MEK and 5 mol% DVB. Each data point represents the average particle diameter from two replicate experiments, where $n \ge 100$ diameters were measured per replicate
<b>Figure 3.3.</b> Particle diameter of THF-swollen Sty/MAn/DVB particles as a function of DVB mole % and vol% MEK. Data points represent an average of 100-5000 measurements
Figure 3.4. SEM micrographs of Sty-MAn-DVB particles crosslinked with 5 mol%

DVB, showing morphology transitions from hard spheres to swellable microgels, as a function of vol% MEK. Microspheres were made in MEK vol% of a) 60, b) 70 and c) 75. Accelerating voltage is 20kV
<b>Figure 3.5</b> . Optical microscope images of BDDA crosslinked microspheres suspended in THF. Microspheres were made in 65 vol% (bottom row) and 70 vol% MEK (top row), crosslinked with (left to right) $5,8$ and $10$ mol% BDDA. Scale bars are $20\mu$ m
<b>Figure A3.1</b> Average particle diameters of poly(4MS-co-MAn-co-DVB) microgels swollen in neat MEK as a function of DVB mol% and MEK vol% as determined by optical microscopy. Microspheres synthesized in 50 vol% MEK with $\geq$ 5 mol% DVB, as well as those made in 60vol% MEK with 10 mol% DVB are too small to resolve by optical microscopy, thus diameters are not reported. It is important to note that both THF ( $\delta$ = 18.6 MPa1/2) and MEK ( $\delta$ = 19.1 MPa1/2) are considered good solvents for the poly(styrene-alt-maleic anhydride) copolymer ( $\delta$ = 19.6 MPa1/2), which can be used as a linear model for the microspheres presented in this work when selecting a solvent that will swell the polymer network (Grulke, E.A. In Polymer Handbook; Brandrup, J., Immergut, E.H., Grulke, E.A., Eds.; Wiley-Interscience. 1999; 675-714)
<b>Figure 3A.2.</b> Optical microscope images of microspheres made with a 4MS mol fraction of (a) 0.1, (b) 0.5 and (d) 0.9. Microspheres were made in solvent mixtures of 65 vol% MEK at 5 mol% DVB loading. Scale bars are 20 μm
<b>Figure A3.3.</b> Scanning electron micrographs of poly(4MS-co-MAn-co-DVB) microspheres crosslinked with 5 mol% DVB made in a) 40 and b) 60 vol% MEK. Accelerating voltage is 20kV
<b>Figure A3.4</b> . Average diameter of 5 mol% BDDA-crosslinked microgels over time at pH 2, 7.4 and 9, heated to 37°C. Error bars are a standard deviation of diameters measured by brightfield microscopy and analyzed using Nikon NIS elements imaging software90
<b>Figure 4.1.</b> poly(HEVE-co-MAn-co-BDVE) microgels formed in 100% MEK polymerization solvent at 2.5 wt% BDVE crosslinker loading. Microgels were labelled with TAMRA-cadaverine at a targeted labeling of 0.1 mol% with respect to anhydride groups. a) As-formed microgels dispersed in THF. b) Microgels with anhydride groups hydrolyzed with 1.0N NaOH and washed multiple times with DI water
<b>Figure 4.2.</b> Optical images of HEVE-MAn microgels crosslinked with 2.5 % BDVE, prepared with MEK:ACN ratios in the polymerization mixture of 95:5, 90:10 and 80:20 (left to right). Anhydride-form microgels (top row) are suspended in DMF and succinic acid-form (bottom row) in saline at pH 7
<b>Figure 4.3.</b> Optical microscope images of crosslinked poly(HEVE-co-MAn) microgels suspended in (a) THF and (b) phosphate buffered saline (PBS, pH = 7.4). For (b), 0.1 mol% of anhydride groups were labelled with TAMRA-cadaverine before hydrolysis of remaining anhydrides. Scale bars = $25 \mu m$
<b>Figure 4.4</b> . 1H NMR spectrum of HEVE and MAn showing acetal formation with time during heating at 50°C in DMSO-d6. Monomer loading was 10 wt%, with 2 wt% AIBN relative to total monomer content. Anisole was used as an internal standard. Offset is 0.05 ppm

<b>Figure 4.5.</b> Overlaid full 1H NMR spectra of HEVE and MAn showing changes with time during heating to 50°C. Anisole was used as an internal standard
<b>Figure 4.6.</b> 1H NMR spectrum of HEVE and MAn after 24 hours of heating at 50°C in DMSO-d6. Monomer loading is 10 wt%, with 2 wt% AIBN relative to total monomer content and anisole as an internal standard. Reactions outlined in red depict the possible ring opening of MAn with HEVE, followed by hydrolysis of the vinyl ether group to yield acetaldehyde and the maleic acid half ester
<b>Figure 4.7.</b> Stacked 1D spectra of diethylene glycol monovinyl ether (DEVE) and MAn after heating at 50°C in DMSO-d6 (0 min to 150 min). Monomer loading was 10 wt%, with 2wt% AIBN relative to total monomer content, with anisole as an internal standard <b>113</b>
<b>Figure 4.8.</b> 1H NMR spectrum of reaction with diethylene glycol monovinyl ether (DEVE) and MAn after 24 hours of heating at 50°C in DMSO-d6. Monomer loading was 10 wt%, with 2wt% AIBN relative to total monomer content, with anisole used as an internal standard
<b>Figure 4.9.</b> Brightfield images of 100/0 microgels suspended in pH 4 (top row), pH 7 (middle row) and pH 12 (bottom row) solutions and heated to 70°C for 24 to 48 hours. Microgels heated in pH 12 solution were completely degraded after 24 hours
<b>Figure 4.10.</b> Confocal images of A) 100/5 poly(HEVE-co-succinic acid) and B) 70/6 poly(4MS-co-succinic acid-co-DVB) microgels after incubation with 0.01wt% FITC-BSA. Microgels were washed with PBS with two centrifugation cycles and allowed to settle prior to imaging. Microgels are labelled with 0.1 mol% TAMRA-cadaverine. Scale bars = 50µm
<b>Figure A4.1.</b> Volume swelling as a function of mol% BDVE for microgels polymerized in neat MEK at 4% monomer loading. The microgels were hydrolyzed and swelling ratios were calculated as microgel diameter at pH 7 / diameter at pH 2, assuming a fully collapsed microgel state at pH = 2
<b>Figure A4.2.</b> Representative brightfield images of poly(DEVE-co-MAn-co-BDVE) microgels suspended THF. Microgels were synthesized with 2.5 mol% (top row) or 5 mol% (bottom row) BDVE, with different MEK vol% in the polymerization solvent, represented by the first number in the inset (e.g. 88/2.5 corresponds to microgels formed in 88 vol% MEK in the MEK/heptane mixture). Hydrolysis of the anhydride groups lead to complete (88/2.5, 88/5) or partial dissolution (90/2.5, 90/5, 95/2.5, 95/5) of the particles. All scale bars = 25 μm
Figure 5.1. Transmission microscope images of as-formed microgels suspended in THF, showing changes in particle diameter and morphology with varying vol% MEK in the polymerization solvent and mol% BAOD . Insets are representative fluorescence images of microgels suspended in water (pH $7.8$ ) following rhodamine labeling and subsequent succinic anhydride hydrolysis. All scale bars are $50  \mu m$
<b>Figure 5.2.</b> Fluorescence images of $70/10$ microgels at t=0, 0.5, 10 and 30 min, following TCEP addition. [TCEP]:[disulfide] is estimated to be $\sim 100:1$ . Scale bars are $50\mu m$

<b>Figure 5.3.</b> 70/10 microgels before (xa) and 0.3s after (last image) exposure to 100-fold excess THPP. Imaged using a fluorescence microscope equipped with Andor Zyla 4.2 sCMOS camera operating at 100fps. Scale bars = 25μm
<b>Figure 5.4.</b> Fluorescence images depicting changes in $70/10$ (TOP) and $65/10$ (BOTTOM) BAOD microgel diameters with time following mixing with $0.1$ eq'v of THPP. Scale bars = $50\mu$ m
<b>Figure A5.1</b> . Isolated particle yields for BAOD-crosslinked microgels at different mol% BAOD loading, made in 60, 65 or 75 vol% MEK in polymerization mixture 143
<b>Figure A5.2.</b> Microgel diameters as a function of pH. Scale bars are standard deviations of particle diameter taken from an average of > 1000 particle diameter measurements using NIS elements software
<b>Figure A5.3.</b> <sup>1</sup> H NMR of BAOD in CDCl <sub>3</sub> . ca. 93% yield
<b>Figure A5.4.</b> 31P NMR of THPP standard in D2O. THPPO = 60.42 ppm, THPP = -30.24
<b>Figure A5.5.</b> 31P NMR of 70/10 microgels and THPP in D2O. Calculated %BAOD = 2.33
<b>Figure A5.6.</b> 31P NMR of 65/10 microgels and THPP in D2O. Calculated % BAOD = 2.25%
Figure A5.7. 31P NMR of 60/10 microgels and THPP in D2O. Calculated %BAOD = 2.04

# **List of Schemes**

Scheme 2.1. Mechanism of particle nucleation and growth. Aggregation and de-solvation of oligomers leads to particle nuclei that grow by capturing monomers and oligomers from solution
Scheme 2.2. a) Schematic of an RT-DC microchannel layout. Particles flow from the sample reservoir – focused by a sheath flow – through the constriction and measurement zone where the image-based shape analysis is performed. All flow rates stated are the sum of sample and sheath flow. b) Image of 73/5 microgel captured at the end of the constriction zone. Flow-rate = $0.08 \ \mu L/s$
<b>Scheme 3.1.</b> Microgel synthesis and hydrolysis to polyanionic microgel particles. Fluorescence microscope images of a) poly(Sty-co-MAn-co-DVB) and b) poly(4MS-co-MAn-co-DVB) microgels functionalized with a rhodamine label, hydrolyzed and swollen in phosphate buffered saline (PBS). Microspheres were made in 70/30 MEK/heptane using 5 mol% DVB-55 crosslinker. Magnification is 20x, NA =
0.4564
<b>Scheme 4.1.</b> Precipitation polymerization of HEVE and MAn in MEK with 0 - 10 mol% BDVE as a crosslinker. Hydrolysis with aqueous base yields crosslinked microgels that swell in aqueous solutions of pH > 4

#### **CHAPTER 1. Introduction**

### 1.1. Microgels and their Applications

Gels are macroscopic networks of crosslinked polymer chains capable of swelling in good solvents.<sup>1,2</sup> When gels are on the colloidal scale, they are referred to as micro- or nanogels depending on their average diameters. The first notable synthesis of covalently crosslinked microgels was reported by Staudinger and Husemann in 1935 from the dilute solution polymerization of divinylbenzene.<sup>3</sup> These colloids constitute a unique class of soft matter, possessing properties between those of hard spheres and flexible polymer coils. In poor solvents, microgels collapse and behave as typical hard colloids. 4-11 Alternatively, in solvents that swell the polymer, microgels adopt an open network structure with a "fuzzy" exterior that allows them to deform and pack beyond the theoretic limit of hard spheres. 7,9,10,12 Their high surface-to-volume ratio and swellable nature also allows for rapid solvent and solute exchange, enabling reversible volume phase transitions (VPPT) in response to external stimuli (e.g. temperature, pH, solvent). 12-24 These features, combined with their tunable nature, facilitate the application of microgels in a range of research areas, such as water treatment, adhesives, drug delivery, sensing, and catalysis. 25-30

A popular research application of microgels is their application in tissue engineering and their assembly into 3D scaffolds for the development of synthetic extracellular matrices (ECM).<sup>31–33</sup> Cell behaviours are strongly influenced by the interaction with their microenvironment, such that factors like scaffold stiffness and

dimensionality (2D versus 3D) directly impact cell attachment, growth and differentiation.<sup>34-40</sup> Here, synthetic microgel assemblies offer advantages over commonly employed 3D matrices made from natural materials like Matrigel or collagen; the use of synthetic polymer can mitigate the batch-to-batch structural variation associated with animal-derived scaffolds, while also allowing for modulation of mechanical properties, a feature that is often fixed in native matrices. 35,41-43 Microgel assemblies can more accurately mimic the natural hierarchical structure of biological tissues because of their granularity. This high surface area provides better mass transport compared to bulk gels, which promotes cell viability. Improved diffusion also facilitates matrix degradation, a process that can be slower and non-uniform on the bulk scale. Importantly, these assemblies have bulk-characteristics of macroscopic gels with features that can be tuned at the single-particle (micro) level. For example, the degree of "hard" or "soft" character depends on microgel swelling capacity and chemical composition, which can be modulated at the synthetic stage through selection of appropriate (co)monomers, crosslinkers, and polymerization conditions. 44-47 This ability to tune final particle characteristics makes the study of synthetic parameters (e.g. monomer selection, polymerization technique) for microgel design especially interesting.

#### 1.2. Methods of Microgel Synthesis

Heterogeneous polymerizations are the most common techniques employed for preparation of colloids in the sub-micron to micron size range.<sup>47–62</sup> These methods are typically differentiated by the number of phases present in the initial reaction mixture;

suspension and emulsion polymerizations begin as biphasic mixtures of monomer(s), stabilizers, and initiators dispersed in an immiscible, continuous phase.<sup>63–69</sup> Dispersion polymerization is homogeneous first, forming a biphasic mixture once polymers reach a critical molecular weight and precipitate from solution.<sup>48,49,67</sup> Similar to dispersion polymerization, precipitation polymerization also begins as a solution process, where the continuous phase is a good solvent for monomers and initiators but a non-solvent for the forming polymer, but differs in that it lacks added steric stabilizers.<sup>50–59</sup> As a result, particles made from precipitation polymerization can have irregular shapes and broad size distributions. In each of these methods, resulting colloid properties are determined by reaction parameters, such as the type and concentration of stabilizing agent, polymerization temperature, mixing shear, solvent, and crosslinker concentration.

This thesis examines a unique case of self-stabilized precipitation polymerization, where the reaction solvent provides steric stabilization to growing nuclei by swelling of surface-bound oligomers, resulting in an extended particle growth phase and a set of monodisperse, spherical microspheres. Within this subclass of self-stabilized precipitation polymerizations, the work presented here focuses on copolymerizations of electron-poor (*e.g.* maleic anhydride) and electron-rich (*e.g.* styrenic, vinyl ether) monomer systems with overall low crosslinker loading that enable the formation of swellable, hydrogel particles in the  $3-20~\mu m$  size range. The aim of this introduction is to familiarise the reader with the mechanism of self-stabilized precipitation polymerization, with focus on the key aspects influencing final particle morphology, such as solvent selection and crosslinker concentration.

#### 1.3. Colloidal Stabilization

In absence of long-range repulsive interactions, attractive van der Waals forces acting between particles in a colloidal dispersion promote their rapid aggregation and coalescence.<sup>70</sup> These forces operate over several tens of nanometres and arise due to fluctuating electric dipoles that exist in all atoms and molecules. Sufficient stabilization is therefore essential for long term storage and application of colloidal dispersions. The next section will review the two main mechanisms for preventing aggregation in colloidal dispersions: electrostatic and steric stabilization.<sup>70</sup>

#### 1.3.1. Electrostatic stabilization

In electrostatic stabilization, charged layers introduced onto particle surfaces prevent aggregation via Coulombic repulsion.<sup>71–73</sup> An example is demonstrated in Figure 1.1, which depicts the electrostatic repulsion between two charged particles in a liquid.

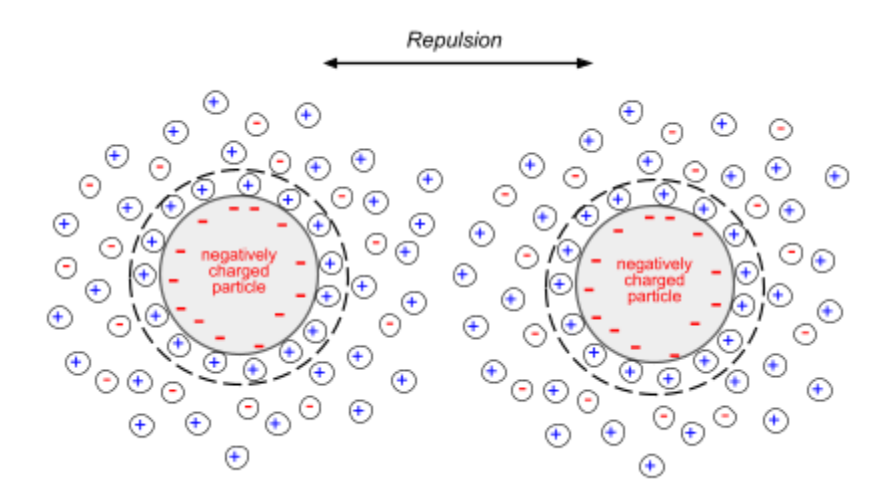
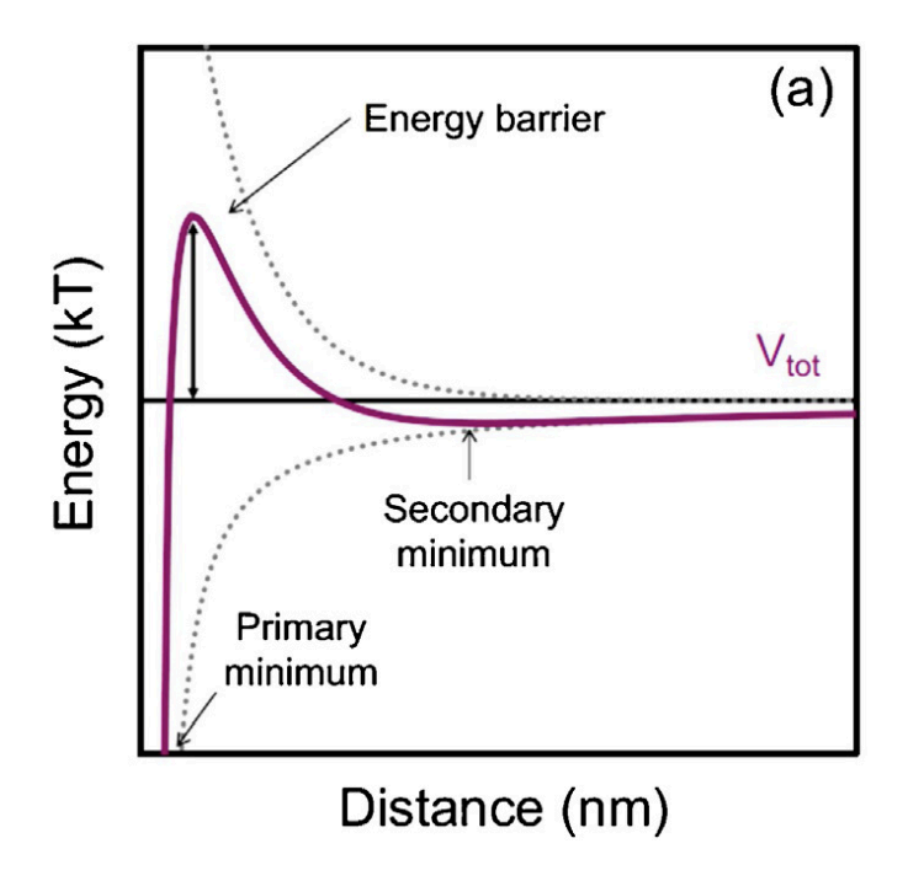


**Figure 1.1.** Schematic representation of electrostatic stabilization of two negatively charged particles in solution. Overlap of the diffuse ion layers at the surface of the particles prevents aggregation. Dashed lines represent the Stern layer.

Counterions from solution create a diffuse electric double layer (EDL) at the particle surface. As particles approach each other, EDL overlap and an increase in local ion concentration generates a repulsive force that has a magnitude proportional to the degree of overlap.<sup>73</sup>

DLVO theory, named after its founders Derjaguin, Landau, Vervey, and Overbeek, can be used to describe the interaction and aggregation behaviour of charged bodies in a liquid. The equation of the energy ( $V_{tot}$ ) between two similarly charged surfaces (e.g. plates or spheres) is taken as the sum of contributions of attractive van der Waals ( $V_A$ ) and repulsive EDL ( $V_R$ ) forces (Equation 1), and modelled as a function of interparticle distance (Fig. 1.2).

$$V_{tot} = V_A + V_R \tag{1}$$



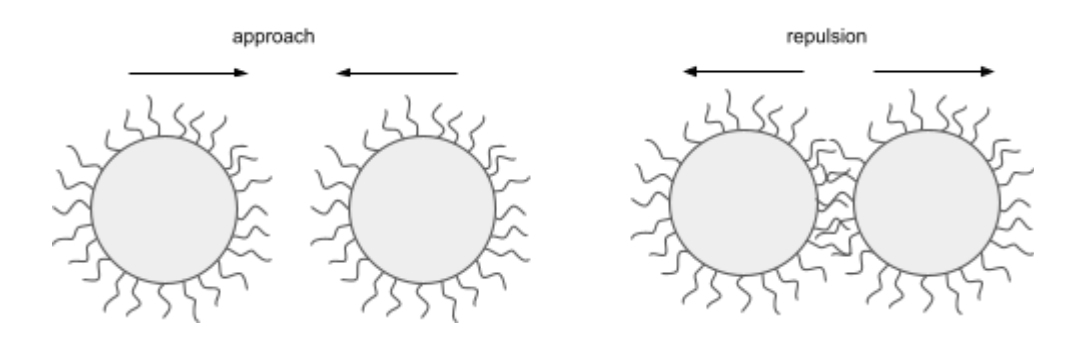
**Figure 1.2.** Representation of DLVO potential showing total interaction energy ( $V_{tot}$ ) as a sum of van der Waals attraction and EDL forces. The deep, primary minimum represents irreversible aggregation at short distances, while the secondary minimum represents reversible aggregation at intermediate distances.<sup>74</sup>

Figure 1.2 shows that there is an energy barrier that particles must overcome to aggregate. At very short distances, attractive van der Waals forces cause particles to fall into a primary potential energy well (Fig. 1.2, primary minimum) where they aggregate irreversibly. At intermediate distances, repulsive EDL forces dominate and the colloidal dispersion is stabilized. Exponential decay of EDL forces over very large distances results in a more shallow, secondary minimum, where particles may aggregate in a

reversible fashion.<sup>75</sup> The primary minimum is considered infinitely deep, while the depth of the secondary potential energy well varies depending on conditions like temperature, ionic strength, and pH of the continuous phase. For example, an increase in ionic strength will screen surface charges on particles, deepening the secondary minimum and decreasing energy barrier for aggregation. Since the effectiveness of electrostatic stabilization ultimately depends on the size and diffusivity of the electric double layer, this method finds its best use in high dielectric media like water.

#### 1.3.2. Steric Stabilization

Unlike electrostatic stabilization, steric stabilization is less sensitive to salt concentration and can be employed in both organic and aqueous media. This method involves adsorption or covalent bonding of a polymer layer onto the particle surface to prevent coalescence through steric repulsion (Figure 1.3).<sup>70</sup>



**Figure 1.3.** Schematic representation of steric stabilization for two particles of equal radius bearing polymer chains on their surface. Upon approach, crowding of surface polymer chains results in a decrease in configurational entropy and a net repulsive force that prevents aggregation.

Here, stabilization is a result of the influx of solvent molecules that work to dilute the increasing local polymer concentration upon particle approach. From a thermodynamic perspective, aggregation is entropically and enthalpically unfavourable when the suspending medium is a good solvent for the stabilizer chains. Locally increasing the stabilizer concentration reduces entropy by restricting configurational freedom of surface bound chains, while breaking strong stabilizer-solvent interactions to form poorer polymer-polymer interactions increases the enthalpy of the system. These surface-bound polymers are selected such that they have an affinity for both particle surface and the continuous phase. Steric stabilizers for polar solvents can be homopolymers like poly(ethylene glycol) (PEG), poly(vinyl alcohol) (PVA), poly(*n*-vinyl pyrrolidone) (PVP), or block copolymers.<sup>76-79</sup>

#### 1.4. Self-Stabilized Precipitation Polymerization

Our group has previously reported on controlled precipitation polymerizations leading to monodisperse, crosslinked polymer microspheres of maleic anhydride, 4-methylstyrene and divinylbenzene-55.<sup>52,54</sup> A minimum amount of crosslinker is typically required to help capture oligomers from solution onto the growing microsphere. Size and morphology of these microspheres can be tailored by changing solvency or crosslinker loading. Polymerization begins as a homogeneous mixture of monomers and initiators. As oligomers form and reach a critical molecular weight, they phase-separate and aggregate to form primary particle nuclei. This nucleation stage continues until there are enough nuclei present to capture growing oligomers from solution, which suppresses

secondary nucleation and prevents broadening of the final particle size distribution. Nuclei are stabilized by a surface layer of solvent-swollen oligomers, which collapses as it undergoes crosslinking and is replaced with a new layer of oligomers. Once nuclei reach colloidal stability, they continue to grow by capturing monomers and oligomers from solution. Ultimately, the number of nuclei at colloidal stability determines the final microsphere number and size.

The key to this process is the interplay between polymer-solvent interactions and polymer crosslinking: the solvent swells oligomers at the particle surface providing stabilization, while crosslinking facilitates capture of more oligomers to the surface, promoting desolvation of the surface-bound polymer layer to become part of the particle core.

#### 1.4.1. Effect of reaction solvent on particle morphology

Understanding the solution behaviour of polymers is important for the formulation of paints, coatings and plastic processing, and in the pharmaceutical industry. S1-S3 In the context of precipitation polymerization, interactions between solvent molecules and growing polymer chains dictate the onset of colloidal stability, and therefore the final particle size distribution and morphology. A method for predicting the magnitude of such polymer-solvent interactions involves the application of Hildebrand and Hansen solubility parameters. The next section provides a brief introduction to solubility parameters as they relate to solvent selection for the preparation of microspheres from precipitation polymerization.

#### 1.4.2. Hildebrand and Hansen Solubility Parameters

Mixing is determined by the magnitude of the Gibbs free energy (Equation 2), where  $\Delta H_{mix}$  and  $\Delta S_{mix}$  are the enthalpy and the entropy of mixing, respectively, and T is the absolute temperature in Kelvin.

$$\Delta G_{mix} = \Delta H_{mix} - T\Delta S_{mix} \tag{2}$$

In ideal solutions, where all molecules are of comparable dimensions, the forces acting between them are equal such that  $\Delta H_{mix}$  is negligible and mixing is purely entropy driven. When considering polymer dissolution, where solute and solvent dimensions are not equivalent, enthalpic contributions must be considered for an accurate representation of  $\Delta G_{mix}$ .

One way to predict polymer-solvent compatibility is through the comparison of their solubility parameters,  $\delta$ . This term comes from a relationship defined by Hildebrand and Scott to describe the enthalpy of mixing ( $\Delta H_{mix}$ ) of binary liquids, which is based on the heats of vaporization of the components in the mixture (Equations 3 and 4).<sup>84,85</sup>

$$\Delta H_{mix} = V \left( \delta_1 - \delta_2 \right)^{1/2} \phi_1 \phi_2 \tag{3}$$

$$\delta_i = \left(\frac{\Delta E_i^v}{V_i}\right)^{1/2} \tag{4}$$

Here, V is the total volume of the mixture, and  $\Delta E_i^v$ ,  $V_i$ , and  $\phi_i$  represent the energy of vaporisation, molar volume, and volume fraction of component i, respectively. The solubility parameter is defined as the square root of cohesive energy density (CED),

 $\frac{\Delta E_i^{\nu}}{V_i}$ , and is a measure of attractive forces holding a substance, *i*, together in a given volume.

The  $\delta$  term is expressed in units of MPa<sup>1/2</sup> and can be directly measured for small molecules and volatile liquids, with values ranging from ~10 MPa<sup>1/2</sup> for non-polar solvents like dimethyl siloxane to 48 MPa<sup>1/2</sup> for water. From equations 2 and 3, we see that mixing is favoured ( $\Delta G_{mix} < 0$ ) when  $\delta_1 = \delta_2$ . In practice, however,  $\delta$  terms need not be exactly equal for a polymer to be miscible with a given solvent; rather, mixing can occur if the  $\delta_1$  and  $\delta_2$  are within ~ 4 to 5 MPa<sup>1/2</sup> of each other. For non-volatile substances like macromolecules,  $\delta$  parameters can be estimated experimentally by testing what solvent best swells a cross-linked analogue of the polymer. The polymer is then assumed to have a similar  $\delta$  value to that of the swelling solvent. Alternatively,  $\delta$  can be determined empirically from the summation of individual thermodynamic contributions of functional groups, atoms, and bonds in the repeat unit of the polymer through use of van Krevelen and Hoftyzer's group contribution values.

While the Hildebrand solubility parameters are good predictors for non-polar systems, such as poly(DVB-55), they are more limited in their application for polar compounds because they do not account for the hydrogen-bonding or dipolar forces. To bridge this gap, Hansen expanded Hildebrand's solubility parameter into a three-dimensional term (Equation 5) that encompasses the corresponding intermolecular contributions.

$$\delta_T^2 = \delta_D^2 + \delta_P^2 + \delta_H^2$$
 (5)

Here,  $\delta_T$  is the total solubility parameter of the mixture, and  $\delta_D$ ,  $\delta_H$  and  $\delta_P$ , represent the dispersion, hydrogen-bonding, and dipolar forces, respectively. These individual contributions provide a more accurate guide for estimating polymer and solvent interactions in polar solutions, providing a valuable framework for solvent selection in precipitation polymerization with more polar (co)monomers.

In precipitation polymerization, the goal is to select a "marginal" solvent: one that dissolves monomers and swells low molecular weight oligomers, but precipitates the forming polymer. This requirement can be rationalised by the mechanism of particle formation. In early stages of polymerization, the solvent promotes the desolvation and aggregation of growing polymers into primary particle nuclei (pre-stabilization). Once nuclei are formed, the solvent prevents further aggregation by swelling surface-bound oligomers, while also facilitating particle growth through the desolvation of new polymer from solution.<sup>54</sup> In the precipitation polymerization of divinylbenzenes (e.g. DVB-55, DVB-80), Frank et al. and Downey et al. found that mixtures of methyl ethyl ketone (MEK,  $\delta = 19.0 \text{MPa}^{1/2}$ ) and heptane ( $\delta = 15.0 \text{ MP}^{1/2}$ ) met the marginal solvency requirements for the formation of narrow-dispersed microspheres. 52,54 When relatively more polar comonomers like maleic anhydride or (meth)acrylates were used, the solvent mixture was adjusted to include more polar solvents to facilitate microsphere formation over aggregation. 51,53,54 Consequently, increasing the amount of good solvent beyond a certain point leads to macrogelation; as the polymer swells, the likelihood of intermolecular reactions between particles increases. These solvent-dependent morphology transitions (e.g. aggregation, microsphere, microgel, and macrogel

formation) can be observed at different solvency ranges, again depending on the difference in Hansen solubility parameters (HSP) between the growing polymer and the reaction solvent.

#### 1.4.3. Effect of crosslinker concentration

Crosslinking is another important aspect of precipitation polymerization, as it limits configurational freedom and reduces overall entropy of mixing to promote desolvation. It is important to note that though the roles of crosslinker and reaction solvent are discussed separately, they function cooperatively in the mechanism of particle formation; at given solvency range where oligomers at the surface of growing nuclei are swollen, there is a corresponding amount of crosslinking required to drive the polymer below its theta-condition to facilitate partial collapse of the network into discrete particles. Thus, morphologies observed at different crosslinker concentrations will depend strongly on the polymerization solvent composition. For example, Frank et al. found that 5 mol% crosslinker was enough to facilitate microgel formation in DVB-55/MAn copolymerizations when the MEK volume fraction of the reaction solvent was 70%, while only soluble polymer was isolated at 80% MEK.<sup>54</sup> In this regime of good solvency (e.g. >80 v/v% MEK in the case of DVB-55/MAn copolymerizations), increasing the crosslinker concentration can result in macrogelation. When the crosslinker concentration is sufficient enough to enable microgel formation, enhanced swelling of polymer chains from better solvent conditions decreases crosslinking efficiency, producing particles with a higher degree of swelling. In their swollen state,

distance between microgels decreases enough to allow for crosslinking with neighbouring particle surfaces.

### 1.5. Thesis Overview

The overall objectives of this thesis are two-fold. The first objective is to further explore the effects of low crosslinker loading and good solvency conditions on the properties of microgels formed by precipitation polymerization of maleic anhydride (MAn) and styrenic monomers, which expands on our earlier work on highly crosslinked DVB-55 microspheres. Here, crosslinker content is kept under 10 mol% DVB and reaction solvent is rich in good solvent, MEK, such that resulting particles are lightly crosslinked and fall in the 3 – 20 µm size-regime when swollen in organic solvents like THF. These results are presented in the first half of the thesis (Chapters 2 and 3). The second goal involves the expansion of the comonomer and crosslinker repertoire to include hydrophilic vinyl ethers (Chapter 4) and replacement of permanent crosslinker DVB with a degradable disulfide-containing diacrylate (Chapter 5) in place of styrenic monomers and DVB. A chapter-by-chapter breakdown is presented below.

In Chapter 2, precipitation polymerization of 4-methyl styrene (4MS), DVB, and MAn is studied to make microgels in the 3 – 20 μm diameter size regime. The effects of polymerization cosolvent and DVB loading on final particle morphology was studied using optical and confocal microscopy. Electron microscopy was used to assess the degree of homogeneity of crosslinking, showing a uniform morphology for microgels with the lowest crosslinker levels (5 mol%). Microgels were functionalized with

fluorescent labels and backbone anhydride groups were ring-opened with aqueous base to study the pH and salt response of aqueous microgels suspensions with confocal and optical microscopy. Inclusion of styrene as a comonomer to the 4MS/DVB/MAn system introduces another handle for controlling final particle size, where increasing the molar percentage of styrene in the 4MS:styrene pool results in smaller microgel diameters at constant crosslinker and cosolvent conditions.

In Chapter 3, precipitation polymerization of 4MS/DVB/MAn is extended to very low crosslinker loadings (3 to 5 mol% with respect to styrenic monomers, or 1.5 – 2.5% relative to total polymer) and the mechanical properties of resulting microgels are studied using microscopy and real-time deformability cytometry (RT-DC), a microfluidic technique developed for the analysis of cell morphology that provides single-particle Young's modulus information. Microgels synthesized in high volume fractions of MEK and with low (*e.g.* 3 mol%) DVB content faceted and deformed under compression due to their soft nature, and had moduli comparable to mammalian cells. This chapter demonstrates the first use of RT-DC for the characterization of soft, polymer particles.

Chapter 4 replaces styrenic monomers with vinyl ethers, and focuses on the study of microgels formed from copolymerization of hydroxyethyl vinyl ether (HEVE) and MAn in neat MEK and MEK/heptane mixtures. Particle morphology was studied as a function of reaction solvency and crosslinker loading; where narrow-dispersed particles ranging from 1 to 7 $\mu$ m in diameter formed high volume fractions of MEK ( $\geq$  95 v/v % MEK) at crosslinker loadings less than 7.5 mol% BDVE. Unlike polymerizations in former chapters, cross-linked microgels were isolated from 1:1 copolymerizations of

HEVE and MAn (*e.g.* 0 mol% crosslinker) when polymerized in neat MEK. These self-crosslinked particles were stable in good organic solvents in their anhydride-form, but degraded when heated in neutral or basic aqueous solutions. <sup>1</sup>H NMR analysis showed that the HEVE monomer undergoes a series of side reactions, including cyclization, hydrolysis, and intermolecular ester formation, when heated in the presence of trace amounts of maleic acid found in maleic anhydride. The combined results of NMR and degradation tests suggest that self-crosslinking is a result of ester-bond formation with anhydride groups on neighbouring chains during polymerization.

Chapter 5 explores the synthesis of degradable microgels from precipitation polymerization of MAn, 4MS and a disulfide-containing diacrylate, bis(2-acryloyl)oxyethyl disulfide (BAOD). Microgels in the 1 to 11 µm size range were formed in mixtures of MEK/heptane ranging from 60% MEK to 70% MEK, at BAOD loadings of 10 to 15 mol%. The solvency and crosslinker range in which spherical, narrow-disperse particles are formed is limited compared to polymerizations presented in previous chapters (*e.g.* DVB cross-linked microgels). Here, when the MEK volume fraction is less than 50% or greater than 70%, irregular aggregates or macrogels are formed, respectively.

### 1.6. References

- 1. Tanaka, T. Gels. Scientific American. 1981, 244, 124–138
- 2. Tanaka, T.; Fillmore, D. J. Kinetics of swelling of gels. *J. Chem. Phys.* **1979**, *70*, 1214–1218
- 3. Staudinger, H.; Heuer, W.; Husemann, E.; Rabinovitch, I. J. The insoluble polystyrene. *Trans. Faraday Soc.* **1936**, *32*, 323–332
- 4. Mourran, A.; Wu, Y.; Gumerov, R. A.; Rudov, A. A.; Potemkin, I. I.; Pich, A.; Möller, M. When Colloidal Particles Become Polymer Coils. *Langmuir.* **2016**, *32*, 723–730
- 5. Lyon, L. A.; Fernandez-Nieves, A. The Polymer/Colloid duality of microgel suspensions. *Annu. Rev. Phys. Chem.* **2012**, *63*, 25–43
- 6. Saunders, B. R.; Vincent, B. Microgel particles as model colloids:theory, properties and applications. *Adv. Colloid Interface Sci.* **1999**, *80*, 1–25
- Mattsson, J.; Wyss, H. M.; Fernandez-Nieves, A.; Miyazaki, K.;Hu, Z.;
   Reichman, D. R.; Weitz, D. A. Soft colloids make strong glasses. *Nature*. 2009, 462, 83–86
- 8. Scotti, A.; Bochenek, S.; Brugnoni, M.; Fernandez-Rodriguez, M. A.; Schulte, M. F.; Houston, J. E.; Gelissen, A. P. H.; Potemkin, I.I.; Isa, L.; Richtering, W. Exploring the colloid-to-polymer transition for ultra-low crosslinked microgels from three to two dimensions. *Nat. Commun.* **2019**, *10*, 1418.

- 9. Keidel, R.; Ghavami, A.; Lugo, D. M.; Lotze, G.; Virtanen, O.; Beumers, P.; Pedersen, J. S.; Bardow, A.; Winkler, R. G.; Richtering, W. Time-resolved structural evolution during the collapse of responsive hydrogels: The microgel-to-particle transition. *Sci. Adv.* **2018**, *4*, eaao7086
- Hellweg, T.; Dewhurst, C. D.; Bruckner, E.; Kratz, K.; Eimer, W. Colloidal crystals made of poly(N-isopropylacrylamide) microgel particles. *Colloid Polym. Sci.* 2000, 278, 972–978
- Deshmukh, O. S. Hard and soft colloids at fluid interfaces: Adsorption, interactions, assembly & rheology. *Advances in Colloid and Interface Science*.
   2015, 222, 215–227.
- 12. Senff, H.; Richtering, W. Temperature sensitive microgel suspensions: Colloidal phase behavior and rheology of soft spheres. *J. Chem. Phys.* **1999**, *111*, 1705–1711
- 13. Agnihotri, P. et al. Temperature- and pH-responsive poly(N-isopropylacrylamide-co-methacrylic acid) microgels as a carrier for controlled protein adsorption and release. *Soft Matter* **2021**, *17*, 9595–9606
- 14. Tanaka, T.; Fillmore, D.J.; Sun, S.T.; Nishio, I.; Swislow, G.; Shah, A. Phase Transitions in Ionic Gels. *Phys. Rev. Lett.* **1980**, *45*, 1636–1639.
- Jelken, J.; Jung, S.; Lomadze, N.; Gordievskaya, Y. D.; Kramarenko, E. Yu.; Pich,
   A.; Santer, S. Tuning the volume phase transition temperature of microgels by
   light. Adv. Func. Mater. 2021, 32, 2107946

- 16. Polotsky, A. A.; Plamper, F. A.; Borisov, O. V. Collapse-to-Swelling transitions in pH- and thermoresponsive microgels in aqueous dispersions: the Thermodynamic Theory. *Macromolecules*. 2013, 46, 8702–8709.
- 17. Pich, A.; Tessier, A.; Boyko, V.; Lu, Y.; Adler, H.-J. P. Synthesis and Characterization of Poly(vinylcaprolactam)-Based Microgels Exhibiting Temperature and pH-Sensitive Properties. *Macromolecules* **2006**, *39*, 7701–7707.
- 18. Snowden, M. J.; Chowdhry, B. Z.; Vincent, B.; Morris, G. E. Colloidal copolymer microgels of N-isopropylacrylamide and acrylic acid: pH, ionic strength and temperature effects. *J. Chem. Soc., Faraday Trans.* **1996**, *92*, 5013.
- 19. Bergman, M. J.; Pedersen, J. S.; Schurtenberger, P.; Boon, N. Controlling the morphology of microgels by ionic stimuli. *Soft Matter* **2020**, *16*, 2786–2794.
- 20. Garcia, A. et al. Photo-, thermally, and pH responsive microgels. *Langmuir*. **2007**, 23, 224–229
- 21. Zhou, S.; Chu, B. Synthesis and Volume Phase Transition of Poly(methacrylic acid- co N -isopropylacrylamide) Microgel Particles in Water. *J. Phys. Chem. B.* **1998**, *102*, 1364–1371
- 22. Brijitta, J.; Schurtenberger, P. Responsive hydrogel colloids: Structure, interactions, phase behavior, and equilibrium and nonequilibrium transitions of microgel dispersions. *Curr. Opin. Colloid Interface Sci.* **2019**, *40*, 87–103
- 23. Hassan, A. et al. Efficient removal of cationic dye from aqueous media using alkali-treated multilayered polymer microspheres prepared via emulsion polymerization. *New J. Chem.* **2025**,*49*, 1377-1390

- 24. Ahiabu, A.; Serpe, M.J. Rapidly Responding pH- and Temperature-Responsive Poly (N-Isopropylacrylamide)-Based Microgels and Assemblies. ACS Omega. 2017, 2, 1769-1777
- 25. Zhang, Q. M.; Berg, D.; Mugo, S. M.; Serpe, M. J. Lipase-modified pH-responsive microgel-based optical device for triglyceride sensing. *Chem. Comm.* **2015**, *51*, 9726–9728.
- 26. Guerzoni, L. P. B.; Bohl, J.; Jans, A.; Rose, J. C.; Koehler, J.; Kuehne, A. J. C.; De Laporte, L. Microfluidic fabrication of polyethylene glycol microgel capsules with tailored properties for the delivery of biomolecules. *Biomater. Sci.* 2017, 5, 1549–1557
- 27. Gao, Y.; Li, X.; Serpe, M. J. Stimuli-responsive microgel-based etalons for optical sensing. *RSC Advances*. **2015**, *5*, 44074–44087
- 28. Wiese, S.; Spiess, A. C.; Richtering, W. Microgel-Stabilized Smart Emulsions for biocatalysis. *Angew. Chem. Int. Ed.* **2012**, *52*, 576–579
- 29. Sharma, B.; Striegler, S. Crosslinked Microgels as platform for hydrolytic catalysts. *Biomacromolecules*. **2018**, *19*, 1164–117
- 30. Yang, D.; Pelton, R. H. Degradable Microgel Wet-Strength Adhesives: A route to enhanced paper recycling. *ACS Sustain. Chem. Eng.* **2017**, *5*, 10544–10550.
- 31. Du, Y.; Lo, E.; Ali, S.; Khademhosseini, A. Directed assembly of cell-laden microgels for fabrication of 3D tissue constructs. *PNAS.* **2008**, *105*, 9522–9527

- 32. Nguyen, P. K.; Snyder, C. G.; Shields, J. D.; Smith, A. W.; Elbert, D. L. Clickable Poly(ethylene glycol)-Microsphere-Based Cell Scaffolds. *Macromol. Chem. Phys.* **2013**, *214*, 948–956.
- 33. Griffin, D.R. et al. Accelerated wound healing by injectable microporous gel scaffolds assembled from annealed building blocks. Nat. Mater. 2015, 14, 737–744
- 34. Reilly, G. C; Engler, A. J. Intrinsic extracellular matrix properties regulate stem cell differentiation. *J. Biomech.* **2010**, 43, 55–62.
- 35. Enemchukwu, N. O. et al. Synthetic matrices reveal contributions of ECM biophysical and biochemical properties to epithelial morphogenesis. *J. Cell Biol.*2016, 212, 113–124
- 36. Engler, A. J.; Sen, S.; Sweeney, H. L.; Discher, D. E. Matrix elasticity directs stem cell lineage specification. *Cell* **2006**, *126*, 677–689.
- 37. Huebsch, N.; Lippens, E.; Lee, K.; Mehta, M.; Koshy, S. T.; Darnell, M. C.; Desai, R. M.; Madl, C. M.; Xu, M.; Zhao, X.; Chaudhuri, O.; Verbeke, C.; Kim, W. S.; Alim, K.; Mammoto, A.; Ingber, D. E.; Duda, G. N.; Mooney, D. J. Matrix elasticity of void-forming hydrogels controls transplanted-stem-cell-mediated bone formation. *Nat. Mater.* 2015, *14*, 1269–1277.
- 38. Yang, C.; DelRio, F. W.; Ma, H.; Killaars, A. R.; Basta, L. P.; Kyburz, K. A.; Anseth, K. S. Spatially patterned matrix elasticity directs stem cell fate. *PNAS*. **2016**, *113*, e4439-45.

- 39. Pelham, R. J.; Wang, Y. L. Cell locomotion and focal adhesions are regulated by substrate flexibility. *PNAS.* **1997**, 94, 13661—13665
- 40. Kloxin, A. M.; Kasko, A. M.; Salinas, C. N.; Anseth, K.S. Photodegradable Hydrogels for Dynamic Tuning of Physical and Chemical Properties. *Science* **2009**, *324*, 59-63
- 41. Kleinman, H. K., Martin, G. R. Matrigel: basement membrane matrix with biological activity. *Semin. Cancer Biol.* **2005**, *15*, 378–386
- 42. Hughes, C. S., Postovit, L. M. & Lajoie, G. A. Matrigel: a complex protein mixture required for optimal growth of cell culture. *Proteomics*, **2010**, *10*, 1886–1890
- 43. Jabaji, Z. et al. Type I collagen as an extracellular matrix for the in vitro growth of human small intestinal epithelium. *PLoS One*. **2014**, *9*, e107814
- 44. Scotti, A.; Denton, A. R.; Brugnoni, M.; Houston, J. E.; Schweins, R.; Potemkin,
  I. I.; Richtering, W. Deswelling of microgels in crowded suspensions depends on
  Cross-Link density and architecture. *Macromolecules* 2019, 52 3995–4007.
- 45. Peng, B.; Van Der Wee, E.; Imhof, A.; Van Blaaderen, A. Synthesis of monodisperse, highly Cross-Linked, fluorescent PMMA particles by dispersion polymerization. *Langmuir* **2012**, *28*, 6776–6785
- 46. Gao, J.; Frisken, B. J. Influence of secondary components on the synthesis of Self-Cross-Linked N-Isopropylacrylamide microgels. *Langmuir* **2004**, *21*, 545–551

- 47. Dupin, D.; Fujii, S.; Armes, S. P.; Reeve, P.; Baxter, S. M. Efficient synthesis of sterically stabilized pH-Responsive microgels of controllable particle diameter by emulsion polymerization. *Langmuir* **2006**, *22*, 3381–3387.
- 48. Song, J.S.; Winnik, M. A. Cross-Linked, monodisperse, Micron-Sized Polystyrene Particles by Two-Stage Dispersion Polymerization. *Macromolecules* **2005**, *38*, 8300–8307.
- 49. Hu, H.; Larson, R. G. One-Step preparation of highly monodisperse Micron-Size particles in organic solvents. *J. Am. Chem. Soc.* **2004**, *126*, 13894–13895.
- 50. Li, K.; Stöver, H. D. H. Synthesis of monodisperse poly(divinylbenzene) microspheres. *J. Polym. Sci., Part A:Polym. Chem.* **1993**, *31*, 3257–3263.
- 51. Li, W.H.; Stöver, H.D.H. Mono- or Narrow Disperse Poly (Methacrylate-co-Divinylbenzene) Microspheres by PrecipitationPolymerization. *J. Polym. Sci., Part A: Polym. Chem.* **1999**, *37*, 2899
- 52. Downey, J. S.; McIsaac, G.; Frank, R. S.; Stöver, H. D. H. Poly(divinylbenzene) Microspheres as an Intermediate Morphology between Microgel, Macrogel, and Coagulum in Cross-Linking Precipitation Polymerization. *Macromolecules*. **2001**, *34*, 4534–4541.
- 53. Goh, E. C. C.; Stöver, H. D. H. Cross-Linked Poly(methacrylic acid-co-poly(ethylene oxide) methyl ether methacrylate) Microspheres and Microgels Prepared by Precipitation Polymerization: A Morphology Study. *Macromolecules.* 2002, 35, 9983–9989.

- S.; S.; K.; D. 54. Frank, R. Downey, J. Yu, Stöver, Н. H. Poly(divinylbenzene-alt-maleic anhydride) Microgels: Intermediates to Microspheres and Macrogels in Cross-Linking Copolymerization. Macromolecules. 2002, 35, 2728–2735.
- 55. Bai, F.; Yang, X.; Huang, W. Synthesis of Narrow or Monodisperse Poly(divinylbenzene) Microspheres by Distillation–Precipitation Polymerization. *Macromolecules.* **2004**, 37, 9746–9752.
- 56. Limé, F.; Irgum, K. Monodisperse polymeric particles by photoinitiated precipitation polymerization. *Macromolecules*. **2007**, *40*, 1962–1968.
- 57. Xu, C.; Chen, C.; Jiang, J.; Zhao, C.; Ma, Y.; Yang, W. Monodisperse Styrene-Maleic Anhydride-Isoprene Terpolymer Microspheres with Tunable Crosslinking Density Prepared by Self-Stabilized Precipitation Polymerization.

  ACS Appl. Polym. Mater. 2022, 4, 7363–7372.
- 58. Cui, H.; Chen, H.; Qu, R.; Wang, C.; Sun, C.; Zhou, W.; Yu, M.; Jiang, H. Highly crosslinked poly(styrene-co-divinylbenzene) microspheres prepared by precipitation polymerization: Effects of the polymerization parameters on the characteristics of the particles. *J. Appl. Polym. Sci.* **2008**, *111*, 3144–3149.
- 59. Shu, H.; Song, C.; Yang, L.; Wang, C.; Chen, D.; Zhang, X.; Ma, Y.; Yang, W. Self-Stabilized precipitation polymerization of vinyl chloride and maleic anhydride. *Ind. Eng. Chem. Res.* **2023**, *62*, 3612–3621.

- 60. Shen, S.; Sudol, E. D.; El-Aasser, M. S. Dispersion polymerization of methyl methacrylate: Mechanism of particle formation. *J. Polym. Sci., Part A: Polym. Chem.* **1994**, *32*, 1087–1100.
- 61. Yan, Q.; Zhao, T.; Bai, Y.; Zhang, F.; Yang, W. Precipitation Polymerization in Acetic Acid: Study of the Solvent Effect on the Morphology of Poly(divinylbenzene). *J. Phys. Chem. B.* **2009**, *113*, 3008–3014.
- 62. Xing, C.; Yang, W. A novel, facile method for the preparation of uniform, reactive maleic Anhydride/Vinyl acetate copolymer micro- and nanospheres. *Macromol. Rapid Commun.* **2004**, *25*, 1568–1574.
- 63. Vivaldo-Lima, E.; Wood, P. E.; Hamielec, A. E.; Penlidis, A. An updated review on suspension polymerization. Ind. Eng. Chem. Res. 1997, 36 (4), 939–965.
- 64. Villalobos, M. A.; Hamielec, A. E.; Wood, P. E. Bulk and suspension polymerization of styrene in the presence of n-pentane. An evaluation of monofunctional and bifunctional initiation. Journal of Applied Polymer Science 1993, 50 (2), 327–343.
- 65. Nishimura, S.-N.; Nishida, K.; Shiomoto, S.; Tanaka, M. Surfactant-Free Suspension Polymerization of Hydrophilic Monomers with an Oil-in-Water System for the Preparation of Microparticles Toward the Selective Isolation of Tumor Cells. Materials Advances 2022, 3 (12), 5043–5054.
- 66. Chern, C. S. Emulsion polymerization mechanisms and kinetics. Prog. Polym. Sci. 2006, 31 (5), 443–486.

- 67. Arshady, R. Suspension, emulsion, and dispersion polymerization: A methodological survey. *Colloid Polym. Sci.* **1992**, *270*, 717–732.
- 68. Smith, W. V.; Ewart, R. H. Kinetics of emulsion polymerization. *J. Chem. Phys.* **1948**, 16, 592–599.
- 69. Lovell, P. A.; Schork, F. J. Fundamentals of Emulsion Polymerization. *Biomacromolecules* **2020**, *21*, 4396–4441.
- 70. Napper, D. H. Steric Stabilization. J. Colloid. Interface Sci. 1977, 58, 390–407
- 71. Derjaguin, B.; Landau, L. Theory of the stability of strongly charged lyophobic sols and of the adhesion of strongly charged particles in solutions of electrolytes. *Prog. Surf. Sci.* **1993**, *43*, 30–59
- 72. Verwey, E. J. W. Theory of the stability of lyophobic colloids. *J. Phys. Colloid Chem.* **1947**, *51*, 631–636
- 73. Van der Hoeven, Ph. C.; Lyklema, J. Electrostatic stabilization in non-aqueous media. *Adv. Colloid Interface Sci.* **1992**, *42*, 205–277
- 74. Matter, F.; Luna, A. L.; Niederberger, M. From colloidal dispersions to aerogels: How to master Nanoparticle gelation. *Nano Today 30*, 100827.
- 75. Canseco, V.; Djehiche, A.; Bertin, H.; Omari, A. Deposition and re-entrainment of model colloids in saturated consolidated porous media: Experimental study. *Colloids Surf. A: Physicochem. Eng. Asp.* 2009, 352, 5–11
- Smith, J. N.; Meadows, J.; Williams, P. A. Adsorption of Polyvinylpyrrolidone onto Polystyrene Latices and the Effect on Colloid Stability. *Langmuir*. 1996, 12, 3773–3778

- 77. Stejskal, J.; Kratochvíl, P.; Helmstedt, M. Polyaniline Dispersions. 5. Poly(vinyl alcohol) and Poly(N-vinylpyrrolidone) as Steric Stabilizers. *Langmuir*. **1996**, *12*, 3389–3392
- 78. Gref, R.; Domb, A.; Quellec, P.; Blunk, T.; Müller, R.H.; Verbavatz, J.M.; Langer, R. The controlled intravenous delivery of drugs using PEG-coated sterically stabilized nanospheres. *Adv. Drug Deliv. Rev.* **2012**, *64*, 316-326.
- 79. Baines, F. L.; Dionisio, S.; Billingham, N. C.; Armes, S. P. Use of block copolymer stabilizers for the dispersion polymerization of styrene in alcoholic media. *Macromolecules* **1996**, *29*, 3096–3102
- 80. Graham, N. B.; Hayes, C. M. G. Microgels 1: Solution polymerization using vinyl monomers. *Macromol. Symp.* **1995**, *93*, 293–300
- 81. Hansen, C. M. On predicting environmental stress cracking in polymers. *Polym. Degrad. Stab.* **2002**, 77, 43–53.
- 82. Hancock, B. C.; York, P.; Rowe, R. C. The use of solubility parameters in pharmaceutical dosage form design. *Int. J. Pharm.* **1997**, *148*, 1–21
- 83. Greenhalgh, D. J.; Williams, A. C.; Timmins, P.; York, P. Solubility parameters as predictors of miscibility in solid dispersions. *J. Pharm. Sci.* **1999**, *88*, 1182–1190
- 84. Hildebrand, J. H.; Scott, R. L. The Solubility of Nonelectrolytes, 3rd ed.; Reinhold: New York, 1959.
- 85. Brandrup, J.; Immergut, E. H.; Grulke, E. A. Polymer Handbook, 4th ed.; **1999**; Vol. II, p 675–683

- 86. Errede, L. A. Polymer Swelling. 5. Correlation of relative swelling of poly(styrene-co-divinylbenzene) with the Hildebrand solubility parameter of the swelling liquid. *Macromolecules*. **1986**, *19*, 1522–1525
- 87. Van Krevelen, D. W.; Hoftyzer, P. J. Prediction of polymer densities. *J. Polym. Sci.* **1969**, *13*, 871–881
- 88. Ahmad, H.; Yaseen, M. Application of a chemical group contribution technique for calculating solubility parameters of polymers. *Polym. Eng. Sci.* **1979**, *19*, 858–863

# **CHAPTER 2: Tunable Polymer Microgel Particles and their Study using**

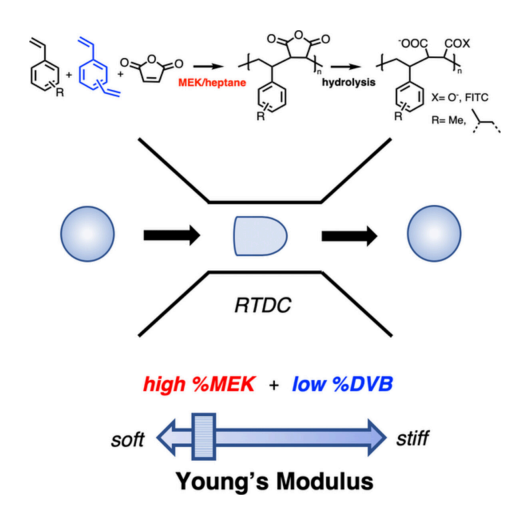
# Microscopy and Real-Time Deformability Cytometry

Sheilan Sinjari<sup>1</sup>, Jessica S. Freitag<sup>2</sup>, Christoph Herold<sup>3</sup>, Oliver Otto<sup>3,4</sup>, David M. Smith<sup>2,5,6</sup>,

Harald D.H. Stöver<sup>1</sup>\*

Contributions: This research was designed by SS and HDHS. Experiments were planned by SS. Microgel syntheses and characterizations were carried out by SS. RT-DC experiments were carried out by JSF and CH and OO, with RT-DC analyses performed by SS using software designed by OO and CH. HDHS provided guidance and editing feedback for the writing of this chapter. This chapter has been reproduced with permission from Sinjari, S.; Freitag, J.S.; Herold, C.; Otto, O.; Smith, D.M.; Stöver, H.D.H. *J. Polym. Sci.* **2020**, *58*, 2317-2326. Copyright © 2020, John Wiley and Sons

#### **Graphical Abstract:**



<sup>&</sup>lt;sup>1</sup>McMaster University, Hamilton, ON L8S 4M1, Canada

<sup>&</sup>lt;sup>2</sup>Fraunhofer Institut für Zelltherapie und Immunologie, Perlickstraße 1, 04103 Leipzig, Germany

<sup>&</sup>lt;sup>3</sup> ZellMechanik Dresden, Tatzberg 47/49, 01307 Dresden, Germany

<sup>&</sup>lt;sup>4</sup> University of Greifswald, Fleischmannstraße 42, 17489 Greifswald, Germany

<sup>&</sup>lt;sup>5</sup>University of Leipzig, Linnéstraße 5, 04103 Leipzig, Germany

<sup>&</sup>lt;sup>6</sup> University of Leipzig Medical Faculty, Johannesallee 30, 04103 Leipzig, Germany

### 2.1 ABSTRACT

We report the preparation and mechanical properties of highly swellable, spherical polymer microgels synthesized by precipitation copolymerization of divinylbenzene-55 (DVB), 4-methylstyrene (4MS) and maleic anhydride (MA) at different cross-linker contents, in a range of methyl ethyl ketone (MEK) and heptane solvent mixtures. Microgels were characterized by optical and confocal microscopy, and their mechanical properties tested using real-time deformability cytometry (RT-DC), a technique developed to analyze cell properties by measuring deformation under shear stress. Hydrolysis of anhydride groups gave microgels with diameters ranging from 10 to 22 µm when swollen in saline, depending on vol\% MEK and cross-linker loading. Young's moduli of the microgels could be tuned from 0.8 kPa to 10 kPa by adjusting cross-linker content and MEK/heptane solvent composition, showing an inverse relationship between the effects of vol% MEK and %DVB on microgel properties. These microgels also show strain-stiffening in response to increasing shear stresses. Extension of the RT-DC method to the study of polymer colloids thus enables high-throughput analysis of microgels with tunable mechanical characteristics.

### 2.2 INTRODUCTION

Microgels that respond to external stimuli, such as pH or temperature, constitute a class of "smart materials" that are relevant to both industry and medicine. Such responsive microgels are available through different heterogeneous polymerization methods like emulsion and suspension polymerization.<sup>1–4</sup> These methods can produce

particles in the sub-micron to >500µm range and typically rely on the addition of surfactants or stabilizers like polyvinylpyrrolidone (PVP) to prevent particle aggregation during polymerization.

The precipitation polymerization of cross-linking monomers in marginal solvents has become an established process for the synthesis of functionalized polymer microspheres with narrow size distribution and surfactant-free surfaces.<sup>5–12</sup> Both cross-linker loading and solvent selection play crucial roles in enabling colloidal stabilization and growth of such particles.<sup>5,6</sup> The cross-linker facilitates capture of oligomers to the particle surface and promotes their subsequent de-solvation to become part of the growing particle core, while reaction solvents are adjusted to swell surface-bound oligomers, which take the place of common steric stabilizers in preventing aggregation during particle growth.<sup>5</sup>

Previous work from our group established formation of monodisperse, cross-linked particles from a broad range of styrenic, acrylic, maleic anhydride and maleimide monomers.<sup>7–12</sup> The technique has since been applied in other groups to form particles with a range of compositions<sup>12–15</sup>, methods of polymerization including photo-initiation<sup>16</sup> and distillation-precipitation, <sup>17,18</sup> and for use in HPLC and solid-phase extractions. <sup>19–21</sup>

Recent work from our group has focused on the synthesis and properties of lightly cross-linked microgels based on 4-methylstyrene (4MS) and maleic anhydride copolymers.<sup>6,8,11</sup> Use of low amounts of cross-linker and hydrolysis of the anhydride groups provides a route to highly swellable microgels that are both pH and salt

responsive.<sup>23</sup> Such lightly cross-linked microgels can be deformable and can form jammed gels under close packing,<sup>24</sup> and thus are potential model systems for studying the role of cell jamming transitions in tissue organization and cancer metastasis.<sup>25,26</sup> Densely packed suspensions of pH and temperature responsive microgels have indeed been used as models to study phase transitions in soft matter systems,<sup>27–30</sup> and more recently have been applied to the 3D printing of soft materials with cells.<sup>31–34</sup> The mechanical properties of such microgels are therefore of significant interest both from a fundamental colloids perspective and for future applications in the field of biomaterials.

A common technique for determining Young's moduli of individual polymer particles and cells is nanoindentation by atomic force microscopy (AFM). This method is limited to measuring the elastic response at the particle surface, however, and has low throughput. Cross-linked microgels can have internal microstructure because of syneresis caused by preferential incorporation of cross-linker during copolymerization. Therefore, methods for rapid assessment of their overall elastic properties is of importance, as is determination of their internal micro- and nanostructure.

Real-time deformability cytometry (RT-DC) was recently developed as a tool to measure the mechanical properties of mammalian cells through analysis of deformation under laminar capillary flow.<sup>39,40</sup> The high-throughput nature of this technique, as well as its ability to precisely determine Young's moduli of cells and cell-sized particles<sup>40</sup> lends itself very well to the mechanical study of soft microgel systems.

In this work, we apply RT-DC to explore the mechanical properties of lightly cross-linked microgels prepared by precipitation polymerization of 4MS and maleic anhydride in a range of MEK and heptane cosolvent mixtures. We measure deformation and Young's moduli of these swellable microgels to investigate the complementary effects of solvent composition and cross-linker loading on microgel physical properties. In doing so, we demonstrate the ability to tune precipitation polymerization to produce microgels with Young's moduli close to those of mammalian cells, and simultaneously highlight the utility of RT-DC for high-throughput characterization of soft colloids. In addition, we use fluorescence and electron microscopy to assess micro- and nanostructure within the swollen microgels.

#### 2.3 EXPERIMENTAL

### 2.3.1 Materials

2,2'-Azobis(2-methylpropionitrile) (AIBN, 99.9%) was purchased from Dupont. Methyl ethyl ketone (MEK) was purchased from Caledon. Fluorescein cadaverine (≥95.0%) was purchased from Biotium. Divinylbenzene (DVB, ≥55% meta- and para-divinylbenzene), 4-methylstyrene (4MS, >95.5%), maleic anhydride (>98.5%), tetrahydrofuran (THF, ≥99.0%), heptane (>98.5%), dimethylformamide were purchased from Sigma-Aldrich. Methylcellulose Cell Carrier Buffer was obtained from ZellMechanik Dresden GmbH. Phosphate buffered saline (PBS, Ca/Mg free) was purchased from ThermoFischer Scientific. All materials were used as received unless otherwise stated.

### 2.3.2. Precipitation Copolymerization of 4MS, Maleic Anhydride and DVB

Microgels were prepared using a method adapted from previous work.<sup>23</sup> To synthesize particles in 70:30 (v/v) MEK:heptane with 5 mol% effective m- and p-DVB relative to total styrenic monomers (notation 70/5), a stock solution of 0.16 g AIBN in 10 g MEK was prepared and stored at -18°C. Maleic anhydride (0.363 g, 3.8 mmol), 4MS (443 μL, 3.4 mmol), DVB (46 µL, 0.35 mmol) and 1 g of AIBN stock solution (0.016 g, 0.10 mmol AIBN), were weighed into a 20 mL screw-cap vial and dissolved in 10.3 g of MEK and 4.10 g of heptane. The combined weight of 10.3 g MEK plus 1 g MEK in the stock solution, or 11.3 g of total MEK, corresponds to 70 vol% MEK in the MEK/heptane cosolvent mixture not counting monomers and initiator, using a density of 0.805 g/mL for MEK and of 0.684 g/mL for the heptane. The vial was rolled at 70 °C and 4 rpm for 24h using a modified commercial hotdog roller. After 24h, the vial was removed from the reactor, briefly opened to admit air and stop the polymerization, and cooled to room temperature. The contents of the vial were transferred to a 50 mL polypropylene centrifuge tube and the vial rinsed three times with THF (8 mL x3), with vial walls being scraped down during each rinse using a microspatula to remove adherent particles. Microgels were sedimented by centrifugation at 3400g for 10 minutes. The supernatant was decanted and the particles resuspended in 40 mL of THF and centrifuged again, for a total of five times. Subsequently, the microspheres were resuspended in 40 mL of THF. A 1 mL aliquot was pipetted into a 4 mL screw-cap vial and dried under nitrogen for 48h to estimate the particle yield. Typical particle yields were in the range of 13 to 73%, depending on % DVB and MEK. The remaining suspension was stored in the dark at -18 °C.

### 2.3.3. Fluorescent Labelling and Hydrolysis of Microgels

As-formed microgels were reacted with 1 mol% fluorescein cadaverine relative to anhydride groups. A typical labelling experiment was performed as follows: 1 mL of a solution of fluorescein cadaverine (2.4 mg, 0.003 mmol) in DMF was added to 5 mL (0.34 mmol anhydride) of THF-suspended 70/5 anhydride-form microgels. The mixture was rotated at room temperature and 20 rpm for 2h. NaOH solution (680 μL of 1.0 N aq. NaOH, 0.68 mmol) was then added to the microsphere suspension and the mixture rotated for 1h. The suspension was transferred to a 50mL polypropylene centrifuge tube, diluted with 20 mL distilled water and rotated at 4 rpm for an additional hour before being centrifuged and resuspended five times in 35 mL of distilled water. Following purification, particles were resuspended in 35 mL of distilled water and stored in the dark at room temperature.

#### 2.3.4 Characterization

### 2.3.4.1. Optical and Confocal Microscopy

Microsphere diameters were assessed with a Nikon Eclipse LV100ND upright optical microscope equipped with NIS-Elements Microscope imaging software. Confocal images of the equatorial sections of microgels were obtained using a Nikon A1 Confocal Eclipse Ti microscope.

# 2.3.4.2. Transmission Electron Microscopy

Internal microgel structures were obtained using a JEOL 1200EX TEMSCAN transmission electron microscope (TEM). TEM samples were prepared by embedding THF-swollen microgels in Spurr epoxy resin and curing at 70 °C overnight. The resin samples were ultra-microtomed to approximately 100 nm thickness and mounted on 3 mm copper TEM grids.

# 2.3.4.3. Mechanical Properties obtained using RT-DC

The method of RT-DC as previously reported by Otto et al.<sup>41</sup> was performed on a Zellmechanik Dresden AcCellerator. Silicon chips with channels having cross-sections of  $15 \times 15 \, \mu m \times \mu m$ ,  $20 \times 20 \, \mu m \times \mu m$  or  $30 \times 30 \, \mu m \times \mu m$  in the measurement region were used with flow rates between 0.08 and 0.32  $\mu L/s$ . For the current experiments, a suspension of microgels in distilled water was centrifuged and resuspended in PBS containing 0.5% methylcellulose, for a microgel concentration of 0.1% wt/vol. The methylcellulose was included for two reasons: it prevents microgel agglomeration and leads to a known increased viscosity resulting in higher forces for particle deformation. An aliquot of about 1 mL of each microgel suspension was placed in a small sample tube and aspirated for the measurements. Microgels were imaged at equilibrium deformation under different flow rates using a high-speed camera (2000 fps) focused on the end of a 300  $\mu$ m long microfluidic channel. Images of the microgels were also collected in the upstream reservoir in absence of deformation. For each sample, images and deformation

as well as size data of 500-8000 microgels were collected at every flow rate, within a few minutes. Deformation is measured from the microgel circularity:

Deformation = 1 - circularity = 1 - 
$$\frac{2\sqrt{\pi A}}{P}$$
,

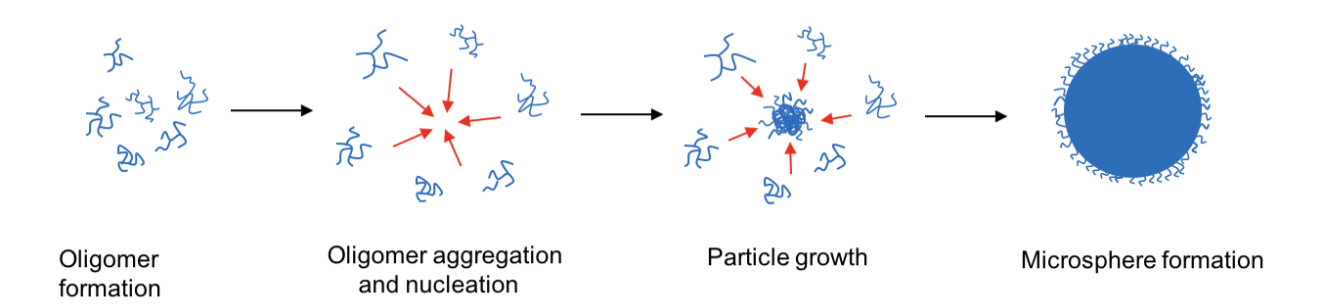
where A is the cross-section area of the particle and P its perimeter.

A conversion of the deformation data to the respective Young's modulus was performed in the analysis software Shape-Out (available at https://github.com/ZELLMECHANIK-DRESDEN/ShapeOut) using look-up tables created by numerical simulation. 42

### 2.4. RESULTS AND DISCUSSION

### 2.4.1. Effects of Solvency and Cross-linker Loading on Particle Size

The narrow size distribution and regular morphology of polymer microspheres synthesized by precipitation polymerization can be attributed to a short particle nucleation period followed by continuous growth under conditions of steric self-stabilization, as illustrated in Scheme 2.1.<sup>5,6</sup> Initially formed oligomers entropically de-solvate through inter- and intramolecular cross-linking reactions and aggregate to form particle nuclei. These nuclei subsequently grow by capturing monomers and newly formed oligomers from solution, which serves to maintain a sterically stabilizing surface layer during the growth period.



**Scheme 2.1.** Mechanism of particle nucleation and growth. Aggregation and de-solvation of oligomers leads to particle nuclei that grow by capturing monomers and oligomers from solution.

This paper focuses on the properties of lightly cross-linked microgels formed by precipitation polymerization of maleic anhydride with 4MS and DVB at 2 wt% total comonomer loading. The effective amount of *m*- and *p*-DVB is varied between 3 and 6 mol% relative to total vinyl groups, and the MEK content in the MEK/heptane cosolvent mixture is varied between 70 and 73 vol%. Equimolar amounts of maleic and total styrenic vinyl groups are used in all samples in order to obtain alternating copolymerizations and minimize compositional drifts towards the end of the polymerization. The microgels are then functionalized with a fluorescent label, residual anhydride groups are hydrolyzed and the microgels suspended in PBS for characterization and analysis.

Figure 2.1 shows representative fluorescent microscope images of three types of maleic anhydride/4MS/DVB particles labelled with fluorescein cadaverine that illustrate the effects of cross-linker level and MEK/heptane solvent composition on hydrolyzed microgels suspended in PBS.

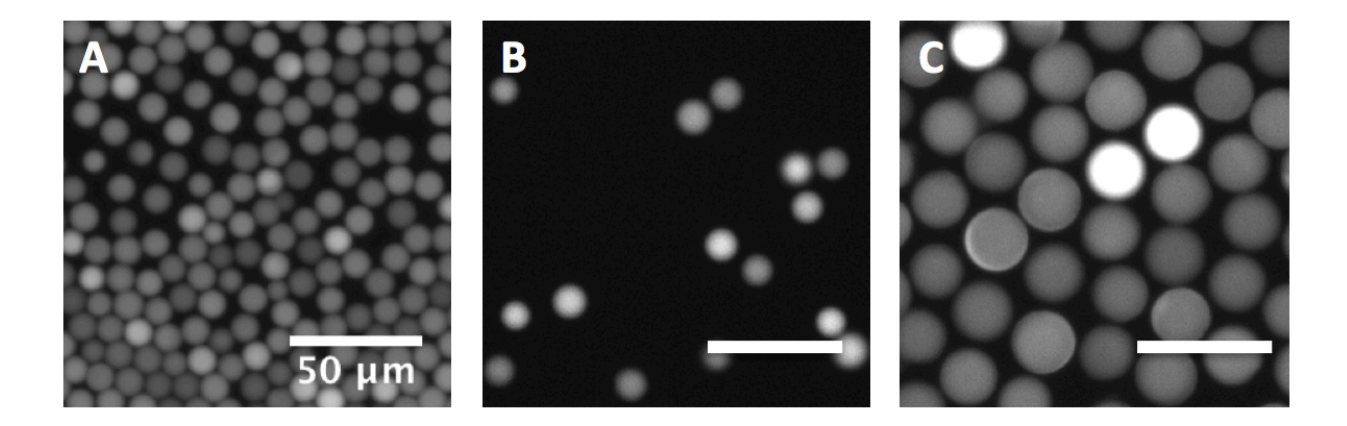


**Figure 2.1.** Fluorescence optical microscope images of representative microgels labelled with fluorescein cadaverine ( $\lambda_{ex}$ =480 nm) formed at A) 70/5, B) 72/5 and C) 72/3, suspended in PBS. Here, the notation '70/5' represents particles synthesized in 70:30 (v/v) MEK/heptane cosolvent mixtures, with 5 mol% effective *m*- and *p*-DVB relative to total styrenic monomers.

As observed previously,<sup>6</sup> final diameters increase with increasing vol% MEK and in particular with decreasing %DVB. Table A2.1 compares the yields and diameters for all 13 types of microgels formed using 3-6 mol% DVB and 70-73 vol% MEK, hydrolyzed and suspended in PBS. We adopt the notation "X/Y" to describe particle types; 'X' denotes the vol% MEK used in the MEK/heptane cosolvent mixture for particle synthesis, and 'Y' denotes the effective mol% of m- and p-DVB relative to total styrenic monomers. Particle sizes ranged from 9 (73/6) to 22  $\mu$ m (73/3). Higher %DVB and lower %MEK, such as at 70/5 particles that have an average diameter of 10  $\mu$ m, promote desolvation of the polymer chains and leads to formation of smaller microgels.

Conversely, the largest diameters are observed at 72/3 (20  $\mu$ m, Table A2.1) and 73/3 (22  $\mu$ m, Table A2.1), where low cross-linker loading and improved solvation of the polymer network co-operate to form larger microgels. Isolated particle yields are lower under these conditions as microgel growth becomes less efficient at higher solvency and lower cross-linker loading.

As such, microgels grow by continuous capture of oligomers and monomers, the decrease in comonomer, cross-linker and initiator levels during the copolymerization may lead to radial gradients in composition and cross-link levels.<sup>43</sup> The use of equimolar anhydride and styrenic double bonds, the strong tendency towards alternating copolymerization, and conversions limited to about 50% for most compositions, suggests these gradients should be minor. We decided to use transmission electron microscopy (TEM) to explore the internal structure of microgels made under low (70 vol% MEK) and high (73 vol%MEK) solvency, as even small changes in compositions can affect particle properties and deformation

Microgels were swollen in THF, embedded in Spurr's resin and characterized using TEM (Figure 2.2). Some graininess is visible in 70/5 (Fig. 2.2a) and especially in and between 73/5 (Fig. 2.2b) microgels. This graininess is more pronounced at the particle surfaces of the 73/5 particles, and has dimensions on the order of 200 nm.

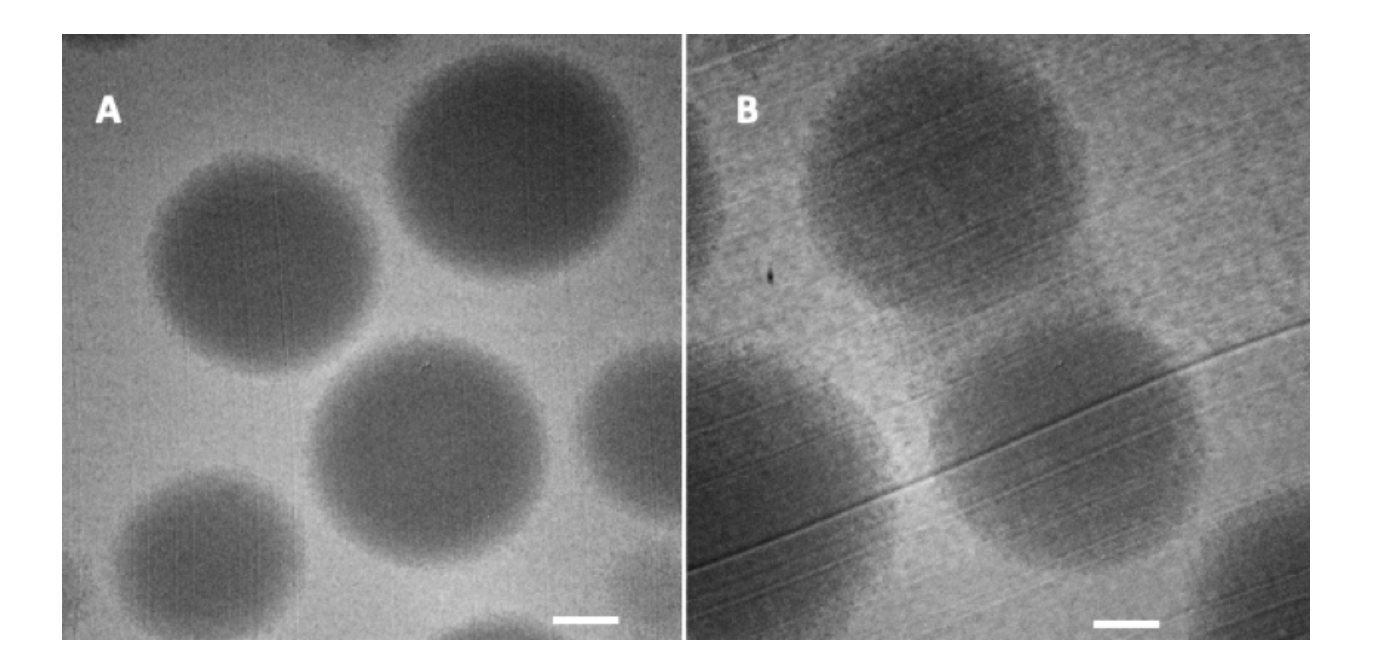


**Figure 2.2.** TEM images of a) 70/5 and b) 73/5 microgels swollen in THF and embedded in Spurr's epoxy resin. Scale bar is 2  $\mu$ m. Contrast has been increased by 20% for all TEM images. The near vertical lines in B are knife artifacts introduced during microtoming.

Microgel size distribution is narrow in most samples, indicating a narrow window of particle nucleation early in these precipitation polymerizations. Fluorescence labelling of final microgels with fluorescein cadaverine is largely consistent between microgels, though with a few microgels appearing much brighter (*e.g.*, Fig. 2.1c and 2.3a) despite rapid introduction of the fluorescent label to the microgel suspension to minimize mixing inconsistencies. The cause of this variation in labelling level is not understood at this point. Confocal fluorescence microscopy was used to obtain radial distributions of fluorescence intensity across equatorial sections, and these images (Fig. A2.1) show the expected even fluorescence intensity distribution across most particle interiors, indicating

no obvious barrier to in-diffusion of the fluorescent labelling agent. Some of these confocal images also show significantly higher internal fluorescence labelling.

The hydrolyzed microgels are colloidally stable in PBS and are highly deformable, evident from the reversible packing of PBS-swollen 72/3 (Fig 2.3). 72/3 microgels have an average diameter of 20 µm and pack into hexagonal arrays with flat interfaces (honeycombs) upon manual vertical compression between glass slides. Figure 2.3 shows the results of microgels before, during, and after vertical compression. The smaller diameter of the microgels in Figure 2.3c is attributed to partial lateral contraction upon vertical recovery.

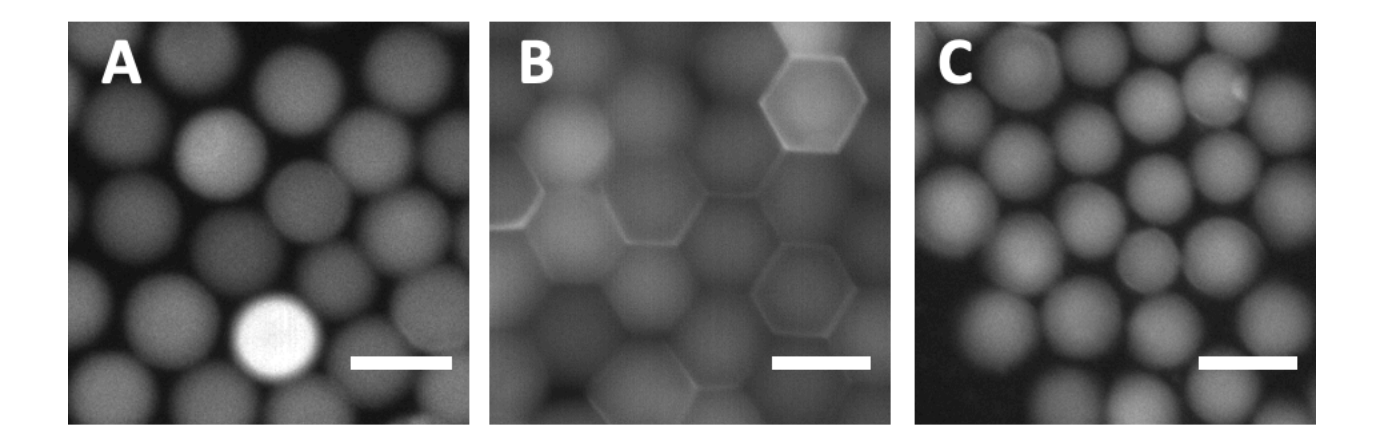
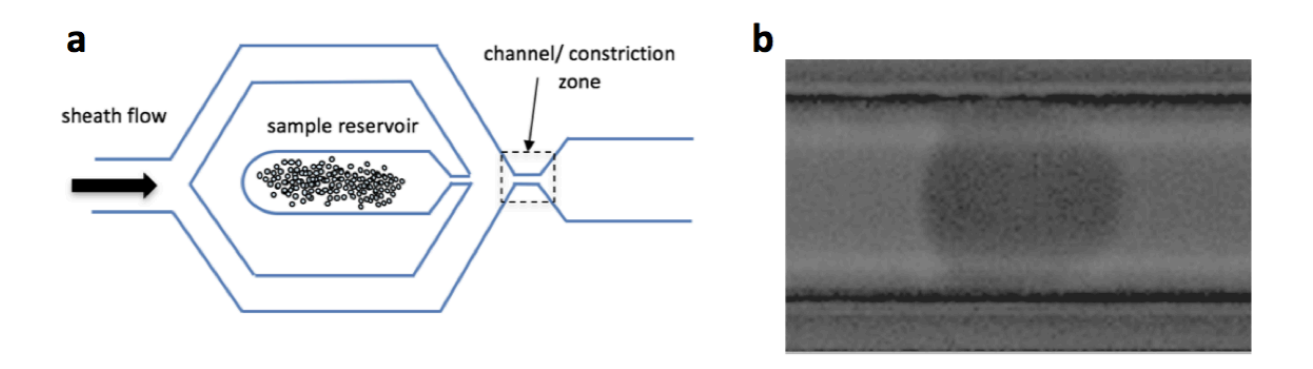


**Figure 2.3.** Deformation of microgels labelled with fluorescein cadaverine upon manual compression between two glass slides: fluorescence microscope images of 72/3 microgels swollen in PBS: A) before compression, B) compressed between two glass slides, and C) post-compression (after removal of top glass slide). Scale bar =  $25 \mu m$ .

Microgels are currently being explored as modular components in cell scaffolds.<sup>3,44</sup> Cell behaviour often depends on mechanical properties of the surrounding environment, as an example, substrate stiffness<sup>45-48</sup>, strain stiffening<sup>49</sup> and stress relaxation<sup>50</sup> have been shown to dictate how cells will differentiate. Considering the deformability and swelling characteristics of the microgels presented here, we sought to test their mechanical properties using RT-DC, a microfluidic technique developed for rapid analysis of cellular mechanical properties.

# 2.4.2. Mechanical Properties of Microgels by RT-DC

In RT-DC, particles enter a microfluidic constriction zone with a cross section larger than the particle size and are deformed by the hydrodynamic forces due to the flow profile inside the constriction zone. Generally, these forces increase with increased flow rate, increased viscosity of the surrounding medium and increased particle size to channel cross-section ratio. Deformed particles, which can adopt a bullet-like shape (Scheme 2.2) that closely resembles cell shape under similar flow conditions, are imaged with a high-speed camera and their deformation is measured. Scheme 2.2 illustrates the instrumental set up.



Scheme 2.2. a) Schematic of an RT-DC microchannel layout. Particles flow from the sample reservoir – focused by a sheath flow – through the constriction and measurement zone where the image-based shape analysis is performed. All flow rates stated are the sum of sample and sheath flow. b) Image of 73/5 microgel captured at the end of the constriction zone. Flow-rate =  $0.08 \,\mu$ L/s.

We analyzed a series of microgels by RT-DC to study the impact of solvency and cross-linker loading during synthesis on mechanical properties of the final, hydrolyzed particles. Microgels were suspended in PBS containing 0.5% methylcellulose primarily to reduce microgel agglomeration on the PDMS chip. The microfluidic nature of the technique allows imaging 3000 – 6000 microgels within under one minute, with real-time evaluation of their deformation.

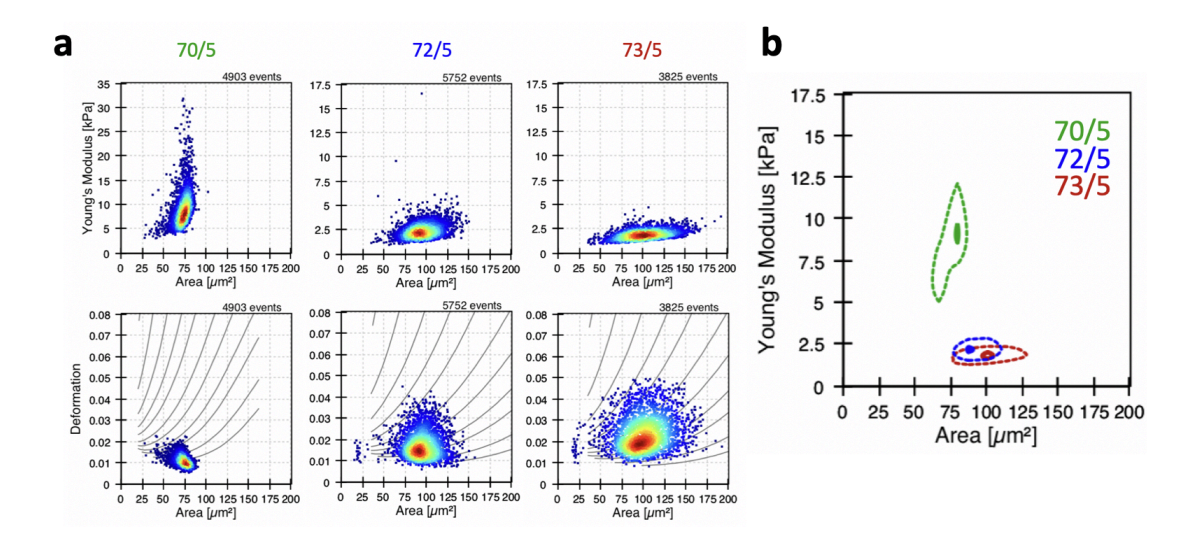


**Figure 2.4.** Effect of MEK content on properties of hydrolyzed microgels in PBS as assessed using RT-DC. a) Scatter plots of Young's Modulus (top row) and deformation (bottom row) versus microgel cross-sectional areas, and b) contour plot of Young's Modulus versus cross-sectional areas, for a series of microgels formed using 5 % effective DVB, formed in 70, 72 and 73 vol% MEK (0.08  $\mu$ L/s flow-rate; 15  $\mu$ m channel for 70/5; 20  $\mu$ m channel for 72/5 and 73/5).

Figure 2.4 shows plots of deformation and Young's modulus versus microgel cross-sectional area, at a flow-rate of 0.08 μL/s, for microgels formed at constant cross-linker loading of 5 mol% DVB but increasing vol% MEK. A minor increase in vol% MEK from 70 to 73 wt% resulted in a five-fold decrease in modulus, from 10 to 2 kPa, in contrast to only a small increase in average cross-sectional area of the microgels (Fig. 2.4a top: scatter plot, Fig. 2.4b: contour plot). The scatter plots of deformation versus cross sectional area (Fig. 2.4a, bottom), show the corresponding raw data.

The remarkable effects of these small increases in the vol% of good solvent (MEK) in the polymerization mixture is attributed primarily to a corresponding drop in cross-linking efficiency. This is supported by the decrease in particle yield when moving from the stiffest microgels (70/5) to the softest (73/3; Table A2.1), reflecting that 73 vol% MEK represents the upper limit of this solvent/monomer/cross-linker regime where particles can be isolated in reasonable amounts. Control experiments at MEK content greater than 74 vol% showed no microgel formation at 3% DVB (Fig. A2.2), or macrogelation at 5% effective DVB, reflecting the critical role of a marginal solvent environment driving internal de-solvation during particle initiation and growth.

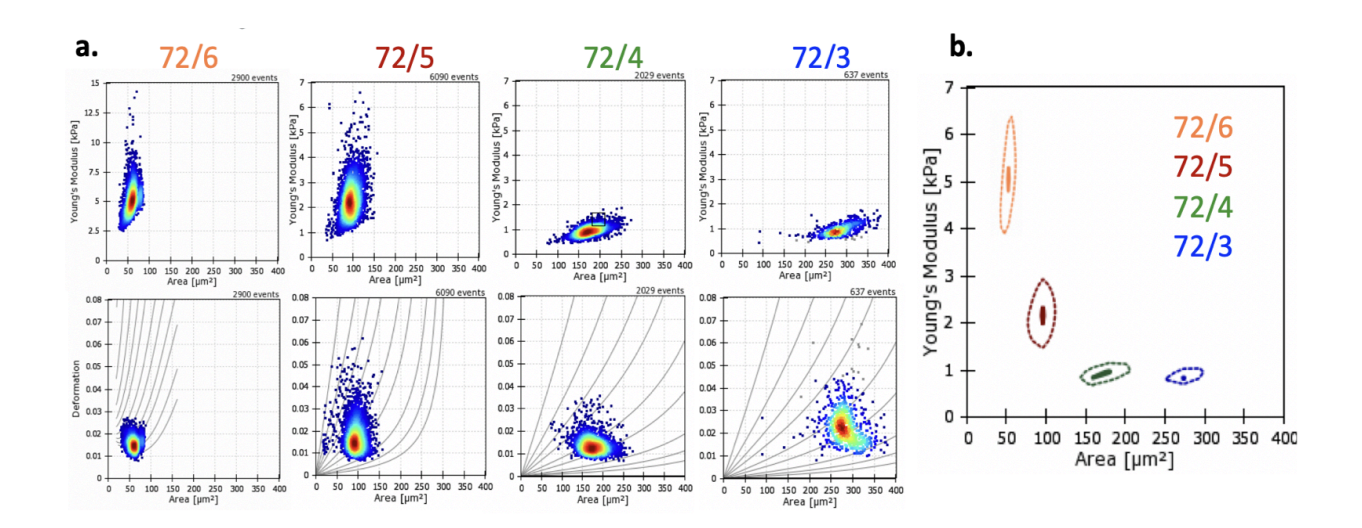


**Figure 2.5.** Effect of cross-linker levels on microgel properties assessed using RT-DC. a) Scatter plots of Young's Modulus (top row) and deformation (bottom row) versus microgel cross-sectional areas, and b) contour plot of Young's Modulus versus cross-sectional areas, for a series of microgels formed using 3 to 6 mol% DVB, in presence of 72 vol% MEK (0.08μL/s flow rate; 30μm channel for 72/3; 15μm channel for 72/4, 72/5 and 72/6).

Similarly, varying the amount of cross-linker within the microgels led to a significant range of control over their mechanical properties. Figure 2.5 shows moduli increasing five-fold from 1kPa (72/3) to 4kPa (72/6) when increasing the cross-linker content from 3 to 6 mol%, at a constant level of 72 vol% MEK. It is remarkable that a 3% decrease in MEK content (from 73 to 70 vol%) affects the modulus as much as a 300% increase in DVB (from 3 to 6 mol%).

Figure A2.2 shows a more complete matrix of Young's moduli as function of DVB (3 - 6 mol%) and MEK (70, 72, 73 vol%), supporting the above interpretation. The

stiffest gels are 10kPa (70/5), observed at high effective mol% of DVB (5 mol%), and moduli decrease with improving solvency. Increased cross-linker is required to compensate for the loss in cross-linker efficiency associated with enhanced solvation of the polymer network at higher vol% MEK, which is supported by the lack of isolated particles at >74 vol% MEK.<sup>23</sup>

Microgels formed at low mol% DVB (3 – 4 mol%) and high vol% MEK (72 – 73 mol%) display the most interesting mechanical and morphological profiles among the particles analyzed. These microgels are highly swellable, having narrow dispersities and sizes ranging from 15  $\mu$ m (72/4 and 73/4, Table 2A.1) to 22  $\mu$ m (72/3 and 73/3, Table 2A.1), with Young's moduli of ~1kPa. This interdependence of crosslinking and solvent composition may permit independent tuning of microgel mechanical properties and size. The Young's moduli of these microgels also closely resemble the moduli of mammalian cells as measured by RT-DC, making them potentially attractive candidates for cell/microgel composites. <sup>51–53</sup>

Many biological materials become stiffer under stress. Actin, <sup>54</sup> collagen, <sup>55</sup> vimentin and keratin <sup>56</sup> are examples of biopolymer networks that undergo strain-stiffening in response to deformation. Interestingly, we observed similar non-linear elastic behaviour in the microgels when they were exposed to different shear stresses (Fig. 2A.3). Figure 6 shows representative data for 72/4 microgels, where Young's modulus doubles from 1 kPa to 2 kPa when flow rate is increased from 0.08  $\mu$ L/s (low shear) to 0.32  $\mu$ L/s (high shear). This behaviour can be attributed to slow de-solvation of the microgel interior

networks under increasing shear forces. Analogous data for other microgels are shown in Figure A2.3.

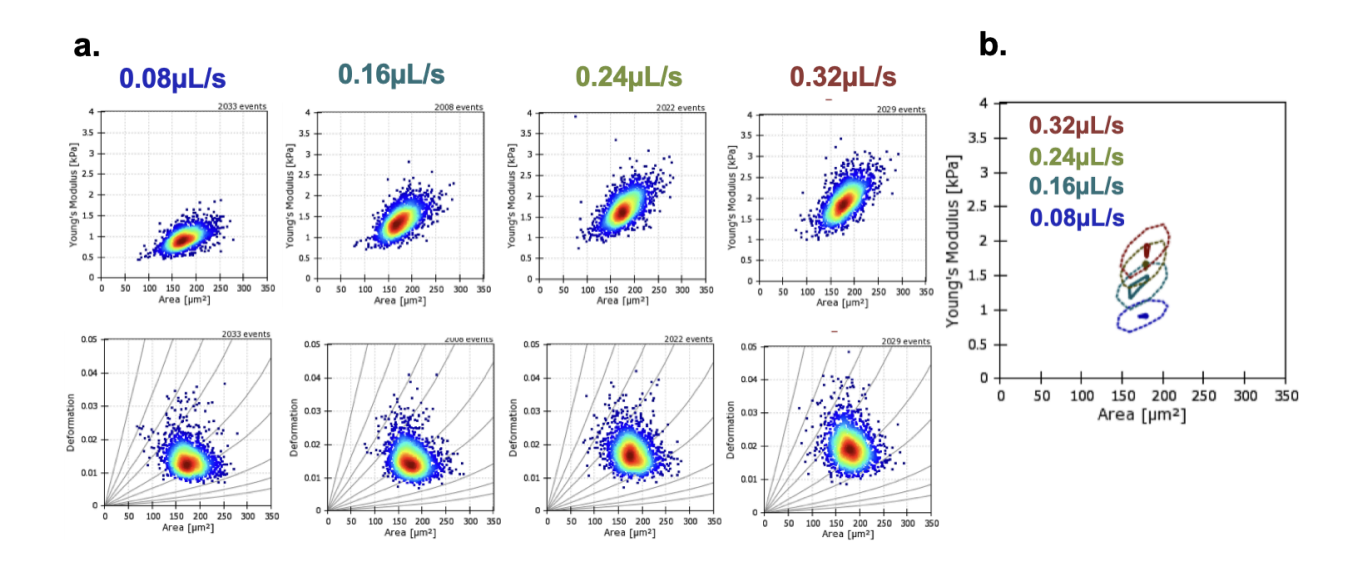


**Figure 2.6**. a) Young's modulus (top) and Deformation (bottom) scatter plots for 72/4 microgels as function of flow rate, and b) contour plot of Young's modulus of 72/4 microgels, showing shear-stiffening with increasing flow rate.

These RT-DC measurements confirm the qualitative observations described in Figures 2.2 and 2.3. Specifically, they demonstrate that two easily accessible experimental parameters, mol% cross-linker and vol% MEK, can be used to deterministically change the microgel deformability and Young's modulus and that these changes can be rapidly assessed using the RT-DC technique. This method will in future be extended to analyze the properties of microgels with different internal morphologies, including more pronounced radial cross-link gradients and core-shell structures, which are of current interest to both the field of fundamental colloids and applied biomedicine.

## 2.5. CONCLUSIONS

A series of microgel particles were prepared by free radical precipitation copolymerization of 4-methylstyrene, divinylbenzene (DVB) and maleic anhydride comonomers, and their properties were assessed using optical and confocal microscopy, and RT-DC. Microgel diameters ranged from 10 to 22 μm, increasing with increasing vol% MEK and decreasing mol% DVB. Young's moduli as measured by RT-DC showed a non-linear dependence on mol% DVB and an inverse dependence on vol% MEK. The observed Young's moduli for hydrolyzed microgels can be easily tuned to fall within the range for mammalian cells, and strain-stiffening roughly resembles similar behaviours in cells and cell biopolymer networks. These cell-like properties not only make these particles interesting candidates for future use in cell/microgel composites, but also constitute basic building blocks for studies into densely packed states of cell organization in tissues.

## 2.6. REFERENCES

- 1. D. Dupuin, S. Fujii, S.P. Armes, P. Reeve, S.M. Baxter, Langmuir 2006, 22, 3381
- 2. H. Senff, W. Richtering, Colloid Polym. Sci. 2000, 278, 830.
- 3. A.S. Caldwell, G.T. Campbell, K.M.T. Shekiro, K.S. Anseth, *Adv. Healthcare Mater.* **2017**, *6*, 1700254.
- 4. J.G. Werner, S. Nawar, A.A. Solovev, D.A. Weitz, *Macromolecules* **2018**, *51*, 5798.
- J.S. Downey, R.S. Frank, W.H. Li, H.D.H Stöver, Macromolecules 1999, 32, 2838.
- 6. R.S. Frank, J.S. Downey, K. Yu, H.D.H. Stöver, Macromolecules 2002, 35, 2728.
- 7. K. Li, H.D.H. Stöver, J. Polym. Sci. A Polym. Chem. 1993, 31, 2473.
- 8. K. Li, H.D.H. Stöver, J. Polym. Sci. A Polym. Chem. 1993, 31, 3257.
- 9. J.S. Downey, R.S. Frank, W.H. Li, H.D.H. Stöver, *Macromolecules* **1999**, *32*, 2838.
- J.S. Downey, G. McIsaac, R.S. Frank, H.D.H. Stöver, *Macromolecules* 2001, 34, 4534.
- 11. E.C.C. Goh, H.D.H. Stöver, *Macromolecules* **2002**, *35*, 9983.
- Y. Zhao, N.A.D. Burke, H.D.H. Stöver, J. Polym. Sci. A Polym. Chem. 2015, 54, 1159.
- 13. G. Li, X. Yang, F. Bai, Polymer. 2007, 48, 3074.
- B. Liu, E. Yan, X. Zhang, X. Yang, F. Bai, J. Colloid Interface Sci. 2012, 369, 144.

- 15. C.D. Jones, A.L. Lyon, *Macromolecules* **2000**, *33*, 8301.
- 16. F. Limé, K. Irgum, Macromolecules 2007, 40, 1962.
- 17. F. Bai, X. Yang, W. Huang, *Macromolecules* **2004**, *37*, 9746.
- 18. F. Bai, B. Huang, X, Yang, W. Huang, *Polymer* **2007**, *48*, 3641.
- 19. E. Turiel, J.L. Tadeo, P.A.G. Cormack, A. Martin-Esteban, *Analyst* **2005**, *130*, 1601.
- 20. J. Wang, P.A.G. Cormack, D.C. Sherrington, E. Khoshdel, *Angew. Chem. Int. Ed.* **2003**, *42*, 5336.
- 21. X. Wang, P. Huang, X. Ma, X. Du, X. Lu. J. Chromatogr. A. 2018, 1537, 35.
- 22. F. Barahona, E. Turiel, P.A.G. Cormack, A. Martín-Esteban, *J. Polym. Sci. A Polym. Chem.* **2010**, *48*, 1058–1066
- 23. S. Sinjari, J. Li, Y. Zhao, M. Skreta, H. Chen, H.D.H. Stöver. *Unpublished Work*
- 24. A. Liu, S. Nagel, *Nature* **1998**, *396* (6706), 21–22
- 25. D. Bi, J.H. Lopez, J.M. Schwarz, L.M. Manning, Nat. Phys. 2015, 11, 1074.
- L. Oswald, S. Grosser, D.M. Smith, J. Käs, J. Phys. D: Appl. Phys. 2017, 50, 483001
- 27. H. Senff, W. Richtering, J. Chem. Phys. **1999**, 111, 1705
- 28. J. Mattsson, H. Wyss, A. Fernandez-Nieves, K. Miyazaki, Z. Hu, D.R. Reichman, D.A. Weitz, *Nature* **2009**, *462*, 83.
- 29. K.N. Nordstrom, E. Verneuil, P.E. Arratia, A. Basu, Z. Zhang, A.G. Yodh, J.P. Gollub, D.J. Durian, *Phys. Rev. Lett.* **2010**, *105*, 175701.
- 30. C. Pellet, M. Cloitre, Soft Matter 2016, 12, 3710.

- 31. T. Bhattacharjee, S.M. Zehnder, K.G. Rowe, S. Jain, R.M. Nixon, W.G. Sawyer, T.E. Angelini, *Sci. Adv.* **2015**, *1*, e1500655.
- Bhattacharjee, C.J. Gil, S.L. Marshall, J.M. Urueña, C.S. O'Bryan, M. Carstens,
   B. Keselowsky, G.D. Palmer, S. Ghivizzani, C.P. Gibbs, W.G. Sawyer, T.E.
   Angelini, ACS Biomater. Sci. Eng., 2016, 2, 1787
- C.S. O'Bryan, C.P. Kabb, B.S. Sumerlin, T.E. Angelini, ACS Appl. Bio Mater.
   2019, 2, 1509
- 34. C.B. Highley, K.H. Song, A.C. Daly, J.A. Burdick, *Adv. Sci.* 2019, *6*, 1801076
- 35. R.E. Mahaffy, S. Park, E. Gerde, J. Käs, C.K. Shih, *Biophys. J.* 2004, 86, 1777.
- 36. S.M. Hashmi, E. Dufresne, *Soft Matter* 2009, *5*, 3682
- 37. J. Wiedemair, M.J. Serpe, J. Kim, J.F. Masson, L.A. Lyon, B. Mizaikoff, C. Kranz. *Langmuir*, **2007**, *23*, 130.
- 38. P. Wu, D.R. Aroush, A. Asnacios, W.C. Chen, M.E. Dokukin, B.L. Doss, P. Durand-Smet, A. Ekpenyong, J. Guck, N.V. Guz, P.A. Janmey, J.S.H. Lee, N.M. Moore, A. Ott, Y.C. Poh, R. Ros, M. Sander, I. Sokolov, J.R. Staunton, N. Wang, G. Whyte, D. Wirtz. *Nat. Methods* 2018, *15*, 491.
- 39. O. Otto, P. Rosendahl, A. Mietke, S. Golfier, C. Herold, D. Klaue, S. Girardo, S. Pagliara, A. Ekpenyong, A. Jacobi, M. Wobus, N. Töpfner, U.F. Keyser, J. Mansfeld, E. Fischer-Friedrich, J. Guck, *Nat. Methods.* 2015, *12*, 199
- 40. A. Mietke, O. Otto, S. Girardo, P. Rosendahl, A. Taubenberger, S. Golfier, E. Ulbricht, S. Aland, J. Guck, E. Fischer-Friedrich, *Biophys. J.* **2015**, *109*, 2023.

- 41. M. Mokbel, D. Mokbel, A. Mietke, N. Träber, S. Girardo, O. Otto, J. Guck, S. Aland, *ACS Biomater. Sci. Eng.* **2017**, *3*, 2962.
- 42. M. Antonietti, W. Bremser, M. Schmidt, *Macromolecules* 1990, 23, 3796.
- 43. T. Gan, Y. Guan, Y. Zhang, J. Mater. Chem. 2010, 20, 5937.
- 44. J.S. Park, J.S. Chu, A.D. Tsou, R. Diop, Z. Tang, A. Wang, S. Li, *Biomaterials* **2011**, *32*, 3921.
- 45. C. Yang, M.W. Tibbitt, L. Basta, K.S. Anseth, Nature Mater 2014, 13, 645.
- A.M. Rosales, S.L. Vega, F.W. DelRio, J.A. Burdick, K.S. Anseth, *Angew. Chem. Int. Ed.* 2017, 56, 12132.
- 47. A.J. Engler, S. Sen, H.L. Sweeney, D.E. Discher, Cell, 2006, 677.
- 48. R. Das, V. Gocheva, R. Hammink, O.F. Zouani, A.E. Rowan, *Nat. Mater.* **2016**, *15*, 318.
- 49. O. Chaudhuri, L. Gu, D. Klumpers, M. Darnell, S.A. Bencherif, J.C. Weaver, N. Huebsch, H. Lee, E. Lippens, G.N. Duda, D.J. Mooney, *Nat. Mater.* **2016**, *15*, 326.
- 50. B. Fregin, F. Czerwinski, D. Biedenweg, S. Girardo, S. Gross, K. Aurich, O. Otto, *Nat. Commun.* **2019**, *10*, 415.
- M. Urbanska, M. Winzi, K. Neumann, S. Abuhattum, P. Rosendahl, P. Müller, A. Taubenberger, K. Anastassiadis, J. Guck, *Development*, 2017, 144, 4313.
- 52. C.N. Holenstein, A. Horvath, B. Schär, A.D. Schoenenberger, M. Bollhalder, N. Goedecke, G. Bartalena, O. Otto, M. Herbig, J. Guck, D.A. Müller, J.G. Snedeker, U. Silvan, *Mol. Biol. Cell.* 2019, 30, 887.

- 53. Xu, J., Tseng, Y., Wirtz, D. J. Biol. Chem. 2000, 275, 35886.
- 54. S. Motte, L.J. Kaufman, *Biopolymers* **2012**, *99*, 35.
- 55. T. Golde, M. Glase, C. Tutmarc, I. Elbalasy, C. Huster, G. Busteros, D.M. Smith,
  - H. Herrmann, J.A. Käs, J. Schnauß. Soft Matter, 2019, 15, 4865.

## 2.7. APPENDIX

%MEK	%DVB	Diameter in PBS (μm)	Yield (%)
70	3	16 ± 1	42
	4	17 ± 1	55
	5	10 ± 1	74
72	3	20 ± 2	57
	4	15 ± 1	37
	4.5	14 ± 2	32
	5	10 ± 1	21
	6	10 ± 1	38
73	3	22 ± 2	13
	4	15 ± 2	20
	4.5	14 ± 1	37
	5	12 ± 1	37
	6	9 ± 1	40

**Table A2.1.** Particle diameters for hydrolyzed microgels formed using 3-6% DVB and 70-73% MEK suspended in PBS. Diameters were obtained using optical microscopy (Nikon Eclipse LV100ND upright optical microscope equipped with NIS-Elements Microscope imaging software). Number of particles analyzed ranged from 100-3000 for each microgel type, which were synthesized and analyzed in triplicate.

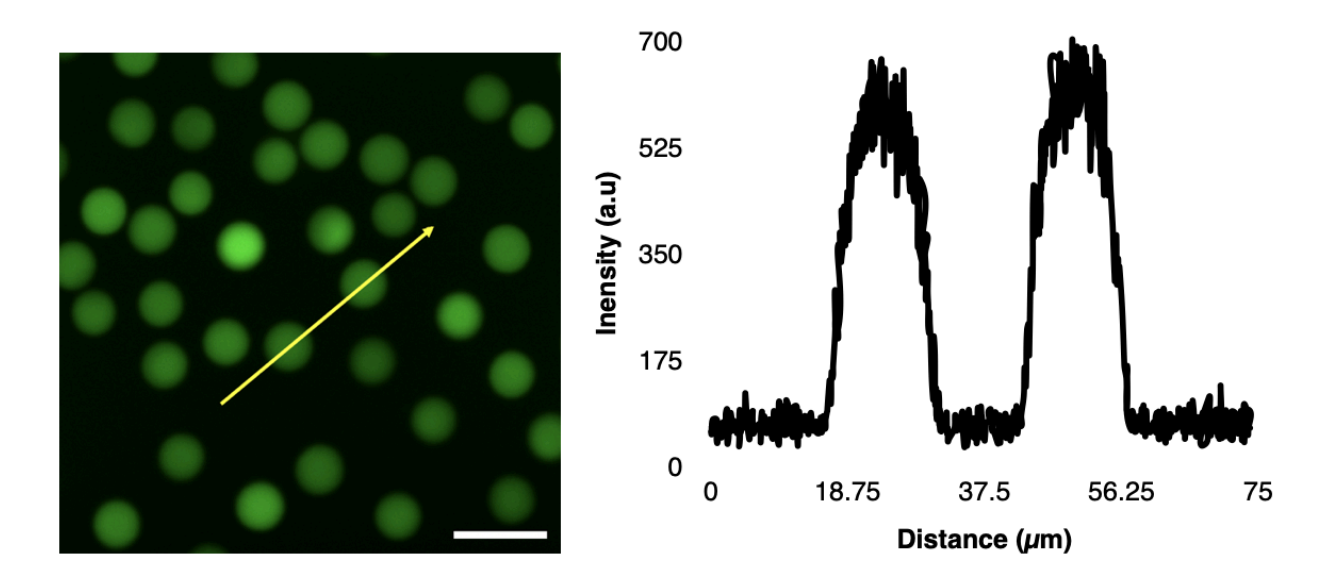


**Figure A2.1.** Microgel homogeneity as assessed by confocal microscopy (Nikon A1 Confocal Eclipse Ti microscope): equatorial sections of 70/5 microgels swollen in water and corresponding line profile. Scale bar is 25μm.

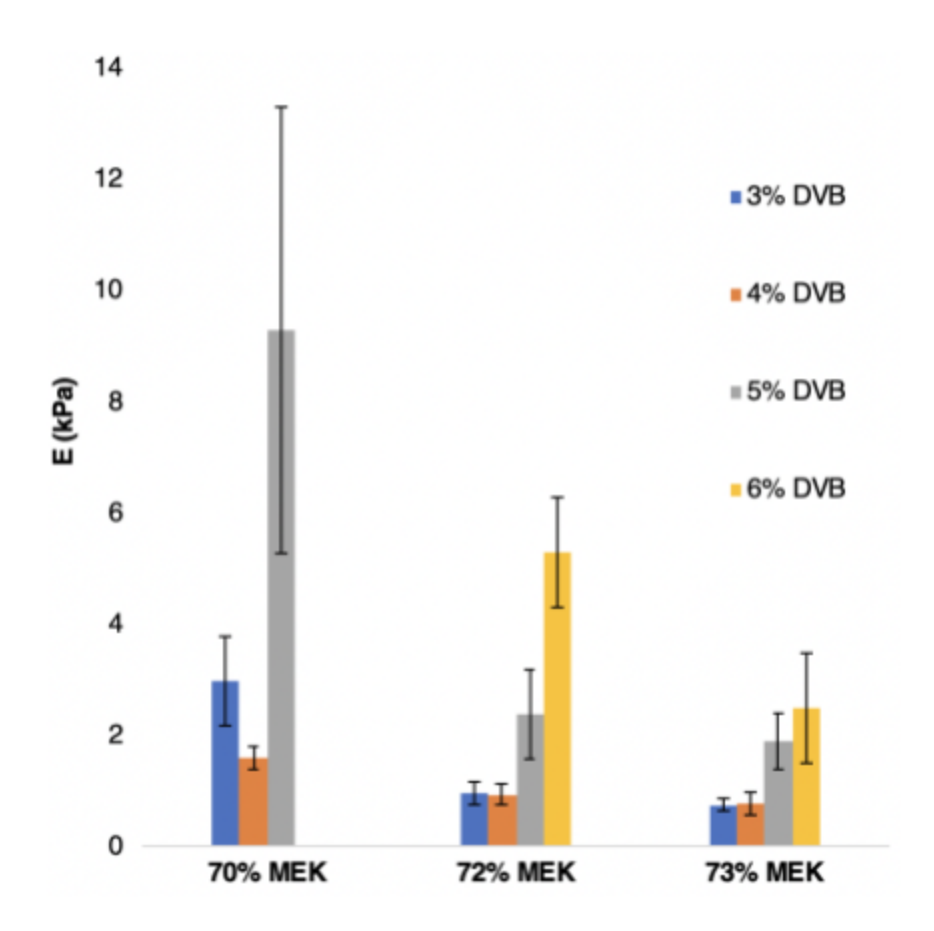
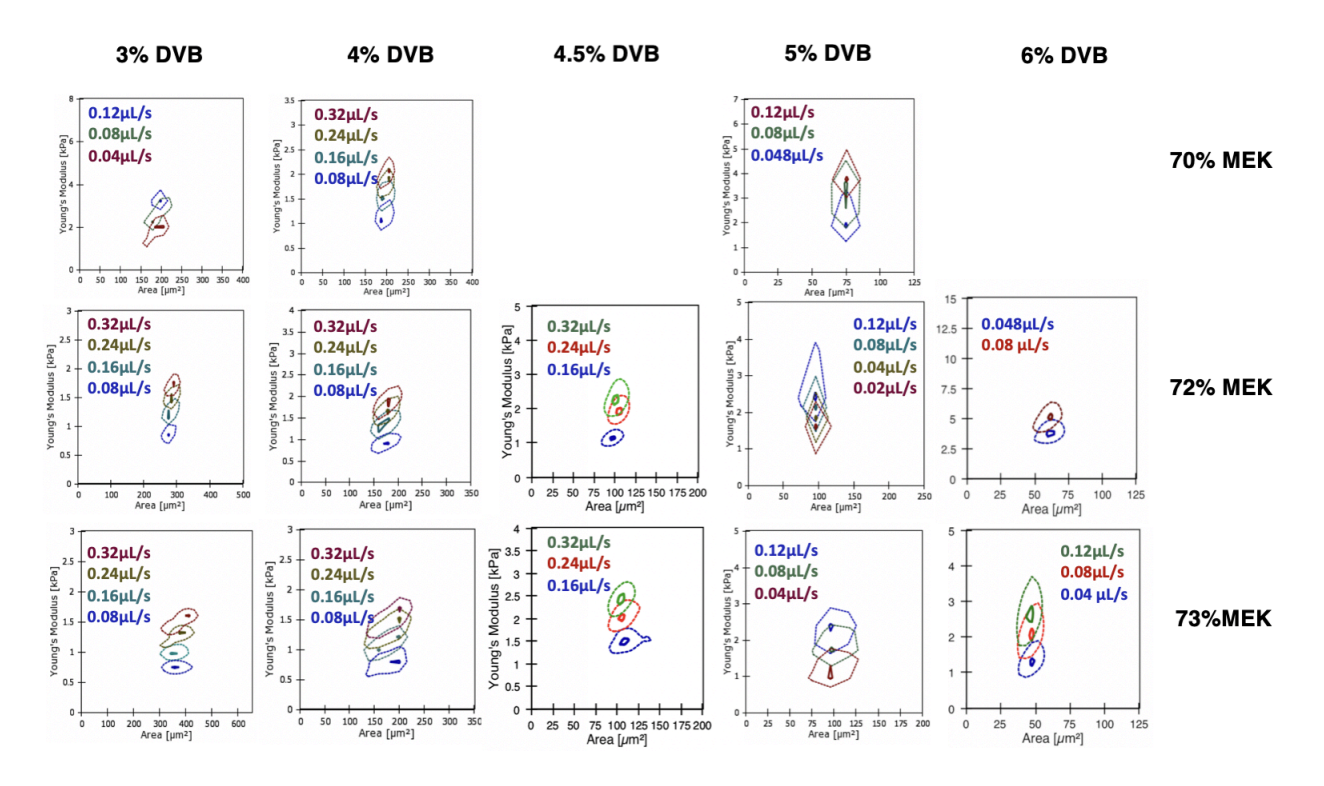


Figure A2.2: Young's moduli of microgels as a function of %DVB and vol% MEK (flow  $rate = 0.08~\mu L/s).$ 



**Figure A2.3**: Young's moduli of microgels as a function of flow-rate, showing strain-stiffening.

# CHAPTER 3: Lightly Crosslinked Microgels by Precipitation Polymerization of Maleic Anhydride and Styrenic Monomers

Sheilan Sinjari<sup>a</sup>, Yuqing Zhao<sup>a</sup>, Jingwen Li<sup>a,b</sup>, Marta Skreta<sup>a</sup>, Heather Sweny <sup>a</sup>, Chen Hong<sup>b</sup>, and Harald D.H. Stöver<sup>a\*</sup>

Contributions: This research was designed by SS and HDHS. Experiments were designed by SS. Microgel syntheses and characterizations were carried out by SS, with assistance from MR and HS. HDHS provided guidance and editing feedback for the writing of this chapter. This chapter has been reproduced with permission from Sinjari, S.; Zhao, Y.; Li, J.; Skreta, M.; Sweny, H.; Hong, C.; Stöver, H. D. H. Lightly Cross-Linked microgels by precipitation polymerization of maleic anhydride and styrenic monomers. *ACS Appl. Polym. Mater.* **2022**, *4*, 5680–5687. Copyright (2022) American Chemical Society

#### **Graphical abstract:**

<sup>&</sup>lt;sup>a</sup> Department of Chemistry and Chemical Biology, McMaster University, Hamilton, ON, L8S 4M1, Canada

<sup>&</sup>lt;sup>b</sup> College of Chemistry, Chemical Engineering and Materials Science, Soochow University, Suzhou, China

### 3.1. ABSTRACT

The synthesis and properties of micron-sized particles by precipitation polymerization of maleic anhydride (MAn), styrene (Sty), 4-methylstyrene (4MS) and divinylbenzene (DVB-55) in methyl ethyl ketone (MEK)/heptane cosolvent mixtures is described. Particles were narrow-disperse with diameters varying as a function of reaction solvent, crosslinker type and loading, and 4MS/Sty ratios. Diameters ranged from 1 to 14 μm when swollen in good organic solvents, with the largest sizes observed at low crosslinker loadings and for polymerization solvents containing ≥70 vol% MEK. At constant crosslinker loading and solvency, increasing the 4MS/Sty ratio from 0.1 to 1 more than doubled the particle diameters, illustrating the impact of comonomer composition on particle nucleation. Switching entirely from 4MS to Sty shifted solvency requirements for microgel formation by 10% of the good solvent, MEK. Similarly, replacing DVB-55 with a diacrylate restricted microgel formation to lower solvency regimes. Hydrolysis of anhydride groups gave microgels with pH-dependent swelling and volume swelling ratios of up to 40 depending on degree of crosslinking.

#### 3.2. INTRODUCTION

Microgels are lightly crosslinked, swellable particles with sizes ranging from hundreds of nanometres to tens of micron.<sup>1–3</sup> The large surface area of these colloids permits rapid response to external stimuli including changes in pH,<sup>4,5</sup> temperature,<sup>6,7</sup> and ionic strength,<sup>8</sup> making microgels interesting candidates for use as cell culture supports,<sup>9,10</sup> optical sensors and model systems for phase transition studies.<sup>13–16</sup> Since

particle size, degree of swelling and stiffness are central to such applications, many reports have focussed on the effects of reaction conditions on the modulation of these properties.

Among the heterogeneous polymerization techniques for microgel fabrication, precipitation polymerization of crosslinking monomers in marginal solvents offers a facile route to narrow-disperse microspheres with stabilizer-free surfaces. First developed for the homopolymerization of divinylbenzene-55 (DVB-55), a commercial mixture of 55% *meta*- and *para*-divinylbenzene isomers and 45% *meta*- and *para*-ethylvinylbenzene isomers, 17,18 this approach has since been adapted to include photo-initiation, 19,20 distillation-precipitation polymerization<sup>21,22</sup> and controlled free radical polymerizations like ATRP<sup>23,24</sup> and RAFT. 25,26

A key requirement for precipitation polymerization is to align polymer and solvent properties. Uniform microspheres are typically formed in marginal, near-theta solvent conditions where newly formed oligomers crosslink and desolvate to form the initial particle nuclei which then grow into colloidally stable microgels by capturing additional oligomer and monomer from the continuous phase. The resulting, self-renewing microgel surface inhibits particle aggregation during the growth stage.<sup>27–30</sup> Neat acetonitrile<sup>31,32</sup> as well as specific ratios of methyl ethyl ketone (MEK) and heptane were found to meet this condition of 'marginal solvency' for precipitation polymerizations of DVB-55 and a range of other styrenic and methacrylic monomers and crosslinkers including maleic anhydride (MAn).<sup>32–33</sup>

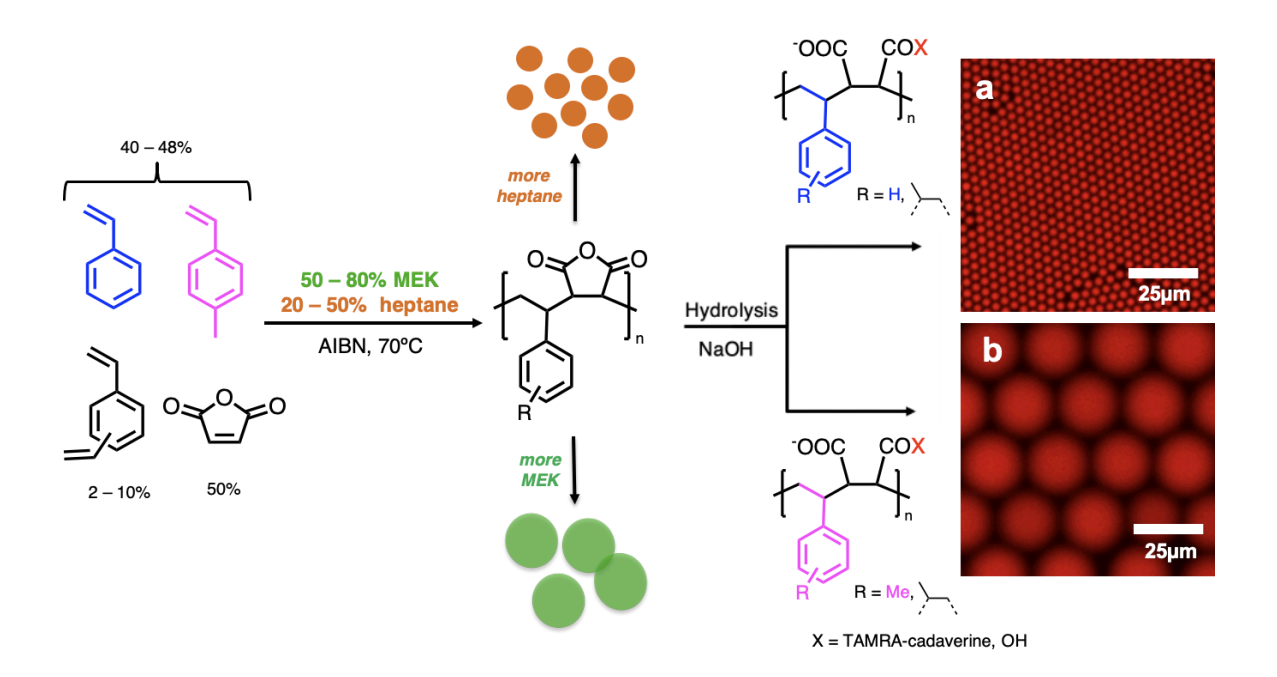
The influence of comonomer polarity on particle morphology was demonstrated by Li et al. for precipitation polymerizations of DVB-80 with different methacrylates.<sup>30</sup> While neat acetonitrile was a suitable solvent for copolymerizations of DVB-80 with polar methacrylic monomers, and polar methacrylic crosslinkers such as ethylene glycol dimethacrylate (EGDMA), less polar cosolvent mixtures were required to obtain narrow-disperse particles for high volume fractions of aliphatic methacrylates.

In 2002, Frank et al. showed that swellable microspheres of up to 5μm in diameter could be obtained from copolymerization of MAn, DVB-55 and 4-methylstyrene (4MS) in MEK/heptane solvent mixtures containing 20 - 70 vol% MEK.<sup>30</sup> A recent study of this comonomer system at low crosslinker loadings of 3 − 5 mol% DVB-55 and increased solvency (≥70 vol% MEK) yielded microgels that could swell up to 22 μm diameter in water after hydrolysis of the anhydride groups.<sup>34</sup> Increasing the MEK content of the copolymerization solvent from 70 to 73 vol% MEK allowed us to tune the Young's moduli of these microgels from 10 down to 0.8 kPa, as measured by real-time deformability cytometry (RT-DC), a microfluidic technique that relates microgel deformation under hydrodynamic shear stress to Young's modulus.<sup>35</sup> The significant effects of such small changes in reaction parameters reflects the fact that microgel initiation and growth takes place near a critical point of network formation.

We report here a deeper study of these lightly crosslinked microgels across a wider parameter space including changes in solvency, comonomer type and crosslinker type.

The anhydride groups of resulting microspheres were then functionalized and/or

hydrolyzed in order to explore the aqueous phase properties of these interesting soft materials.



**Scheme 3.1**. Microgel synthesis and hydrolysis to polyanionic microgel particles. Fluorescence microscope images of a) poly(Sty-co-MAn-co-DVB) and b) poly(4MS-co-MAn-co-DVB) microgels functionalized with a rhodamine label, hydrolyzed and swollen in phosphate buffered saline (PBS). Microspheres were made in 70/30 MEK/heptane using 5 mol% DVB-55 crosslinker. Magnification is 20x, NA = 0.45.

Here, we are using optical and electron microscopy to determine the competing effects of crosslinker type and loading, solvent polarity and 4MS/Sty ratios on final microsphere size and size dispersity. Base hydrolysis of anhydride groups yields polyanionic microgels that rapidly swell/de-swell in response to changes in pH, with

extent of swelling depending on crosslink density. The hydrolytic stability of diacrylate crosslinked microgels is explored as a step towards incorporating degradation into such particles. By controlling monomer and solvent ratios, and leveraging reactive anhydride chemistry, these microspheres may be tailored for applications ranging from tissue engineering to condensed matter modelling.

### 3.3. EXPERIMENTAL

#### 3.3.1. Materials

2,2'-azobis(2-methylpropionitrile) (AIBN) was purchased from Dupont and recrystalized from methanol. Tetramethylrhodamine 5-(and-6)-carboxamide cadaverine (TAMRA-cadaverine, 95%) was purchased from AnaSpec. Divinylbenzene-55 (DVB-55, 55% mixture of divinylbenzene isomers, 45% ethyl vinylbenzene isomers), 4-methylstyrene (4MS, >95.5%), maleic anhydride (MAn, >98.5%), styrene (Sty, ≥99.9%), acetonitrile (≥99.5%), tetrahydrofuran (THF, ≥99.0%), methanol (≥99%), methylethylketone (MEK, ≥99.0%), heptane (>98.5%), dimethylformamide (DMF, ≥99.8%) were purchased from Sigma-Aldrich. All materials were used as received unless otherwise stated.

## 3.3.2. Synthesis of Microspheres by Precipitation Copolymerization

Microgel syntheses were adapted from a procedure previously reported, with a monomer loading of 4% w/v and a targeted 1:1 overall ratio of styrenic to anhydride vinyl groups.<sup>34</sup> The procedure to synthesize particles with equimolar amounts of Sty and 4MS, 5 mol%

of effective DVB-55 (with respect to styrenic monomers; DVB-55, Sty and 4MS) and 50 mol% MAn is given as an example, reaction mixtures are not deoxygenated prior to heating. Briefly, AIBN (16mg; 2 mol% relative to total monomer loading) and MAn (0.363g, 3.70mmol) were weighed into a 20mL screw cap vial and dissolved in 10.47g of MEK and 4.79 g of heptane, corresponding to an MEK/heptane ratio of 65/35 v/v. Sty (193 μL, 1.68 mmol), 4MS (222 μL, 1.68 mmol) and DVB-55 (46.0 μL, 0.320 mmol vinyl groups) were added to the MAn/AIBN solution using a micropipette. The vial was rotated for 24h about its horizontal axis at 4 rpm in an insulated commercial hotdog roller (Model 12, Star International Chrome Hot Dog Roller) fitted with a resistive heating pad, pre-heated to 70 °C. Vials were cooled and opened, content transferred into 50 mL polypropylene tubes. As-formed microspheres were isolated by centrifugation at 3200g and washed by re-suspending in THF (5x40mL) to remove soluble polymer, residual monomer and solvent. Microspheres were then re-suspended in 20 mL of THF and stored in the dark at -18 °C. Isolated particle yields were determined by drying an aliquot of microsphere suspension under reduced pressure.

#### 3.3.3. Fluorescent Labelling and Anhydride Hydrolysis of Microspheres

Microspheres were fluorescently labelled using TAMRA-cadaverine with a targeted degree of labelling of 0.05 mol% relative to anhydride groups (0.025 mol% of total monomer units). THF-swollen microspheres (corresponding to ca. 1.3 mmol anhydride groups) were washed and re-suspended in DMF (3x10mL) before addition of 284  $\mu$ L of a 1% w/v solution of TAMRA-cadaverine in DMF (0.334 mg, 6.5x10<sup>-4</sup> mmol). The solution was agitated by rotation for 12h in the dark at room temperature. Remaining

anhydride groups were reacted with a two-fold excess of 1.0N NaOH, followed by dilution with distilled water. Microsphere suspensions were transferred to a 50 mL polypropylene tube, centrifuged at 3200g and resuspended in distilled water (5x25ml) to remove organic solvents as well as unreacted TAMRA-cadaverine. The microgel suspension was adjusted to pH  $\geq$  7.4 using HCl and stored in the dark at 4°C.

## 3.3.4. Optical and Fluorescence Microscopy

Microsphere images were obtained with a Nikon Eclipse LV100ND upright microscope equipped with Andor Zyla 5.5 sCMOS camera. Particles were imaged at least 30 minutes following washes with THF (as-formed particles) or water (hydrolyzed particles) to ensure complete swelling. Diameters were measured using NIS-Elements Microscope Imaging Software and ImageJ software. Size dispersity was calculated as the standard deviation of mean microgel diameter, determined by averaging  $n \ge 100$  measurements for each microsphere sample.

### 3.3.5. Scanning Electron Microscopy (SEM)

As-formed microspheres were washed and resuspended in a 1:6 v/v THF/acetonitrile solution (3x10mL), deposited onto aluminum studs with double-sided adhesive carbon tape and dried in an oven at 70 °C for 20 min. After drying, studs were sputter coated with 36 nm of gold for conductivity and imaged with a Tescan Variable Pressure Scanning Electron Microscope (SEM) at an accelerating voltage of 20 kV. Particle deposition from a 1:6 v/v THF/acetonitrile solvent mixture serves to deswell/collapse

microspheres without causing aggregation, and without excessive flattening of softer particles.

# 3.3.6. Synthesis and stability of 1,4-butanediol diacrylate (BDDA) crosslinked microspheres

BDDA-crosslinked microspheres were synthesized by the same procedure described above for DVB-crosslinked microspheres, using 4MS and MAn as comonomers. To test the hydrolytic stability of the diacrylate, anhydride groups of microspheres made in 65 vol% MEK containing 5 mol% BDDA (relative to styrenic and acrylic vinyl groups, 2.5 mol% with respect to total vinyl groups) were hydrolyzed using the same procedure described above for DVB-55 analogs. The washed microgels were resuspended in distilled water with pH adjusted to 2, 7.4 and 9 and rotated at 7 rpm in a hybridizer oven heated to 37 °C. The pH of each suspension was monitored daily and microgels were imaged every 12 hours for the first 84 hours, then every 24 hours for 3 days. Changes in particle diameter were assessed using a Nikon Eclipse LV100ND optical microscope running NIS-Elements Microscope Imaging and analysis software.

### 3.4. RESULTS AND DISCUSSION

## 3.4.1. Precipitation copolymerization of styrenic monomers, MAn and DVB-55

Our group previously reported on the precipitation copolymerization of varying styrenic and methacrylic monomers, where low monomer loadings and near-theta conditions enabled the formation of narrow-disperse microspheres with clean surfaces.<sup>27–33</sup> Here, we employ precipitation copolymerization of 4MS and Sty, as well as

mixtures of these two monomers, with 2-10 mol% DVB-55 and stoichiometric amounts of MAn to synthesize swellable microspheres as depicted by Scheme 3.1. Mixtures of MEK and heptane are used as polymerization cosolvents, with MEK content varied from 50 to 80 vol%. A near equimolar overall ratio of styrenic to anhydride vinyl bonds is used to maintain a rapid alternating copolymerization, which affords isolated particle yields of up to 80% despite the relatively low total monomer loading (4% w/v).

## 3.4.1.2. Properties of poly(4MS-co-MAn-co-DVB) microspheres

Figure 3.1 shows the effect of reaction solvency (MEK/heptane) and DVB concentration the diameter morphology of as-formed on and poly(4MS-co-MAn-co-DVB) microspheres. The roles of crosslinker and solvent can be explained in terms of the mechanism of microsphere formation elucidated earlier by our group. 28,29 Initially, a combination of crosslinking events and unfavourable polymer-solvent interactions causes the desolvation and aggregation of oligomers into primary particles or nuclei. The solvent still provides a measure of steric stability by swelling lower molecular weight chains on the particle surface, limiting homocoagulation of nuclei during particle growth. Final particle size is thus a reflection of the number of colloidally stable particles present at the end of the nucleation period, which is dictated by comonomer composition and volume fraction of good solvent (MEK). This is reflected in Figure 3.1 (a and c), and in the trends of average particle diameter (Fig. A3.1).

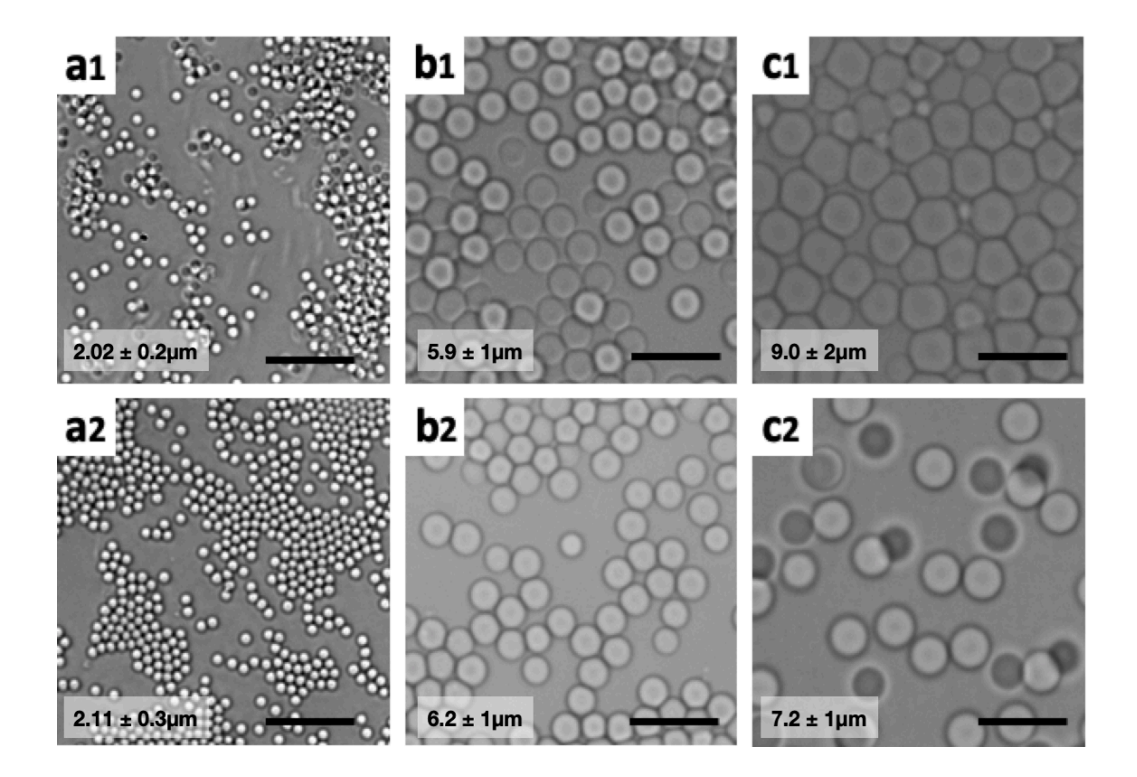


**Figure 3.1.** Optical microscope images of poly(4MS-*co*-MAn-*co*-DVB) microspheres swollen in THF, reflecting the impact of crosslinker content and solvent composition on morphology and diameter. Microspheres are crosslinked with 3 mol% DVB (top row) and 5 mol% DVB (bottom row), made in MEK/heptane mixtures of a) 60/40 b) 65/35 and c) 70/30. Scale bars are 20 μm.

From Figure 3.1, it is apparent that the effect of crosslinker content on particle morphology strongly depends on solvency. Fast desolvation of oligomers at lower solvency (60 vol% MEK) results in more nuclei present at the point of colloidal stability and hence smaller final particles, regardless of crosslinker concentration (Fig. 3.1., a1 and a2). In contrast, higher solvency (65%, 70 vol% MEK) allows for extended aggregation of nuclei prior to attainment of colloidal stability, leading to fewer but larger final

microspheres (Fig. 3.1, b1, c1). At these higher solvencies, increasing the crosslinker level from 3 to 5 mol% again promotes faster desolvation and formation of smaller particles (Fig. 3.1 b2, c2).

It is important to note that formation of well-defined poly(4MS-co-MAn-co-DVB) microspheres is limited to approximately 73 vol% MEK or less in the polymerization solvent.<sup>34</sup> Higher solvency at sufficiently low crosslinker concentration can lead to formation of Staudinger nanogels, irregular microgels, or macrogelation to form space-filling gels.<sup>36,37</sup>

# 3.4.1.3 pH-dependent swelling of hydrolyzed poly(4MS-co-MAn-co-DVB) microspheres

While as-formed particles swell in organic solvents, hydrolysis of anhydride units enables significant and reversible pH-dependent swelling in aqueous media. Table 1 summarizes the diameters of these microspheres with different mol% DVB as function of pH, showing that they swell by a volume factor of up to 40 when moving from acidic to basic media. At pH=2, particles appear largely dehydrated and collapsed as a result of protonation of succinic acid groups that are known to have pKa<sub>1</sub> of around 4.5, depending on the surrounding ionic environment and copolymer composition.<sup>38–40</sup>

		Average diameter (μm) at pH <sup>a</sup>				
DVB (mol%)	2.0	4.0	7.4	9.0	$\left(\frac{d_{swollen}}{d_{collapsed}}\right)^3$	
2	$6.1 \pm 0.3$	$18 \pm 0.5$	$20 \pm 0.8$	$21 \pm 0.8$	37	
3	$5.7 \pm 0.3$	13 ± 0.9	19 ± 0.8	19 ± 1.0	39	
4	$4.2 \pm 0.3$	13 ± 0.9	14 ± 0.9	15 ± 0.8	40	
5	$4.2 \pm 0.4$	$10 \pm 0.6$	12 ± 0.5	$12 \pm 0.5$	23	
8	$2.9 \pm 0.3$	$5.6 \pm 0.6$	$7.1 \pm 0.5$	$7.0 \pm 0.6$	14	

**Table 3.1.** Average microgel diameter and swelling as a function of DVB% loading and pH for microspheres synthesized in 70/30 MEK/heptane solvent mixtures.

Similarly, some particle compositions swell so extensively following anhydride hydrolysis that the use of brightfield imaging is limited by poor optical contrast. Microspheres were therefore reacted with TAMRA-cadaverine prior to anhydride hydrolysis and microgel morphology was assessed by fluorescence microscopy. This process also illustrates the potential of the reactive anhydride groups for post-functionalization/modification (Scheme 3.1, images a and b).

## 3.4.1.4. Precipitation polymerization with mixtures of 4MS and Sty

4MS was chosen as a monovinyl component in copolymerizations with DVB because of its structural similarities to the ethylvinylbenzenes that make up 45% of commercial DVB-55 mixtures.<sup>28</sup> We thus explored the relationship between styrenic

<sup>&</sup>lt;sup>a</sup> Diameters were determined by optical microscopy.

<sup>&</sup>lt;sup>b</sup> Errors are standard deviations of mean microgel diameters collapsed and swollen correspond to particle diameters at pH 2 and 9, respectively

comonomer composition and particle diameter by preparing a series of microspheres containing different 4MS:Sty ratios and constant mol% DVB in different MEK/heptane solvent mixtures, and assessed their diameters by optical microscopy (Figure 3.2).

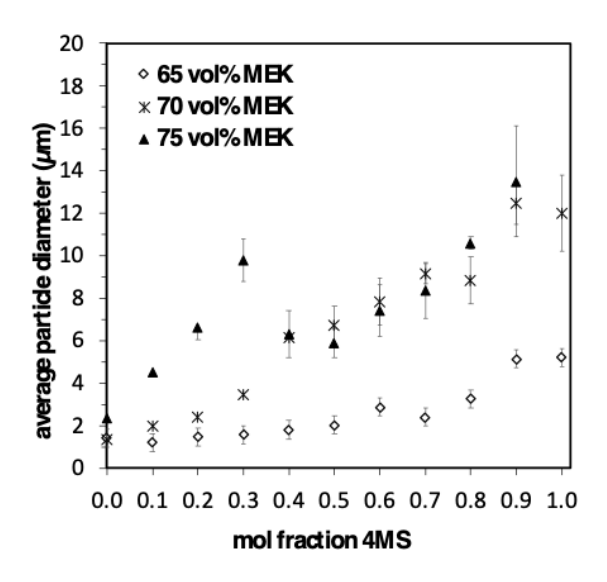


**Figure 3.2.** Average diameters for THF-swollen microspheres as a function of 4MS:Sty comonomer ratios for particles made in MEK/heptane solvent mixtures containing 65, 70 and 75 vol% MEK and 5 mol% DVB. Each data point represents the average particle diameter from two replicate experiments, where  $n \ge 100$  diameters were measured per replicate.

As the mol fraction of 4MS increases in the styrenic monomer pool (4MS+Sty), diameters increase monotonically from 2 to 3.5, and 12 μm, for particles made in 65 and 70 vol% MEK, respectively. These trends suggest that incorporating 4MS decreases the number of nuclei present at colloidal stability, resulting in larger final microgels.<sup>27,28</sup> This is also seen for 75 vol% MEK, though diameter increase is more limited once the mol

fraction of 4MS exceeds 0.3. This is attributed to excessive solvation of 4MS-rich networks at 75 vol% MEK, which may lead to decreasing efficiency of both oligomer capture and crosslinking. No particles were isolated for 4MS mol fractions > 0.9 at 75 vol% MEK, in agreement with the previously observed upper limit of MEK content for the formation of 4MS-MAn-DVB microgels (Fig. A3.1).

## 3.4.1.5. Properties of poly(Sty-co-MAn-co-DVB) microspheres

The effects of crosslinker loading on the diameters of styrene-based particles at different vol% MEK are summarized in Figure 3.3.

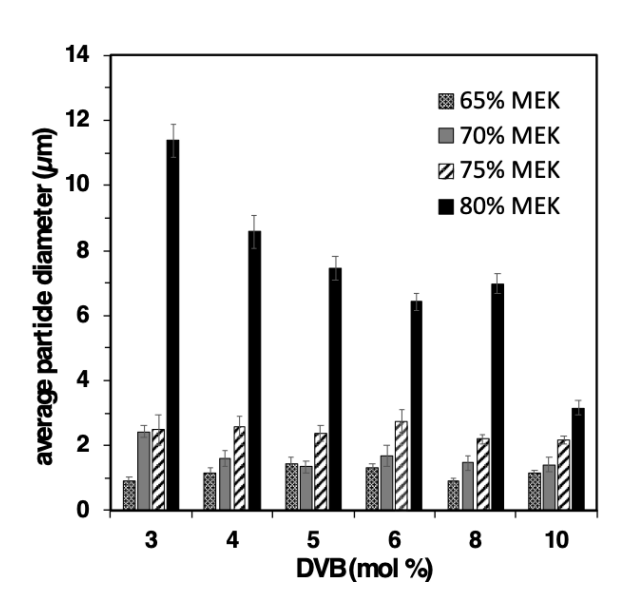


**Figure 3.3**. Particle diameter of THF-swollen Sty/MAn/DVB particles as a function of DVB mole % and vol% MEK. Data points represent an average of 100-5000 measurements.

Narrow-disperse microspheres were formed between 65 and 80 vol% MEK, where ≤60 vol% MEK led to the formation of sub-micron sized particles that could not reliably be measured using optical microscopy. Particles formed at 65 to 80 vol% MEK exhibited a significant increase in diameter with increasing vol% MEK and decreasing mol% DVB, with largest diameters observed at 3 mol% DVB and 80 vol% MEK. It is worth noting that the onset of large particle formation for the Sty-based particles is shifted to 80 vol% MEK, compared to that of the 4MS-based particles, which show maximum diameters at 70 vol% MEK (Fig. A3.1). This corresponds to the offset of polymer-solvent matching between the Sty- and 4MS-networks also observed in Figure 3.2.

SEM images in Figure 3.4 reveal an increase in both diameter and entanglement of swellable surface layers of the particles when DVB loading is held constant at 5 mol%, and solvency is increased from 60 vol% MEK (Fig. 3.4a) to 75 vol% (Fig. 3.4c). Particles are narrow-disperse with smooth surfaces across all three solvent compositions, with evidence of rare dimer formation at 75 vol% MEK (Fig. 3.4c), which is an example of late homocoagulation and growth.

A similar transition is seen in the SEM images of poly(4MS-co-MAn-co-DVB) microspheres when moving from 40 to 60 vol% MEK (Fig. A3.3), again reflecting the off-set in solvent matching between the two copolymer systems.

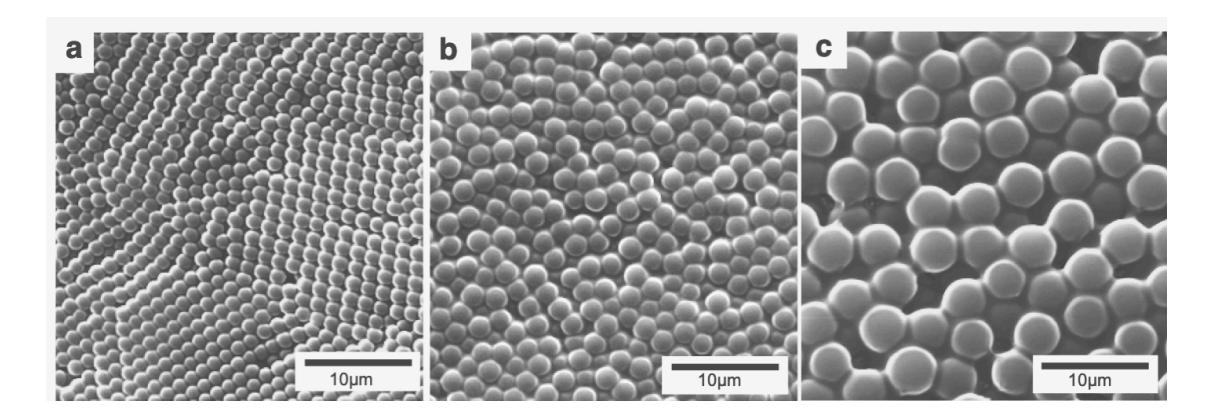


**Figure 3.4**. SEM micrographs of Sty-MAn-DVB particles crosslinked with 5 mol% DVB, showing morphology transitions from hard spheres to swellable microgels, as a function of vol% MEK. Microspheres were made in MEK vol% of a) 60, b) 70 and c) 75. Accelerating voltage is 20kV.

We explored the use of Hansen solubility parameters in attempts to explain the offset in solvent matching on the basis of specific molecular features of solvents and polymers. Solubility parameter values ( $\delta$  MPa<sup>1/2</sup>) for different MEK/heptane solvent mixtures are given in Table A3.1. In practice, polymer and solvent are compatible when the difference between their  $\delta$  values falls within 4MPa<sup>1/2</sup> of each other. For the 70 - 80 vol% MEK solvency regime, differences between estimated  $\delta$  values of the polymers (poly(Sty-alt-MAn) = 19.6 MPa<sup>1/2</sup> and poly(4MS-alt-MAn) = 19.7 MPa<sup>1/2</sup>)<sup>42</sup> and solvent alone are not significant enough to explain the ca. 10 vol% MEK offset in conditions for largest particle formation. Estimated solubility parameters are still useful for predicting polymer – solvent interactions at points below the critical limit of solvency (e.g. at MEK volume fractions < 70 and 80% for 4MS- and Sty-based copolymers, respectively).

# 3.4.1.6. Precipitation polymerization of 4MS, MAn and 1,4-butanediol-diacrylate (BDDA)

Li and Goh have demonstrated that precipitation polymerization can be extended to include polar dimethacrylates and methacrylate monomers while retaining control over particle size and distributions.<sup>31,33</sup> Since it is known that increased hydrophobicity in the polymer backbone makes methacrylic esters stable to hydrolysis,<sup>43</sup> we aimed to replace DVB-55 with a diacrylate crosslinker, 1,4-butanediol diacrylate (BDDA), to assess its effects on microsphere properties and probe the hydrolytic stability of acrylate esters.

## 3.4.2 Properties of poly(4MS-co-MAn-co-BDDA) particles

For a series of BDDA crosslinked microgels, morphologies appeared to be similarly dependent on solvent composition (Fig. 3.5), where individual particles are formed in 65 vol% MEK at BDDA loadings of 5 to 10 mol%. Figure 3.5 (top row) shows aggregation and macrogelation at 70 vol% MEK for BDDA loadings of 5 mol% (similar to those used in the styrenic copolymerizations).

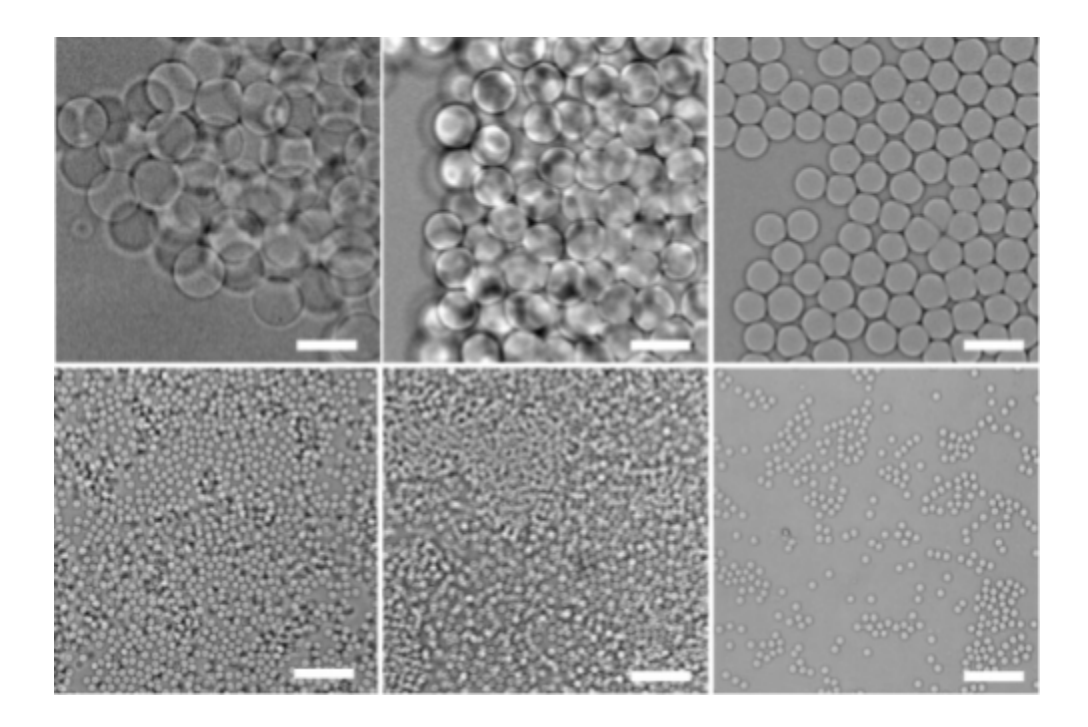


**Figure 3.5.** Optical microscope images of BDDA crosslinked microspheres suspended in THF. Microspheres were made in 65 vol% (bottom row) and 70 vol% MEK (top row), crosslinked with (left to right) 5, 8 and 10 mol% BDDA. Scale bars are 20 μm.

Microgels made in 65 vol% MEK with 5 mol% BDDA were used to assess the hydrolytic stability of the diacrylate. Microgel suspensions were adjusted to pH 2, 7 and 9, and changes in diameter were monitored over the course of one week while heating solutions at 37°C. Optical microscopy affords a simple approach to visualizing hydrolysis, as particle swelling resulting from de-crosslinking should be easily observed.

Results summarized in Figure A.3.4 show that particle diameter remains unchanged across the tested pH range over 7 days. The lack of noticeable swelling may stem from reduced accessibility of the ester to incoming nucleophiles. Protonation of succinic acid groups at pH 2 may produce a local hydrophobic environment by collapsing the polymer

network, while at high pH, hydrolysis may be limited by repulsion of hydroxide ions by neighbouring anionic carboxylates.

Moreover, depending on copolymer composition, polymeric esters are more stable to hydrolysis than their small-molecule analogues.<sup>41</sup> In the BDDA system, the butyl spacer and ca. 47.5 mol% of styrenic groups add significant hydrophobic bulk that may contribute to ester stability. Though decrosslinking was not observed for the presented microgel composition, future incorporation of a more labile and hydrophilic acrylate-based crosslinker may facilitate microgel degradation.

### 3.5. CONCLUSIONS

The effects of crosslinker type and loading, solvent composition and comonomer ratios on the formation and properties of lightly crosslinked microgels by precipitation copolymerization of styrenic monomers and maleic anhydride was explored. Anhydride groups were functionalized and hydrolyzed to give pH-responsive hydrogel particles ranging from 1–20µm in diameter, where diameters and swelling depended on polymerization cosolvent ratio, mol% DVB-55 and solution pH. 4MS-based microgels had diameters an order of magnitude larger than their Sty-based counterparts under conditions of constant crosslinker loading and solvency. Sizes increased significantly at 70 and 80 vol% MEK for 4MS and Sty particles, respectively, across a range of crosslink densities, with the difference in the onset of large particle formation reflecting the significant effect of monomer structure on microgel properties. Morphologies of acrylate-crosslinked particles showed similar dependence on reaction solvency and

crosslinker content as those crosslinked with DVB-55. Particles crosslinked with 5 mol% BDDA were hydrolytically stable, with no decrosslinking observed following one week of exposure to acidic and basic conditions. The effects of monomer-solvent matching and crosslinker content on final microgel diameters were largely attributed to their impact on the nucleation process, e.g. the onset of colloidal stability. This work demonstrates that polymerization conditions need to be adjusted for minor changes in comonomer or crosslinker properties, enabling the formation of reactive microgels in the  $3-20~\mu m$  range.

## 3.6. REFERENCES

- (1) Kawaguchi, H. Functional Polymer Microspheres. *Prog. Polym. Sci.* **2000**, *25*, 1171–1210.
- (2) Plamper, F. A.; Richtering, W. Functional microgels and microgel systems. *Acc. Chem. Res.* **2017**, *50*, 131–140.
- (3) Scheffold, F. Pathways and challenges towards a complete characterization of microgels. *Nat. Commun.* **2020**, *11*, No. 4315.
- (4) Zhou, S.; Chu, B. Synthesis and volume phase transition of poly(methacrylic acid-co-N-isopropylacrylamide) microgel particles in water. *J. Phys. Chem. B.* **1998**, *102*, 1364–1371.
- (5) Hoare, T.; Pelton, R. H. Highly pH and Temperature Responsive Microgels Functionalized with Vinylacetic Acid. *Macromolecules* **2004**, *37*, 2544–2550.
- (6) Debord, J. D.; Lyon, A. Synthesis and Characterization of pH Responsive Copolymer Microgels with Tunable Volume Phase Transition Temperatures. *Langmuir* **2003** *19*, 7662–7664.
- (7) Dupin, D.; Rosselgong, J.; Armes, S. P.; Routh, A. F. Swelling Kinetics for a pH-Induced Latex-to-Microgel Transition. *Langmuir* **2007**, *23*, 4035–4041.

- (8) Daly, E.; Saunders, B. R. A Study of the Effect of Electrolyte on the Swelling and Stability of Poly(N-isopropylacrylamide) Microgel Dispersions. *Langmuir* **2000**, *16*, 5546–5552.
- (9) Bhattacharjee, T.; Gil, C. J.; Marshall, S. L.; Uruena, J. M.; O'Bryan, C. S.; Carstens, M.; Keselowsky, B.; Palmer, G. D.; Ghivizzani, S.; Gibbs, C. P.; Sawyer, W. G.; Angelini, T. E. Liquid-like Solids Support Cells in 3D. *ACS Biomater. Sci. Eng.* **2016**, *2*, 1787–1795.
- (10) Morley, C. D.; Tordoff, J.; O'Bryan, C. S.; Weiss, R.; Angelini, T. E. 3D aggregation of cells in packed microgel media. *Soft Matter* **2020**, *16*, 6572–6581.
- (11) Zhang, Q. M.; Xu, W.; Serpe, M. J. Optical Devices Constructed from Multiresponsive Microgels. *Angew. Chem., Int. Ed.* **2014**, *53*, 4827–4831.
- (12) Gao, Y.; Li, X.; Serpe, M. J. Stimuli-Responsive Microgel-Based Etalons for Optical Sensing. RSC Adv. 2015, 5, 44074–44087. (13) Senff, H.; Richtering, W. Temperature sensitive microgel suspensions: colloidal phase behaviour and rheology of soft spheres. *J. Chem. Phys.* **1999**, *111*, 1705–1711.
- (14) Trappe, V.; Prasad, V.; Cipelletti, L.; Segre, P. N.; Weitz, D. A. Jamming phase diagram for attractive particles. *Nature* **2001**, *411*, 772–775.
- (15) Mattsson, J.; Wyss, H. M.; Fernandez-Nieves, A.; Miyazaki, K.; Hu, Z.; Reichman, D. R.; Weitz, D. A. Soft colloids make strong glasses. *Nature* **2009**, *462*, 83–86.

- (16) Paloli, D.; Mohanty, P. S.; Crassous, J. J.; Zaccarelli, E.; Schurtenberger, P. Fluid-solid transitions in soft-repulsive colloids. *Soft Matter* **2013**, *9*, 3000–3004.
- (17) Li, K.; Stöver, H. D. H. Synthesis of monodisperse poly(divinylbenzene) microspheres. *J. Polym. Sci., Part A: Polym. Chem.* **1993**, *31*, 3257–3263.
- (18) Li, W. H.; Stöver, H. D. H. Porous Monodisperse Poly- (divinylbenzene) Microspheres by Precipitation Polymerization. *J. Polym. Sci., Part A: Polym. Chem.* **1998**, *36*, 1543–1551.
- (19) Limé, F.; Irgum, K. Monodisperse Polymeric Particles by Photoinitiated Precipitation Polymerization. *Macromolecules* **2007**, *40*, 1962–1968.
- (20) Limé, F.; Irgum, K. Preparation of Divinylbenzene and Divinylbenzene-co-Glycidyl Methacrylate Particles by Photoinitiated Precipitation Polymerization in Different Solvent Mixtures. *Macromolecules* **2009**, *42*, 4436–4442.
- (21) Bai, F.; Yang, X.; Huang, W. Synthesis of Narrow or Monodisperse Poly(divinylbenzene) Microspheres by Distillation Precipitation Polymerization. *Macromolecules* **2004**, *37*, 9746–9752.
- (22) Bai, F.; Huang, B.; Yang, X.; Huang, W. Synthesis of Monodisperse Poly(methacrylic acid) Microspheres by Distillation Precipitation Polymerization. *Eur. Polym. J.* **2007**, *43*, 3923–3932.

- (23) Zheng, G.; Stöver, H. D. H. Grafting of Polystyrene from Narrow Disperse Polymer Particles by Surface-Initiated Atom Transfer Radical Polymerization. *Macromolecules* **2002**, *35*, 7612–7619.
- (24) Jiang, J.; Zhang, Y.; Guo, X.; Zhang, H. Narrow or Monodisperse, Highly Cross-Linked, and "Living" Polymer Microspheres by Atom Transfer Radical Precipitation Polymerization. *Macromolecules* **2011**, *44*, 5893–5904.
- (25) Barner, L.; Li, C. E.; Hao, X.; Stenzel, M. H.; Barner-Kowollik, C.; Davis, T. P. Synthesis of core-shell poly(divinylbenzene) microspheres via reversible addition fragmentation chain transfer graft polymerization of styrene. *J. Polym. Sci., Part A: Polym. Chem.* **2004**, *42*, 5067–5076.
- (26) Zheng, C.; Zhou, Y.; Jiao, Y.; Zhang, H. Narrow or Monodisperse, Physically Cross-Linked, and "Living" Spherical Polymer Particles by One-Stage RAFT Precipitation Polymerization. *Macromolecules* **2019**, *52*, 143–156.
- (27) Frank, R. S.; Downey, J. S.; Stöver, H. D. H. Synthesis of Divinylbenzene–Maleic Anhydride Microspheres Using Precipitation Polymerization. *J. Polym. Sci., Part A: Polym. Chem.* **1998**, *36*, 2223–2227.
- (28) Downey, J. S.; Frank, R. S.; Li, W. H.; Stöver, H. D. H. Growth Mechanism of Poly(divinylbenzene) Microspheres in Precipitation Polymerization. *Macromolecules* **1999**, *32*, 2838–2844.

- (29) Downey, J. S.; McIsaac, G.; Frank, R. S.; Stöver, H. D. H. Poly(divinylbenzene) Microspheres as an Intermediate Morphology between Microgel, Macrogel, and Coagulum in Cross-Linking Precipitation Polymerization. *Macromolecules* **2001**, *34*, 4534–4541.
- (30) Frank, R. S.; Downey, J. S.; Yu, K.; Stöver, H. D. H. Poly(divinylbenzene-alt-maleic anhydride) Microgels: Intermediates to Microspheres and Macrogels in Cross-Linking Copolymerization. *Macromolecules* **2002**, *35*, 2728–2735.
- (31) Li, W. H.; Stöver, H. D. H. Mono- or narrow disperse poly(methacrylate-co-divinylbenzene) microspheres by precipitation polymerization. *J. Polym. Sci., Part A: Polym. Chem.* **1999**, *37*, 2899–2907.
- (32) Zhao, Y.; Burke, N. A. D.; Stöver, H. D. H. Structured Poly(divinylbenzene-co-chloromethylstyrene) Microspheres by Thermal Imprinting Precipitation Polymerization. *J. Polym. Sci., Part A: Polym. Chem.* **2016**, *54*, 1159–1166.
- (33) Goh, E. C. C.; Stöver, H. D. H. Cross-Linked Poly(methacrylic acid-co-poly(ethylene oxide) methyl ether methacrylate) Micro spheres and Microgels Prepared by Precipitation Polymerization: A Morphology Study. *Macromolecules* **2002**, *35*, 9983–9989.
- (34) Sinjari, S.; Freitag, J. S.; Herold, C.; Otto, O.; Smith, D. M.; Stöver, H. D. H. Tunable polymer microgel particles and their study using microscopy and real-time deformability cytometry. *J. Polym. Sci.* **2020**, *58*, 2317–2326.

- (35) Otto, O.; Rosendahl, P.; Mietke, A.; Golfier, S.; Herold, C.; Klaue, D.; Girardo, S.; Pagliara, S.; Ekpenyong, A.; Jacobi, A.; Wobus, M.; Töpfner, N.; Keyser, U. F.; Mansfeld, J.; Fischer-Friedrich, E.; Gück, J. Real-time deformability cytometry: on-the-fly cell mechanical phenotyping. *Nat. Methods.* **2015**, *12*, 199–202.
- (36) Daoud, M.; Joanny, J. F. Conformation of Branched Polymers. J. Phys. 1981, 42, 1359–1371.

## 3.7. APPENDIX

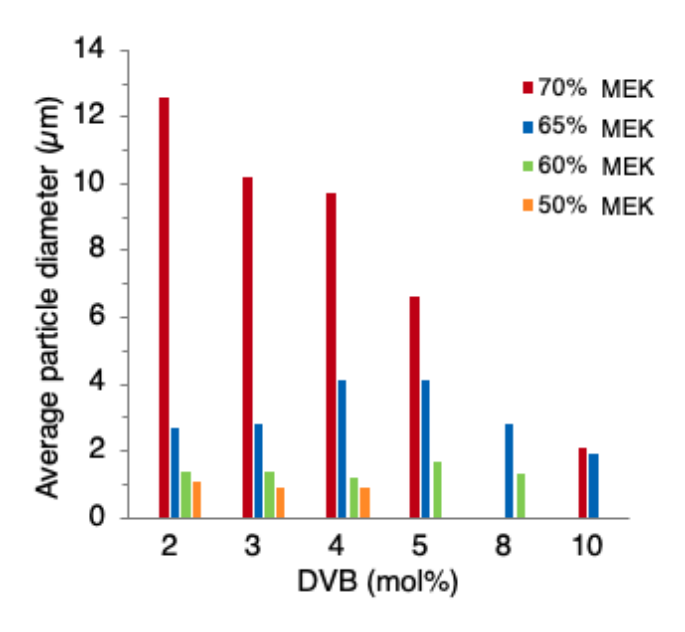


**Figure A3.1** Average particle diameters of poly(4MS-co-MAn-co-DVB) microgels swollen in neat MEK as a function of DVB mol% and MEK vol% as determined by optical microscopy. Microspheres synthesized in 50 vol% MEK with  $\geq$ 5 mol% DVB, as well as those made in 60vol% MEK with 10 mol% DVB are too small to resolve by optical microscopy, thus diameters are not reported. It is important to note that both THF ( $\delta = 18.6$  MPa1/2) and MEK ( $\delta = 19.1$  MPa1/2) are considered good solvents for the poly(styrene-alt-maleic anhydride) copolymer ( $\delta = 19.6$  MPa1/2), which can be used as a linear model for the microspheres presented in this work when selecting a solvent that will swell the polymer network (Grulke, E.A. In Polymer Handbook; Brandrup, J., Immergut, E.H., Grulke, E.A., Eds.; Wiley-Interscience. 1999; 675-714).

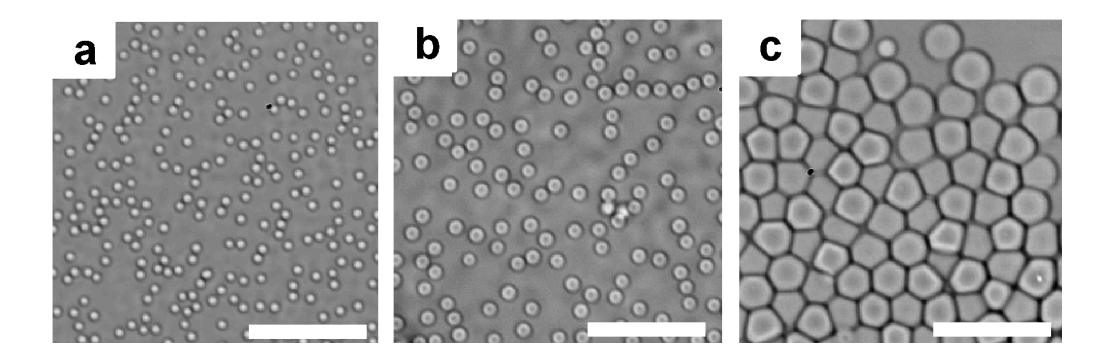


**Figure A3.2** Optical microscope images of microspheres made with a 4MS mol fraction of (a) 0.1, (b) 0.5 and (d) 0.9. Microspheres were made in solvent mixtures of 65 vol% MEK at 5 mol% DVB loading. Scale bars are 20  $\mu$ m.

vol% of solvent		Solubility Parameter (MPa <sup>1/2</sup> )			
MEK	Heptane	$oldsymbol{\delta}_{\sf d}$	$oldsymbol{\delta}_{ extsf{p}}$	$oldsymbol{\delta}_{h}$	δ
100	0	16.0	9.0	5.1	19.1
90	10	15.9	8.1	4.6	18.5
80	20	15.9	7.2	4.1	17.9
70	30	15.8	6.3	3.6	17.4
60	40	15.7	5.4	3.1	16.9
50	50	15.7	4.5	2.6	16.5
40	60	15.6	3.6	2.0	16.1
30	70	15.5	2.7	1.5	15.8
20	80	15.4	1.8	1.0	15.6
10	90	15.4	0.9	0.5	15.4
0	100	15.3	0.0	0.0	15.3

**Table A3.1.** Partial and total Hansen solubility parameters for MEK/heptane solvent mixtures. Estimated by  $\delta = \varphi_a \ \delta_a + \varphi_b \ \delta_b$ ; where  $\varphi$  is the volume fraction, and solvents (e.g. MEK and heptane) are represented by subscripts a and b.

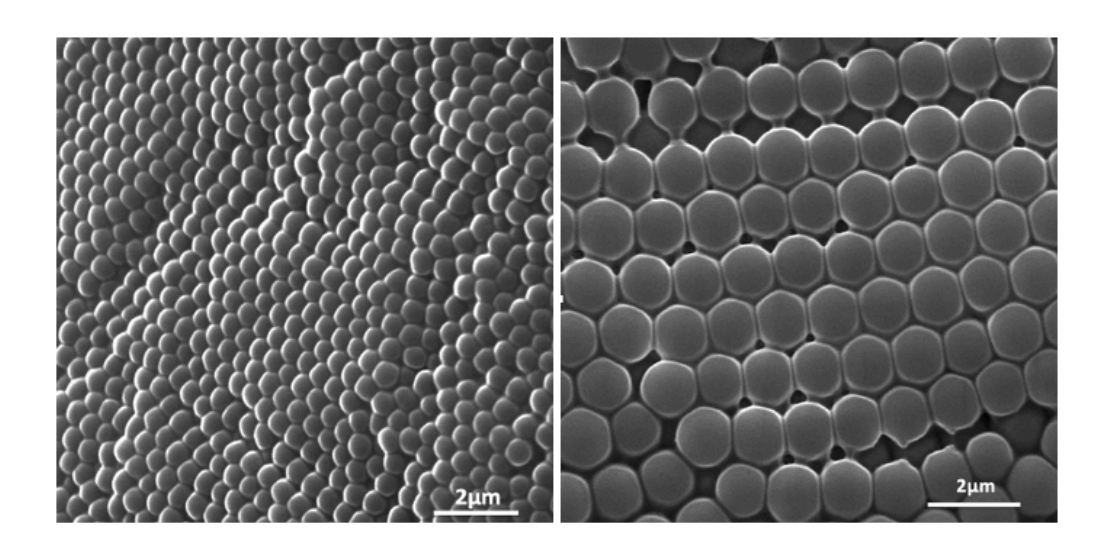


**Figure A3.3** Scanning electron micrographs of poly(4MS-co-MAn-co-DVB) microspheres crosslinked with 5 mol% DVB made in a) 40 and b) 60 vol% MEK. Accelerating voltage is 20kV

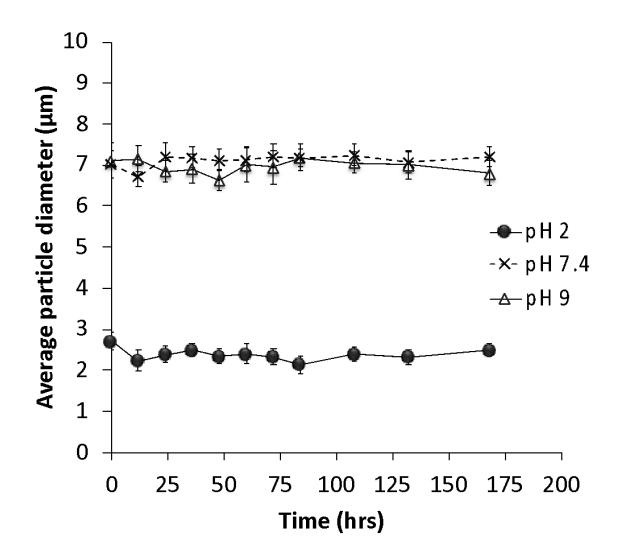


**Figure A3.4**. Average diameter of 5 mol% BDDA-crosslinked microgels over time at pH 2, 7.4 and 9, heated to 37°C. Error bars are a standard deviation of diameters measured by brightfield microscopy and analyzed using Nikon NIS elements imaging software.

## CHAPTER 4: Microgels formed by precipitation copolymerization of vinyl ethers and maleic anhydride

To be submitted for publication to J. Polym. Sci., Part A Polym Chem.

Sheilan Sinjari, Aleksandra Redzic, Heather Sweny, Swaroop Namathirtham, Mitchell Johnson,

#### Harald D.H. Stöver\*

Contributions: This research was designed by SS and HDHS. Experiments were planned by SS. Microgel syntheses and characterizations were carried out by SS, with assistance from AR and HS. NMR experiments were carried out by SS, with assistance from NB for analysis. Degradation experiments were designed by SS and carried out by SS and SN. Confocal experiments/protein binding experiments were designed by SS, and carried out by AR with assistance from MJ. NB and HDHS provided guidance and editing feedback for the writing of this chapter.

#### 4.1. ABSTRACT

The synthesis of reactive and polar microgels by free radical precipitation copolymerization of vinyl ethers with maleic anhydride (MAn) in methyl ethyl ketone (MEK)/heptane or MEK/acetonitrile (ACN) solvent mixtures is reported. Copolymerization of 2-hydroxyethyl vinyl ether (HEVE), MAn, and 1,4-butanediol divinyl ether (BDVE) in MEK-rich solvents yielded spherical microparticles with diameters of 1 to 7 μm when dispersed in THF. The largest microgel diameters were observed for polymerizations conducted in neat MEK with low (≤ 2.5 mol%) overall crosslinker loading. Varying the BDVE crosslinker between 2.5 and 7.5 mol% did not have a significant effect on particle size or dispersity, but increasing BDVE content above 10 mol% resulted in aggregation or macrogelation in the studied cosolvent regime. Interestingly, even in the absence of BDVE crosslinker, copolymerization of equimolar

amounts of HEVE and MAn in neat MEK produced crosslinked microspheres in isolated yields of up to 40%. The nature of this self-crosslinking reaction was probed by <sup>1</sup>H NMR, revealing a series of reactions involving HEVE, including intermolecular ester formation. The chemical stability of these self-crosslinked microgels was studied as a function of pH at 70 °C, using optical microscopy to track changes in particle diameter and morphology. Microgels suspended at pH 4 had slightly increased diameters after 48 hours of heating, while particles kept at pH 7 and 12 dissolved completely after 24 and 48 hours, respectively, suggesting the crosslinking involved ester linkages.

#### **4.2. INTRODUCTION**

Polymer microspheres represent a unique class of solvent-swollen particles that exhibit the properties of either hard spheres or soft microgels, depending on their swelling state.<sup>1,2</sup> There is considerable interest in water-swollen microgels, driven by their tendency to undergo rapid, reversible volume phase transitions (VPT) in response to different stimuli including temperature, pH, and ionic strength.<sup>3-7</sup> This responsive behaviour has motivated the study of such microgels in areas ranging from tissue engineering to fundamental colloid science.<sup>8-12</sup>

Precipitation polymerization is a well-established method for the synthesis of microspheres with narrow size distributions and surfactant-free surfaces. A major research effort of our group has been the synthesis of microgels and microspheres by precipitation copolymerization of crosslinking monomers in low-viscosity marginal solvents or solvent mixtures such as acetonitrile and MEK/heptane mixtures. Initially

demonstrated for the synthesis of divinylbenzene-55 (DVB) particles, the technique has since been extended to multiple styrenic and (meth)acrylic monomers, and maleic anhydride (MAn). Specifically, the rapid, alternating copolymerization of styrenic monomers with maleic anhydride affords high isolated particle yields (e.g.  $\geq$  70%) even at relatively low monomer loadings (4-6 wt%), while also providing a convenient handle for post-modification with a range of nucleophiles.

Recently, we reported on the synthesis of lightly cross-linked microgels from precipitation copolymerization of MAn, 4-methylstyrene (4MS) and DVB in MEK/heptane solvent mixtures.<sup>23</sup> Particles ranged from submicron, hard spheres to large, swellable microgels, depending on the volume fraction of MEK and the DVB crosslinker level. Hydrolysis of the succinic anhydride groups yielded deformable microgels of up to 20 µm in diameter, resembling mammalian cells. While the tunable nature of the poly(4MS-co-MAn-co-DVB) microgel system makes it an attractive candidate for biological model studies, the significant hydrophobic styrenic content can be undesirable in applications where non-specific protein adsorption must be avoided.

The present study is focussed on replacing 4MS and DVB with more polar, electron-rich vinyl ether-based monomers and crosslinkers, while retaining the reactive anhydride chemistry.

Vinyl ethers have a strong tendency for alternating radical copolymerization with electron-poor monomers including maleic anhydride, which should lead to copolymers with MAn content of 50 mol% that have high capacity for post-functionalization. Poly(methyl vinyl ether-*alt*-maleic anhydride) (PMMAn) is produced on an industrial

scale and has been widely used in biomedical research due to its ease of functionalization and hydrophilicity following anhydride hydrolysis. <sup>24-27</sup> While methyl vinyl ether is more hydrophilic than styrenic monomers, its low boiling point (6 °C) makes it inconvenient for the thermally initiated free radical copolymerizations used in this work. Butyl vinyl ether (bp = 94 °C) would be a better candidate but is more hydrophobic. For this reason, alkyl vinyl ethers bearing polar substituents such as hydroxyl groups were considered. Among the simplest hydroxy vinyl ethers is 2-hydroxyethyl vinyl ether (HEVE), a small, hydrophilic and commercially available monomer. A concern in pairing HEVE with MAn is the potential esterification reaction between the alcohol and anhydride, though this reaction is typically slow in organic solvents.<sup>28</sup> Thus, we explored the precipitation copolymerization of MAn with 2-hydroxyethyl vinyl ether (HEVE) and di(ethyleneglycol) vinylether (DEVE) in the presence of small amounts of 1,4-butanediol divinyl ether (BDVE) crosslinker.

In this work, a series of vinyl ether and maleic anhydride microgels were prepared by AIBN-initiated free radical copolymerization in neat MEK, or MEK/Heptane and MEK/acetonitrile (ACN) cosolvent mixtures, and the effects of solvent composition and crosslinker content on microgel morphology studied using optical microscopy.

**Scheme 4.1.** Precipitation polymerization of HEVE and MAn in MEK with 0 - 10 mol% BDVE as a crosslinker. Hydrolysis with aqueous base yields crosslinked microgels that swell in aqueous solutions of pH  $\geq$  4.

Interestingly, cross-linked particles were formed from HEVE and MAn even in absence of BDVE crosslinker, implying a crosslinking reaction. The chemical nature of self-crosslinking in these poly(HEVE-co-MAn) microgels was explored by <sup>1</sup>H-NMR and by examining the hydrolytic stability of self-crosslinked particles formed using HEVE and DEVE. Lastly, a proof-of-concept study is presented to compare the degree of protein binding to poly(4MS-co-MAn-co-DVB) microgels and poly(HEVE-co-MAn) microgels.

#### 4.3 EXPERIMENTAL

#### 4.3.1. Materials

2,2'-Azobis(2-methylpropionitrile) (AIBN, 99.9%) was purchased from Dupont and used as a 1.6 w/w% stock solution in MEK. Maleic anhydride (MAn, >98.5%), methyl ethyl ketone (MEK, ≥ 99%), n-heptane (>98.5%), acetonitrile (ACN, ≥ 99.5%), di(ethylene glycol) vinyl ether (DEVE, 98%), 1,4-butanediol divinyl ether (BDVE, 98%), 4-methylstyrene (4MS, ≥95.5%), divinylbenzene (DVB, ≥55% mixture of m- and p-divinylbenzene isomers), tetrahydrofuran (THF, ≥99.0%), dimethylformamide (DMF, ≥ 99.8%), DMSO-d₀ (99.9% D atom), acetonitrile-d3 (CD₃CN, 99.9% D atom), acetone-d₀ (99.9% D atom), ethylene carbonate (99%), anisole (99.5%), bovine serum albumin–fluorescein isothiocyanate conjugate (FITC-BSA) were purchased from Sigma-Aldrich and used as received. Tetramethylrhodamine 5-(and-6)-carboxamide cadaverine (TAMRA-cadaverine, 95%) was purchased from AnaSpec and used as received. 2-hydroxyethyl vinyl ether (HEVE, 97%) and di(ethyleneglycol) vinylether (DEVE, 98%) were purchased from Sigma-Aldrich and purified by precipitation in cold MEK to remove oligomers³7 and used as a 10 w/w% stock solution in MEK.

#### 4.3.2. Precipitation copolymerization of vinyl ethers and maleic anhydride

Microgel syntheses were adapted from a procedure previously reported for poly(MAn-4MS-DVB) particles.<sup>23</sup> The ratio of MAn to total vinyl ether (HEVE/DEVE and BDVE) vinyl groups was targeted at 1:1 to promote alternating polymerization, with total monomer loadings of 4 w/v% (monomer wt/solvent vol). The precipitation

copolymerization of HEVE, MAn, and 2.5 mol% BDVE in 94/6 (v/v) MEK/heptane, with a monomer loading of 4 wt%, is presented here as an example: in an 8 mL glass screw-cap vial, MAn (0.168 g, 1.71 mmol) was dissolved in 5.535 g (6.876 mL) of MEK and 0.328 g (0.480 mL) of heptane. To this solution, 0.40 g (0.50 mL) of AIBN stock solution (0.064 g/0.10 mmol AIBN, 2 wt% relative to monomers), 147 µL of HEVE stock solution (0.143 g, 1.63 mmol) and 11.6 µL of BDVE (11.5 mg, 0.08 mmol) were added. The 94:6 volume fractions of MEK and heptane were calculated using a density of 0.805 g/mL and 0.684 g/mL for MEK and heptane at 20 °C, respectively. Multiple vials were rotated at 7 rpm about their horizontal axis at 70 °C for 12–24 hrs on a commercial hotdog roller equipped with controlled resistive heating and an insulating cover. Polymerizations in mixed MEK/ACN solvents were carried out as described above, using ACN instead of heptane. In this work, most of the microgels were prepared in MEK/heptane and are identified by the vol% MEK and mol% BDVE used for synthesis. For example, "100/5" corresponds to poly(HEVE-co-MAn-co-BDVE) microgels prepared in 100% MEK with 5 mol% BDVE loading. For mixed solvents, the identity of the cosolvent, MEK or ACN, is explicitly stated in the text.

#### 4.3.3. Microgel isolation and purification

Microgels were purified by multiple centrifugation and resuspension cycles with THF as described in previous reports.<sup>23</sup> Briefly, microgels were sedimented by centrifugation at 3200g for 10 min, followed by resuspension in 40 mL total volume of THF. This washing procedure was repeated an additional three times, for four total wash cycles. After the

final wash cycle, the supernatant was carefully decanted and purified microgels were re-suspended to a total volume of 10 mL in THF. A 1 mL aliquot of microgel suspension was subsequently dried under nitrogen for 24 hrs to determine particle yield, which ranged from 30 to 50% for polymerizations carried out in neat MEK at crosslinker loadings of 0 to 10 mol% BDVE (Table A4.1).

#### 4.3.4. Fluorescent labeling and anhydride hydrolysis

Microgels were fluorescently labelled using TAMRA-cadaverine with a targeted labeling degree of 0.1 mol% relative to anhydride groups (0.05 mol% relative to polymer repeat units). A typical labeling experiment of 95/5 microgels is presented as an example. Briefly, 44 μL of a 1 mg/mL solution of TAMRA-cadaverine (8.6x10<sup>-5</sup> mmol) in DMF was added to 1 mL of a 1.6 wt% suspension of microgels in THF (0.086 mmol of anhydride). The mixture was mixed for 24 hours in the dark at room temperature (25 °C). Microgels were washed with DMF (three centrifugation cycles) and remaining anhydride groups hydrolyzed by reaction with a two-fold molar excess of 1.0 N NaOH for 15 min at room temperature (25°C). Microgel suspensions were diluted to a total volume of 25 mL with deionized water and rotated at 20 rpm for 12-18 hours to facilitate mixing. The final microgel suspension was washed three times with 15 mL of deionized water and resuspended to a total volume of 10 mL with PBS or deionized water, and stored in the dark at 4 °C.

## 4.3.5. Confocal microscopy - FITC-BSA protein binding

100/5 HEVE microgels and 70/6 4MS microgels, each labelled with 0.1 mol% TAMRA-cadaverine relative to microgel anhydride groups, were used in the following experiments. 70/6 poly(4MS-co-MAn-co-DVB) microgels were synthesized and purified as described above, using a 70/30 MEK/heptane mixture for the polymerization solvent, 6 mol% DVB and 4 wt% monomer loading. All microgels were washed and resuspended three times in 10 mL PBS prior to incubation with FITC-BSA. FITC-BSA, 1 mL at 0.01% w/w in PBS, was added to 500 μL aliquots of 100/5 HEVE or 70/6 DVB microgels. Suspensions were agitated at 4 rpm for 18 hours in the dark at room temperature (23 °C). Microgels were subsequently washed twice by centrifugation (3200 g, 10 min each) with 12 mL PBS to remove unbound FITC-BSA, then resuspended in 2 mL PBS. 100 μL of each microgel suspension was transferred to a 96 well plate and particles were allowed to settle for 1 hour prior to imaging. Microgel equatorial sections were imaged using a Nikon A1 Confocal Eclipse Ti microscope.

#### 4.3.6. Hydrolytic stability of poly(HEVE-co-MAn) microgels

Stability experiments were conducted using poly(HEVE-co-MAn) microgels synthesized in neat MEK at 4% total monomer loading, in absence of divinyl crosslinker BDVE. Microgels were synthesized and purified using the procedures listed in 4.3.2 and 4.3.3, respectively. Following purification and isolation by centrifugation, microgels were resuspended to a total volume of 10 mL in deionized water and converted to their succinic acid form by hydrolysis using 1N NaOH. Three, 2 mL aliquots (0.11 mmol, 19.2)

mg of polymer) of this hydrolyzed 100/0 HEVE microgel suspension were pipetted into 4 mL screw-cap vials and adjusted to pH 4.00, pH 7.00, or pH 12.0 using dilute HCl and NaOH solutions. Following pH adjustment, suspensions were heated at 70 °C without agitation in an oven. At t=0, 24 and 48 hrs, the suspensions were removed from the oven and agitated to ensure full mixing before imaging using a Nikon LV100ND equipped with a Zyla sCMOS 5.5 camera.

#### 4.3.8. <sup>1</sup>H NMR experiments

<sup>1</sup>H NMR spectra were collected using a Bruker AV 500 (500MHz) or AV 600 (600 MHz) spectrometer in DMSO-d<sub>6</sub>.

#### **4.4 DISCUSSION**

Initial attempts to prepare lightly crosslinked HEVE/MAn microspheres were based on the experimental conditions used previously to prepare 4-MS/MAn particles, including a 1:1 ratio of vinyl ether groups to MAn, 4% monomer loading, 0-10 mol% BDVE crosslinker and 2 wt% AIBN initiator. While MEK/heptane cosolvent mixtures containing about 70 v/v% MEK worked well for the 4MS/DVB/MAn system, it was anticipated that a more polar solvent would be required in the presence of the polar, hydroxy-functional HEVE. 15-23 For this reason, the polarity of the polymerization medium was adjusted by adding small amounts of either ACN or heptane to MEK.

## 4.4.1. Effects of polymerization solvent on microgel formation and morphology 4.4.1.1. Precipitation Polymerization in MEK/heptane and MEK/acetonitrile

#### cosolvent mixtures

The effect of reaction solvency on particle formation in precipitation polymerization has previously been explored for a range of styrenic and (meth)acrylic monomers, where matching polymer and solvent Hansen solubility parameters facilitated the formation of discrete, narrow-dispersed microspheres.<sup>15-23</sup> Typically, monomer systems containing more polar monomers (*e.g.* hydroxyethyl methacrylate, methacrylic acid) were found to require more polar solvents to stabilize the growing particle nuclei.<sup>21,22</sup>

To establish a solvency range for discrete microgel formation in vinyl ether/MAn copolymerizations, HEVE, MAn, and 2.5 mol% BDVE were first copolymerized in MEK/heptane cosolvent mixtures containing 85 - 100% MEK. For polymerizations carried out with MEK volume fractions < 95%, significant polymer deposition was observed on the walls of the glass reaction vessels. Particles obtained from these polymerizations were either sub-micron in diameter or irreversibly aggregated. When solvents containing ≥95% MEK were used, small, narrow-disperse particles were obtained in yields averaging 40%, which is typical for precipitation polymerizations with relatively low amounts of monomer and crosslinker. These results match previous results from the precipitation polymerization of styrenic or methacrylic monomers, where microgels formed across a cosolvent window from 70 to 100 vol% MEK.<sup>22,23</sup> Following particle isolation, 0.1 mol% of backbone anhydride groups in some of the microgels were

reacted with a rhodamine-based fluorescent label (TAMRA-cadaverine) to facilitate particle observation in the swollen state. In all cases, the remaining anhydride groups were hydrolyzed to yield water-swollen particles. The diameters of the water-swollen microgels ranged from 1 to 8 µm as assessed by optical and fluorescence microscopy, with the largest microgels obtained from polymerizations carried out in neat MEK, the most polar solvent used in this series of experiments. Figure 4.1 illustrates the change in microgel size and dispersity as polymerization solvency is increased from 95% to 100% v/v% MEK for microgels crosslinked with 2.5% BDVE. The trend of increasing particle diameter with increasing amount of good solvent (MEK) in the polymerization solvent aligns with previous chapters, where styrenic microgels exhibited similar solvent-dependent diameter changes.

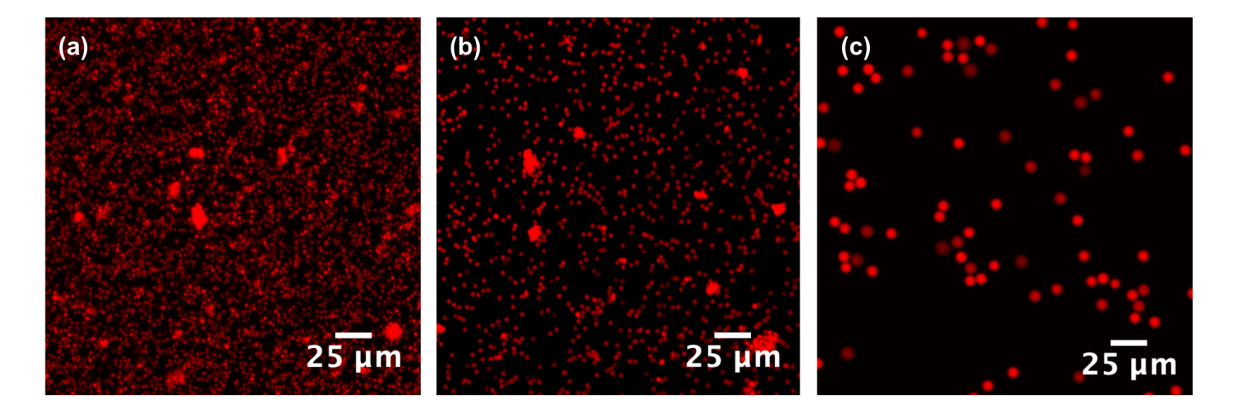


**Figure 4.1.** Poly(HEVE-*co*-MAn-*co*-BDVE) microgels made with 2.5 wt% BDVE crosslinker, formed in a) 95%, b) 97% and c) 100% v/v MEK as the polymerization solvent. Microgels were labelled with TAMRA-cadaverine at a targeted labeling of 0.1 mol% with respect to anhydride groups and re-suspended in deionized water prior to imaging.

#### 4.4.1.2. Polymerization in MEK/ACN mixtures

In our previous work on precipitation copolymerization of MAn and styrenic monomers (Chapter 3), microgels up to 20  $\mu$ m in diameter were formed using a combination of low crosslinker loadings and high volume fractions of good solvent (*e.g.* MEK) in the polymerization mixture.<sup>23</sup> With increasing solvency, the morphology of the polymer formed often changes from microgels to space-filling gels and even soluble branched polymer. Such transitions were not observed for the solvency and crosslinker range explored in poly(HEVE-*co*-MAn-*co*-BDVE) syntheses, suggesting that neat MEK ( $\delta_T = 19.1 \text{ MPa}^{1/2}$ ) does not yet exceed the upper limit of polymerization solvency for

microsphere formation. To reach a higher  $\delta_T$ , acetonitrile (ACN,  $\delta_T$  = 24.4 MPa<sup>1/2</sup>;  $\delta_D$ =15.3,  $\delta_p$ =16 and  $\delta_H$ = 8.1) was added to the polymerization solvent mixture in efforts to produce larger microgels.

Figure 4.2 shows both anhydride-form and hydrolyzed p(HEVE-MAn-BDVE) particles prepared in MEK/ACN mixtures comprising of 5 to 20 v/v% ACN. The particle diameter increases upon increasing the vol% of ACN in the polymerization mixture, reaching ~15  $\mu$ m for hydrolyzed microgels formed in presence of 20 vol% ACN. However, increasing ACN from 5% to 20% is also accompanied by a significant reduction in isolated particle yield to below 10%, attributed to narrowing of the  $\delta_T$  gap between polymer and solvent. The higher polymer solubility will decrease the efficiency of oligomer capture and precipitation, and thus increase the yield of soluble oligomers formed during the polymerization. These results correspond to analogous observations previously seen in 4MS/MAn/DVB copolymerizations, as described in Chapter 2.

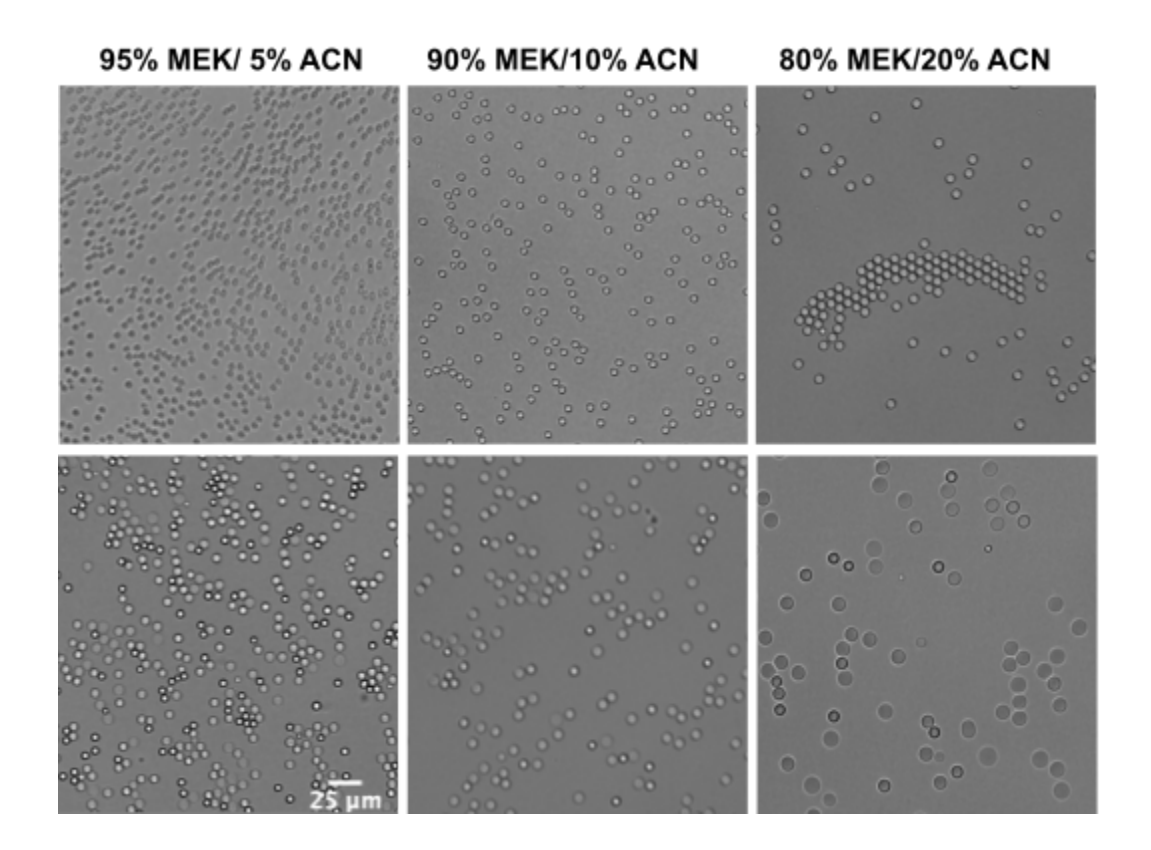


**Figure 4.2.** Optical images of HEVE-MAn microgels crosslinked with 2.5 % BDVE, prepared with MEK:ACN ratios in the polymerization mixture of 95:5, 90:10, and 80:20 (left to right). Anhydride-form microgels (top row) are suspended in DMF and succinic acid-form (bottom row) in saline (150 mM NaCl) at pH 7.

# 4.4.2. Effect of Crosslinker Loading on HEVE-MAn Polymerizations - Self cross-linking reactions

We further explored the effects of crosslinker on microgel morphology for polymerizations conducted in neat MEK. Polymerizations were conducted with BDVE content varying from 0 to 10 mol% at a constant monomer loading of 4 wt%. From previous work, we expected particle yield to decrease with decreasing crosslinker level,

with only soluble polymer formed in absence of crosslinker. Surprisingly, narrow-disperse particles were produced in good yields (30 - 50%) in all cases, including from copolymerization of HEVE and MAn alone in neat MEK (Figure 4.3).

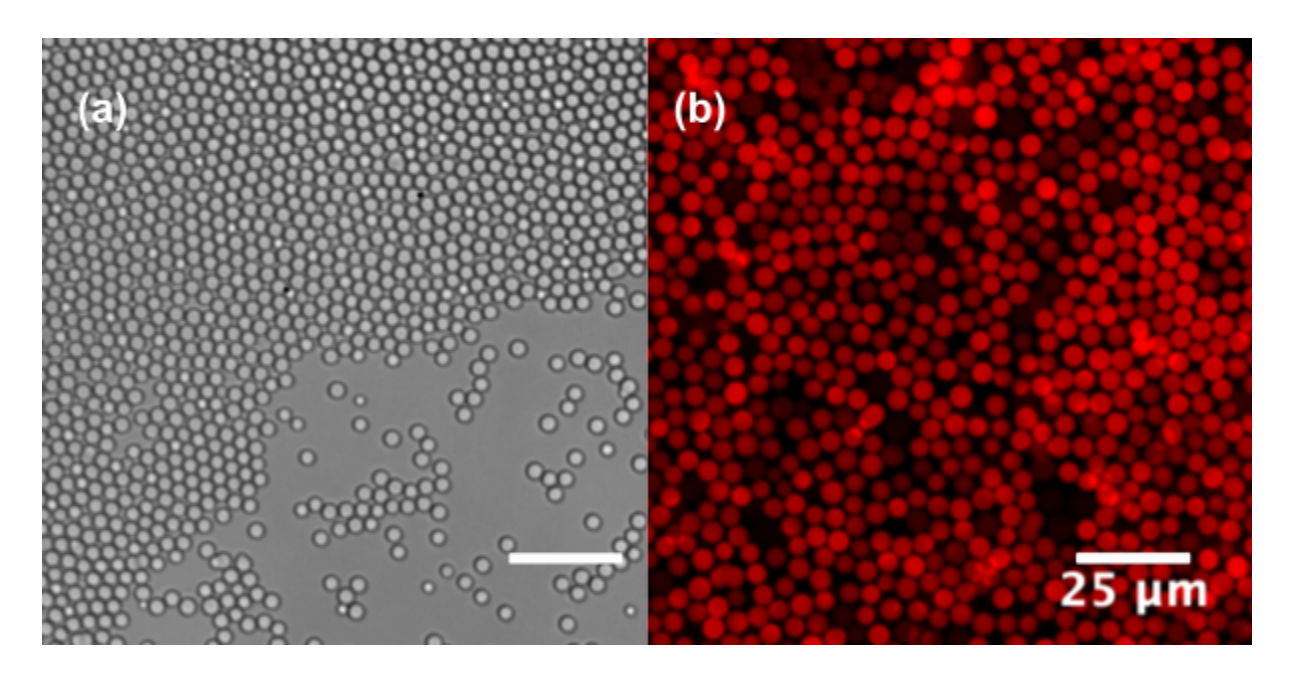


**Figure 4.3.** Brightfield (a) and fluorescence (b) images of poly(HEVE-co-MAn) microgels suspended in (a) THF and (b) phosphate buffered saline (PBS, pH = 7.4). For (b), 0.1 mol% of anhydride groups were labelled with TAMRA-cadaverine before hydrolysis of remaining anhydrides. Scale bars = 25  $\mu$ m

These poly(HEVE-*co*-MAn) particles prepared without BDVE crosslinker were stable in both organic solvents (*e.g.* THF and DMF; Fig. 4.3a) and aqueous solutions (pH 7.4, Fig. 4.3b) following hydrolysis of anhydrides, suggesting that the particles are covalently crosslinked.

Self-crosslinking events in free-radical polymerizations are common, often resulting from hydrogen abstraction from the polymer backbone or side chain, followed by radical coupling.<sup>29–31</sup> Although radical coupling is possible due to the multiple activated methylene and methine hydrogens in poly(HEVE-*co*-MAn), covalent crosslinking may also proceed via intermolecular esterification between HEVE hydroxyl groups and anhydride on neighbouring chains, a reaction that can occur both before and after polymerization.

To further probe the mechanism of crosslinking, <sup>1</sup>H NMR was used to follow the reactions of the monomers. HEVE, MAn (10 wt%), and AIBN (2 wt% relative to total monomers) were dissolved in DMSO-d<sub>6</sub> and heated at 50 °C in the spectrometer, with <sup>1</sup>H NMR spectra collected at regular intervals (Fig. 4.4: 3 – 5 ppm region, and Fig. 4.5: full spectrum).

Peaks due to HEVE at 3.6, 3.7, 4.0, 4.2, and 6.5 ppm (not shown in Fig. 4.4) disappeared completely within 150 min, while a new set of peaks for 2-methyl-1,3-dioxolane appeared at 1.25 (not shown), 3.65, 3.9, and 4.9 ppm. 2-methyl-1,3-dioxolane is an isomer of HEVE formed by acid-catalyzed cyclization, a well-known reaction for hydroxyalkyl vinyl ethers.<sup>32–38</sup> In addition to cyclization, in the presence of traces of water, and catalyzed by of succinic acid, some of the dioxolane hydrolyzes to acetaldehyde and ethylene glycol (Fig. 4.5).

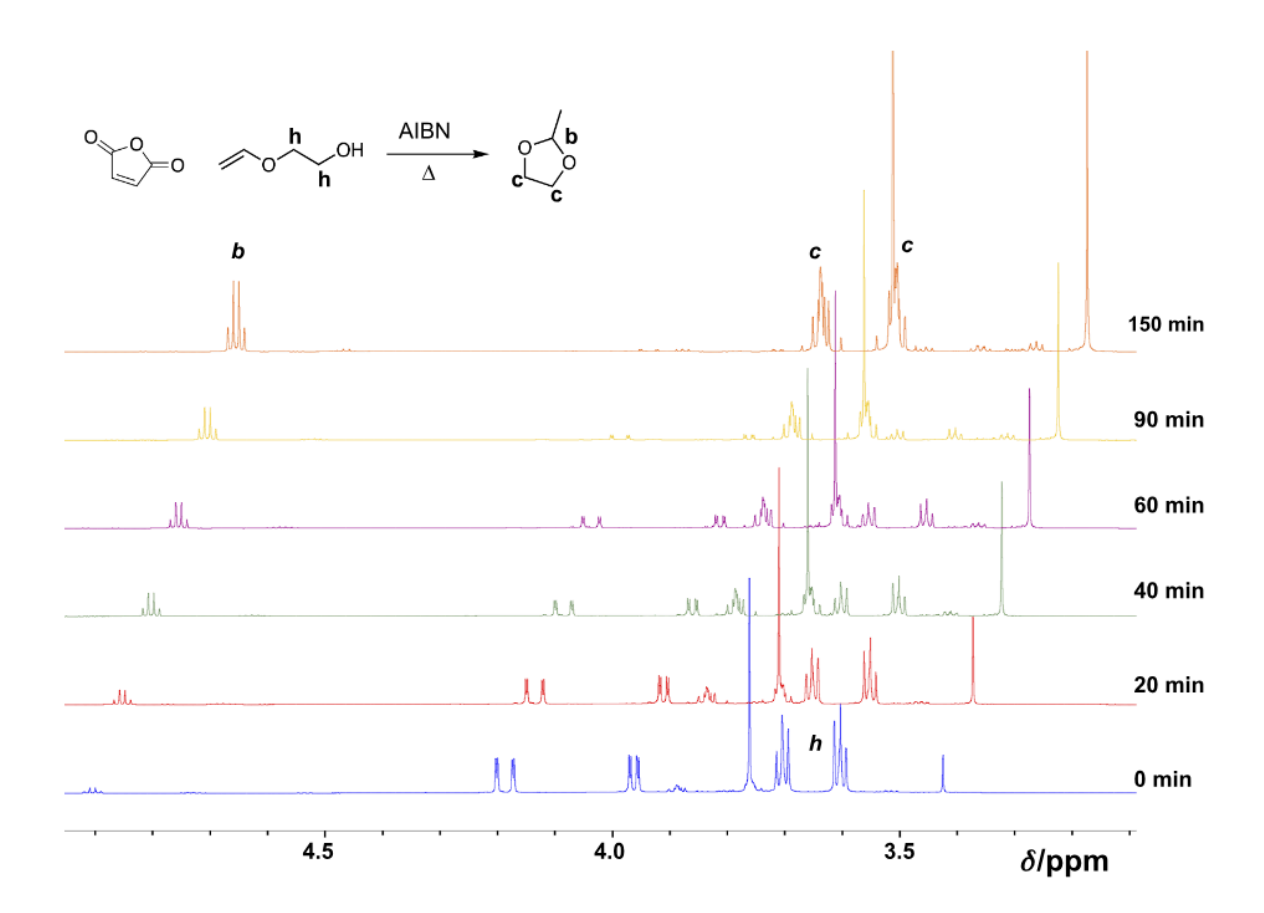


**Figure 4.4.** <sup>1</sup>H NMR spectrum of HEVE and MAn showing acetal formation with time during heating at 50 °C in DMSO-d<sub>6</sub>. Monomer loading was 10 wt%, with 2 wt% AIBN relative to total monomer content. Anisole was used as an internal standard. Offset is 0.05 ppm.

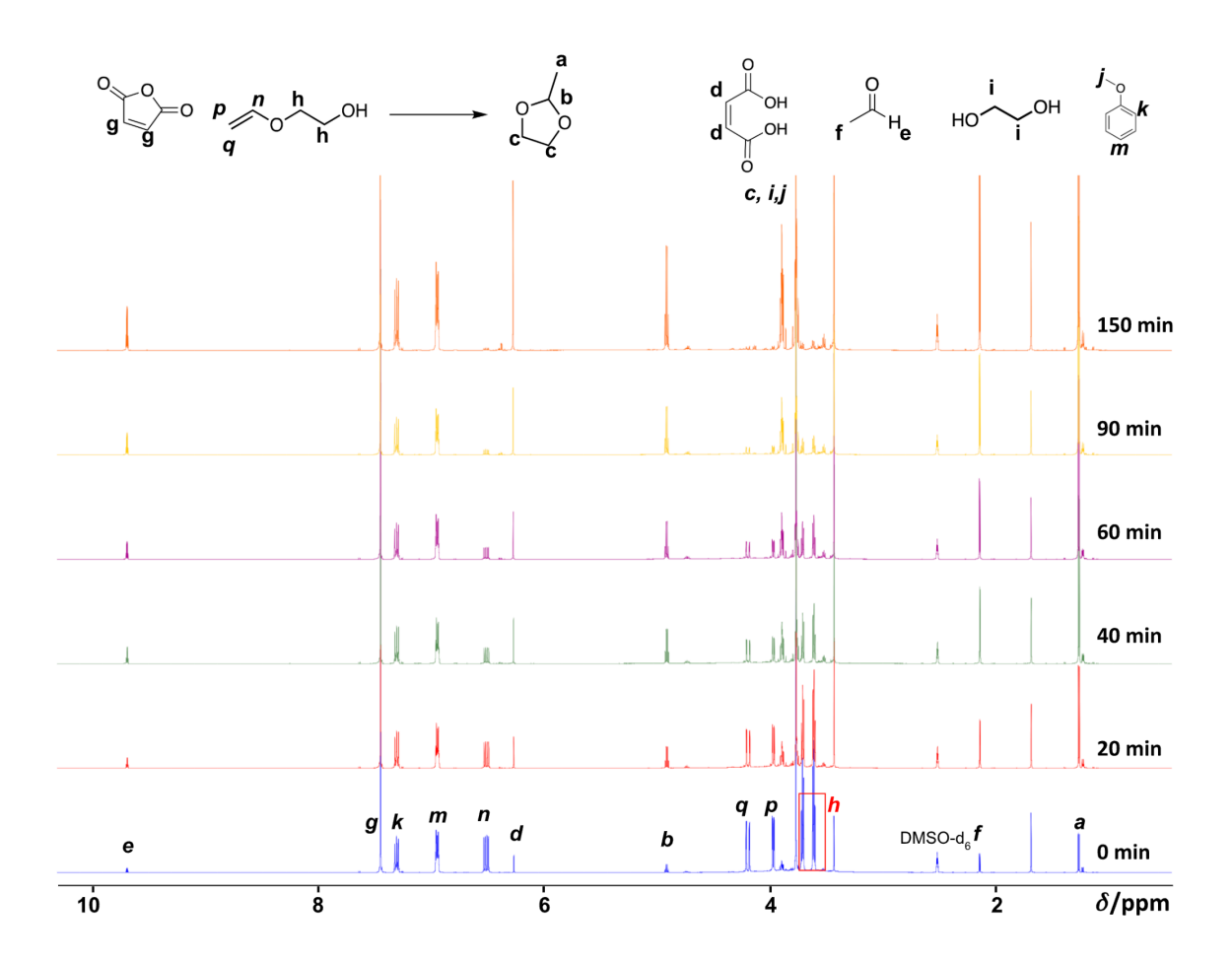


**Figure 4.5.** Overlaid full <sup>1</sup>H NMR spectra of HEVE and MAn showing changes with time during heating to 50 °C. Anisole was used as an internal standard.

While this study was originally designed to probe ester formation, there is little evidence of this reaction at 150 min (Fig. 4.5, orange spectrum), suggesting that the ester may only be formed during reaction of MAn with HEVE hydroxyl groups at elevated temperatures, and after longer periods of time.

Figure 4.6 shows evidence of ester formation when heating at 50 °C is extended to 24 hrs: peaks at 6.41 ppm (1H, d, J=12Hz), 6.37 ppm (1H, d, J=12 Hz), 4.1 ppm (2H, t), and 3.6 ppm (2H, t) are indicative of a maleic acid half ester, the product from MAn ring-opening by an alcohol by ethylene glycol or by HEVE hydroxyl groups on neighbouring polymer chains. The data show that after 24 hrs, about 10% MAn remains, while 75% has been converted to succinic acid and ~15% to ester. The large amount of acid suggests presence of a significant amount of water leading to hydrolysis of the maleic anhydride used.

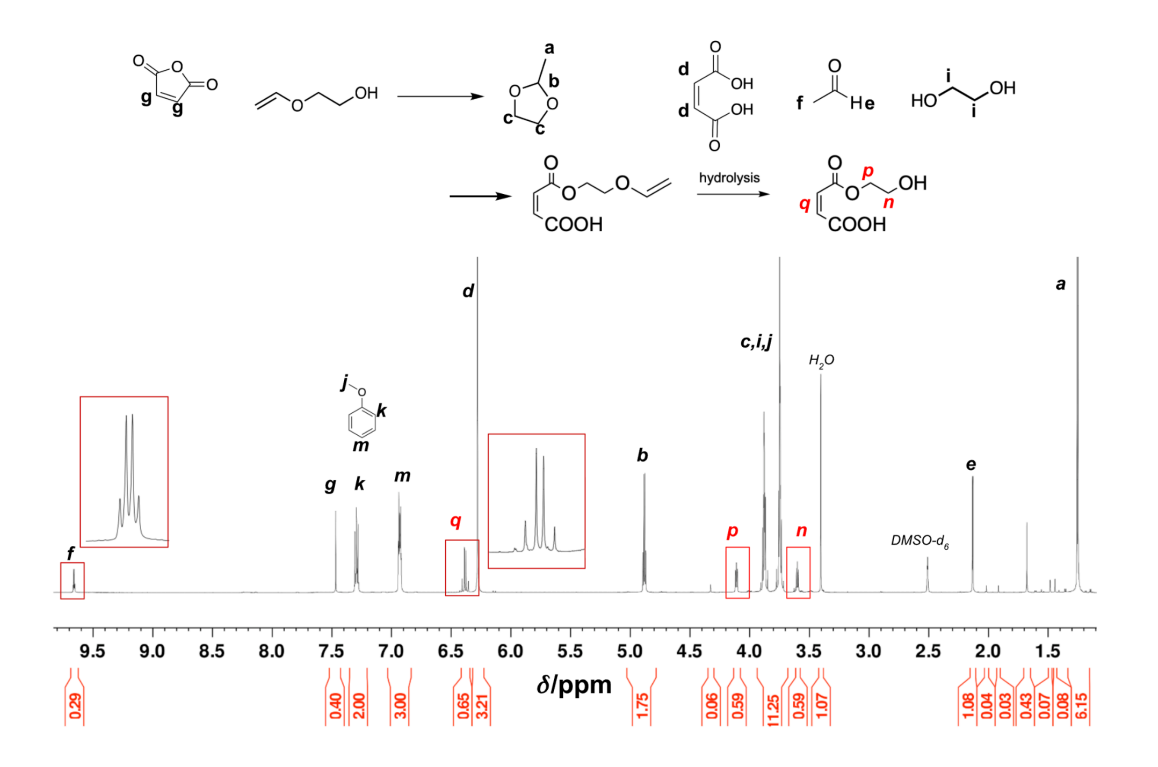


**Figure 4.6.** <sup>1</sup>H NMR spectrum of HEVE and MAn after 24 hours of heating at 50°C in DMSO-d<sub>6</sub>. Monomer loading is 10 wt%, with 2 wt% AIBN relative to total monomer content and anisole as an internal standard. Reactions outlined in red depict the possible ring opening of MAn with HEVE, followed by hydrolysis of the vinyl ether group to yield acetaldehyde and the maleic acid half ester.

Assuming that the observed reactions and their rates are similar in MEK compared to DMSO, it suggests that polymerization must take place before HEVE is converted. Copolymerization of MAn and HEVE as electron-poor and electron-rich comonomers is known to be rapid, and microgels are largely formed within 90 minutes, with the ester crosslinking occurring at least in part after polymerization. This implies that crosslinking by esterification between polymer-bound anhydride and alcohol groups will continue until the as-formed particles are hydrolyzed to their succinic-acid forms. Microgels would hence become increasingly crosslinked the older they are, where those hydrolyzed just after polymerization should be more swellable and degradable than those that have been aged (e.g. allowed to crosslink for longer). This may be further explored in subsequent studies.

The data show that acetalization and hydrolysis (HEVE and MAn) are fairly rapid, so the good yield (30 - 50%) of particles also reflects that polymerization occurs at a comparable or faster rate. The relatively slow formation of ester seen in the NMR experiment suggests that ester crosslinks in the particles are formed post-polymerization by reaction of a polymer-bound anhydride with polymer-bound hydroxy groups of HEVE. Future work will explore NMR experiments at conditions closer to those used in polymerization, e.g.  $70^{\circ}$ C, with similar solvency conditions (e.g. MEK-d<sub>8</sub>).

#### 4.5. Reactions between DEVE and MAn

Cyclization of hydroxyalkyl vinyl ethers to form cyclic acetals occurs efficiently when the products are five- or six-membered rings, but less so for larger rings.<sup>32</sup> In efforts

to reduce the loss of vinyl ether through the dioxolane path, the use of diethylene glycol vinyl ether (DEVE) was explored. DEVE, an analog of HEVE, is also hydrophilic and was expected to show similar copolymerization rates with MAn. However, acid-catalyzed cyclization to an 8-membered cyclic acetal would be comparatively slower, potentially allowing greater conversion to polymer.

While microgels were not isolated from DEVE/MAn copolymerizations conducted in neat MEK or MEK/Heptane mixtures, Fig 4.7 shows that cyclization proceeds slowly, as indicated by the absence of acetal methine signal (4.8ppm, 1H) for the first 150 minutes of reaction. Consistent with the HEVE/MAn reaction, DEVE vinyl signals have almost entirely disappeared by 90 min (Fig. 4.7, yellow spectrum), with no significant evidence of ester formation until 24 hours (Fig. 4.8). Unlike HEVE, the primary loss pathway of DEVE appears to be conversion of the monomer to diethylene glycol and acetaldehyde. After heating for 24 hours, similar peaks to those seen with HEVE/MAn were observed in the 1H NMR spectrum of DEVE/MAn (Fig. 4.8). Acetal methine protons appear in the 4.7ppm region, with characteristic ester signals at 6.41 ppm (1H, dd, J=12Hz), 4.1, and ~3.6ppm.

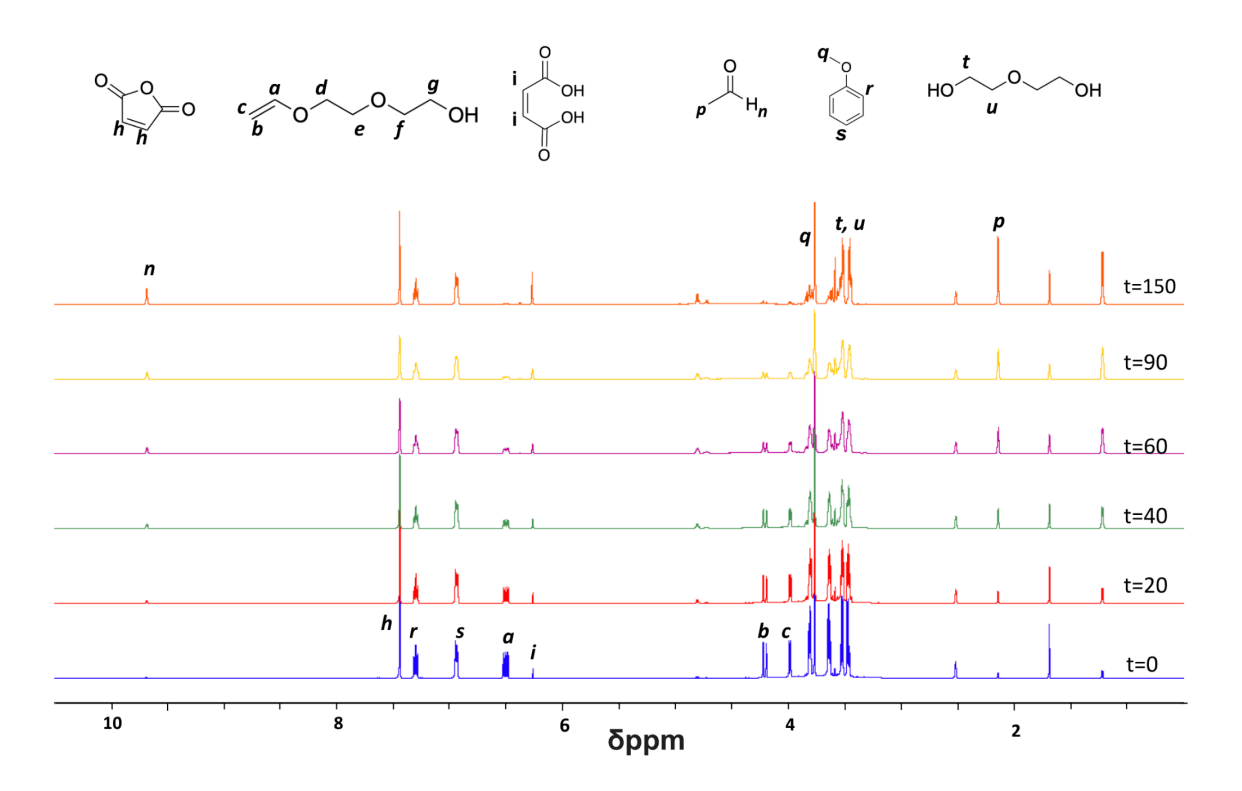


**Figure 4.7.** Stacked 1D <sup>1</sup>H NMR spectra of diethylene glycol monovinyl ether (DEVE) and MAn after heating at 50°C in DMSO-d<sub>6</sub> (0 min to 150 min). Monomer loading was 10 wt%, with 2wt% AIBN relative to total monomer content, with anisole as an internal standard.

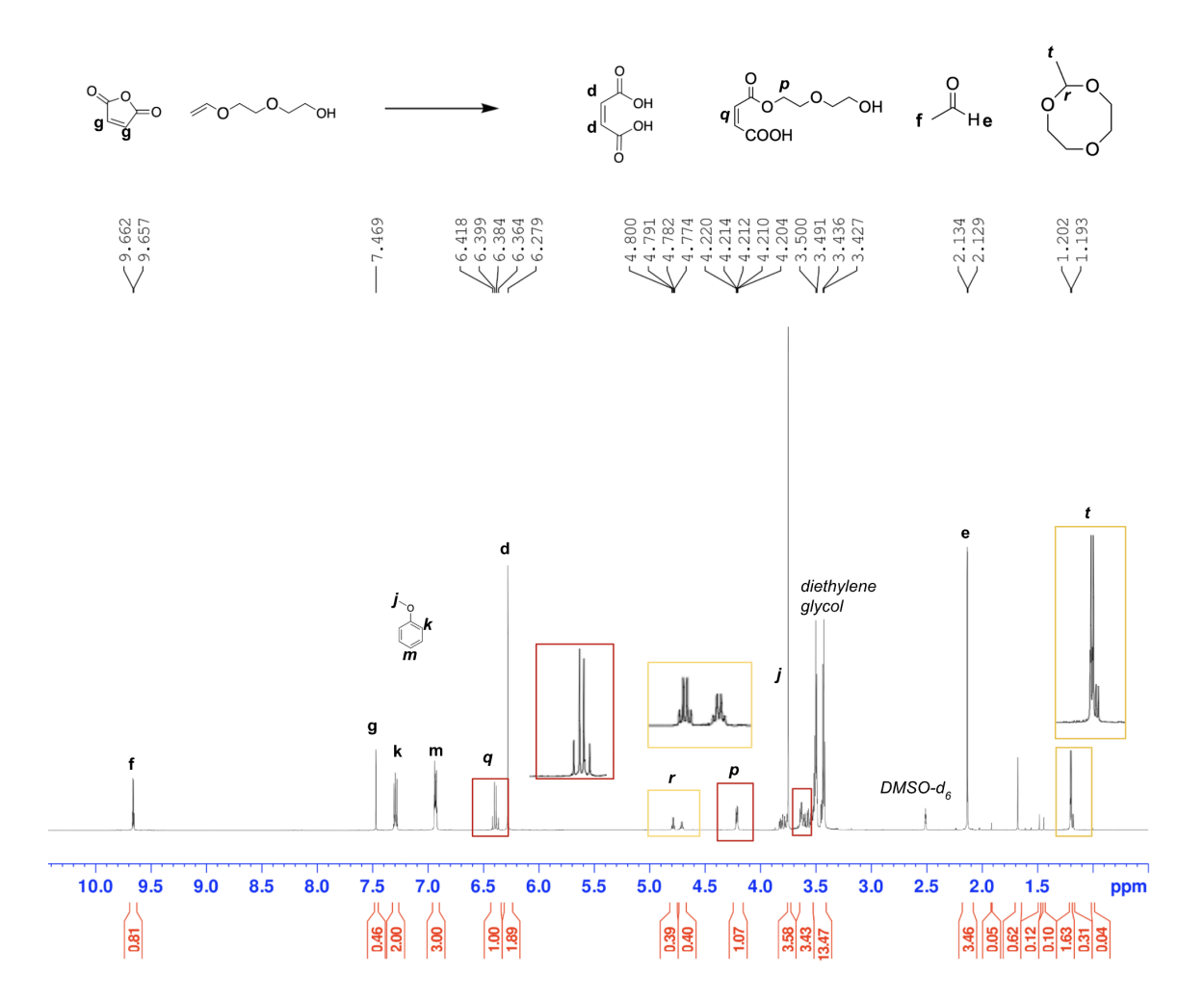


**Figure 4.8.** <sup>1</sup>H NMR spectrum of reaction with diethylene glycol monovinyl ether (DEVE) and MAn after 24 hours of heating at 50°C in DMSO-d<sub>6</sub>. Monomer loading was 10 wt%, with 2wt% AIBN relative to total monomer content, with anisole used as an internal standard.

After 24 hours, the DEVE monomer has been converted to acetal(s), reacted to form maleic acid half-ester, or hydrolyzed to yield diethylene glycol and acetaldehyde. The apparently lower rates of acetal formation suggest an opportunity to increase yield of

polymer microgels once an appropriate solvency range for precipitation polymerization is determined, but this was not further pursued in this study. Future work will include a time series at 50°C and 70°C showing progress of side-reactions relative to conversions of polymer.

## 4.4.3. poly(HEVE-co-MAn) Microgel Degradation via Hydrolysis

The ester crosslinks formed during and following polymerization are succinic half-esters and should be sensitive to hydrolysis due to neighbouring group effects. This suggests that these crosslinks should be cleavable under fairly mild conditions. In absence of BDVE, these microgels would dissolve, while in presence of low amounts of BDVE, they may swell but should persist.

As a qualitative test for ester crosslinking, 100/0 microgels were heated in aqueous suspension at pH 4, 7, or 12 to 70 °C for up to 48 hours. Optical microscopy was used to assess changes in particle morphology over this time period (Fig. 4.9).

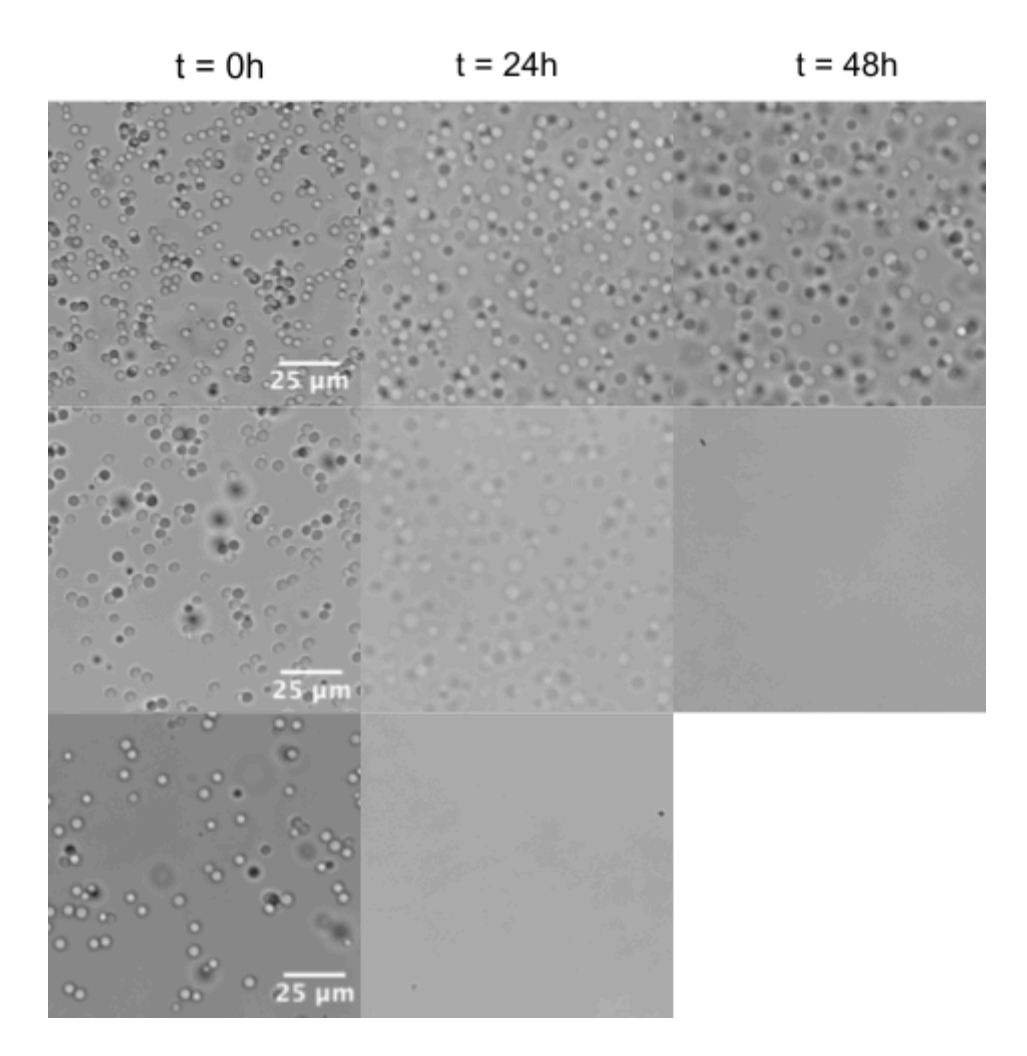


**Figure 4.9.** Brightfield images of 100/0 microgels suspended in pH 4 (top row), pH 7 (middle row) and pH 12 (bottom row) solutions and heated to 70°C for 24 to 48 hours. Microgels heated in pH 12 solution were completely degraded after 24 hours.

Here, particle degradation is evident after 24 and 48h at pH 12 (Fig. 4.9, bottom row) and pH 7 (Fig. 4.9, middle row), respectively, and negligible at pH 4, in agreement with the minimum rate of ester hydrolysis between pH 3 and 4.

## 4.4.4. Comparison of protein binding to vinyl ether and styrenic microgels

A proof-of-concept study was performed to compare the anti-fouling properties of poly(HEVE-co-MAn) microgels and analogous poly(4MS-co-MAn-co-DVB) microgels against bovine serum albumin (BSA) (Fig. 4.8). Microgels were incubated with fluorescent BSA (FITC-BSA) protein (0.01wt%) and imaged after washing with PBS with confocal microscopy. From Figure 4.8, styrenic microgels (Fig 4.8 A) adsorb a significant amount of protein compared to vinyl ether microgels (Fig 4.8 B), which do not exhibit noticeable binding of FITC-BSA. Future studies should address differences in particle concentration and swelling capacity, as HEVE microgels have a modest swelling ratio compared to styrenic particles. Additionally, a more complex and representative protein should be used to assess anti-fouling behaviour of vinyl ether particles.

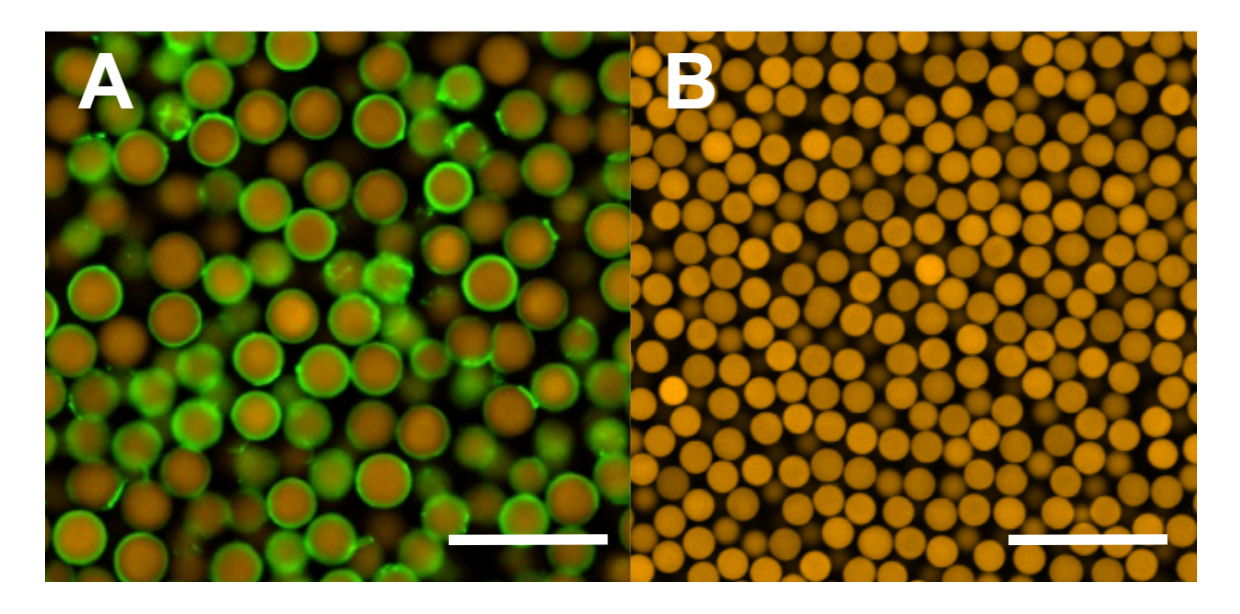


**Figure 4.10.** Confocal images of A) 70/6 poly(4MS-*co*-DVB-*co*-succinic acid), and B) 100/5 poly(HEVE-*co*-succinic acid) microgels after incubation with 0.01wt% FITC-BSA. Microgels were washed with PBS with two centrifugation cycles and allowed to settle prior to imaging. Microgels are labelled with 0.1 mol% TAMRA-cadaverine. Scale bars are 50μm.

#### 4.5. CONCLUSIONS

A series of hydrophilic microgels was prepared by precipitation copolymerization of two vinyl ether monomers and maleic anhydride (MAn) in methyl ethyl ketone (MEK) and MEK cosolvent mixtures. Copolymerization of hydroxy ethyl vinyl ether (HEVE), MAn with 2.5 or 5 mol% butanediol divinyl ether (BDVE) in 94 - 100 v/v% MEK produced narrow-disperse microgels in isolated yields of 30 - 50%, with diameters ranging from 1 to 7 µm when swollen in THF, with largest particles formed in neat MEK as polymerization solvent. Microgel diameter increased to 11 µm upon incorporation of up to 20 vol% ACN as cosolvent, though with decreased vields. HEVE/MAn copolymerizations in neat MEK led to uniform particles formed at BDVE loadings  $\leq 7.5$ mol%, and macrogelation and aggregation at higher loadings of 20-30 mol% BDVE. Crosslinked microgels were also formed without added BDVE, in isolated yields of up to 40%. These self-crosslinked poly(HEVE-co-MAn) microgels had diameters of ~9 um when swollen in water at pH 7.4, and were stable in room temperature agueous solutions at pH 4 to 9. When heated in acidic and basic solutions, self-crosslinked microgels degraded at 70°C over 24 to 48 hours at pH 7 and 12, but remained stable at pH 4, supporting the notion that crosslinking involved ester formation between polymeric HEVE hydroxy and succinic anhydride groups. <sup>1</sup>H NMR revealed cyclic acetal formation, as well as maleic half-ester formation from the reaction between HEVE and MAn in DMSO-d<sub>6</sub>.

## 4.6. REFERENCES

- Mourran, A.; Wu, Y.; Gumerov, R. A.; Rudov, A. A.; Potemkin, I. I.; Pich, A.;
   Möller, M. When Colloidal Particles Become Polymer Coils. *Langmuir* 2016, 32, 723–730
- 2) Scotti, A.; Bochenek, S.; Brugnoni, M.; Fernandez-Rodriguez, M. A.; Schulte, M. F.; Houston, J. E.; Gelissen, A. P. H.; Potemkin, I. I.; Isa, L.; Richtering, W. Exploring the colloid-to-polymer transition for ultra-low crosslinked microgels from three to two dimensions. *Nat. Commun.* 2019, 10, 1418
- 3) Pelton, R.; Chibante, P. Preparation of aqueous lattices with N-isopropylacrylamide. *Colloids Surf.* **1986**, *20*, 247–256
- 4) Debord, J.D.; Lyon, L.A. Synthesis and Characterization of pH-Responsive Copolymer Microgels with Tunable Volume Phase Transition Temperatures. *Langmuir.* **2003**, *19*, 7662–7664
- 5) Su, W.; Yang, M.; Zhao, K.; Ngai, T. Influence of charged groups on the structure of microgel and volume phase transition by dielectric analysis. *Macromolecules*. **2016**, *49*, 7997–8008
- 6) Elancheliyan, R.; Del Monte, G.; Chauveau, E.; Sennato, S.; Zaccarelli, E.; Truzzolillo, D. Role of charge content in the Two-Step Deswelling of Poly(N-isopropylacrylamide)-Based Microgels. *Macromolecules*. 2022, 55, 7526–7539

- 7) Snowden, M. J.; Chowdhry, B. Z.; Vincent, B.; Morris, G. E. Colloidal copolymer microgels of N-isopropylacrylamide and acrylic acid: pH, ionic strength and temperature effects. *J. Chem. Soc., Faraday Trans.* **1996**, *92*, 5013–5016
- 8) Feng, Q.; Li, D.; Li, Q.; Cao, X.; Dong, H. Microgel assembly: Fabrication, characteristics and application in tissue engineering and regenerative medicine. *Bioact. Mater.* **2022**, *9*, 105–119
- 9) Pellet, C.; Cloitre, M. The glass and jamming transitions of soft polyelectrolyte microgel suspensions. *Soft Matter.* **2016**, *12*, 3710–3720.
- 10) Pusey, P. N.; Van Megen, W. Phase behaviour of concentrated suspensions of nearly hard colloidal spheres. *Nature*. **1986**, *320*, 340–342
- 11) Appel, J.; Fölker, B.; Sprakel, J. Mechanics at the glass-to-gel transition of thermoresponsive microgel suspensions. *Soft Matter.* **2016**, *12*, 2515–2522.
- 12) Sierra-Martin, B.; Fernandez-Nieves, A. Phase and non-equilibrium behaviour of microgel suspensions as a function of particle stiffness. *Soft Matter.* **2012**, *8*, 4141
- 13) Limé, F.; Irgum, K. Monodisperse Polymeric Particles by Photoinitiated Precipitation Polymerization. *Macromolecules*. **2007**, *40*, 1962–1968
- 14) Bai, F.; Huang, B.; Yang, X.; Huang, W. Synthesis of monodisperse poly(methacrylic acid) microspheres by distillation–precipitation polymerization. *Eur. Polym. J.* **2007**, *43*, 3923–3932
- 15) Li, K.; Stöver, H. D. H. Synthesis of monodisperse poly(divinylbenzene) microspheres. *J. Polym. Sci., Part A: Polym. Chem.* **1993**, *31*, 3257–3263

- 16) Li, W.-H.; Stöver, H. D. H. Monodisperse Cross-Linked Core-Shell polymer microspheres by precipitation polymerization. *Macromolecules*. 2000, 33, 4354–4360
- 17) Downey, J. S.; McIsaac, G.; Frank, R. S.; Stöver, H. D. H. Poly(divinylbenzene) Microspheres as an Intermediate Morphology between Microgel, Macrogel, and Coagulum in Cross-Linking Precipitation Polymerization. *Macromolecules*. **2001**, *34*, 4534–4541.
- 18) Downey, J. S.; Frank, R. S.; Li, W.-H.; Stöver, H. D. H. Growth Mechanism of Poly(divinylbenzene) Microspheres in Precipitation Polymerization. *Macromolecules.* 1999, 32, 2838–2844.
- 19) Frank. R. S.; Downey. J. S.; Yu, K.; Stöver. Н. D. H. Poly(divinylbenzene-*alt*-maleic anhydride) Microgels: Intermediates to Microspheres and Macrogels in Cross-Linking Copolymerization. Macromolecules. 2002, 35, 2728–2735.
- 20) Zhao, Y.; Burke, N. A. D.; Stöver, H. D. H. Structured poly(divinylbenzene-co-chloromethylstyrene) microspheres by thermal imprinting precipitation polymerization. *J. Polym. Sci., Part A: Polym. Chem.* **2015**, *54*, 1159–1166
- 21) Li, W. H.; Stöver, H. D. H. Monodisperse or narrow poly(methacrylate-*co*-divinylbenzene) microspheres precipitation by polymerization. J. Polym. Sci., Part A: Polym. Chem. 1999, 37, 2899–2907
- 22) Goh, E. C. C.; Stöver, H. D. H. Cross-Linked Poly(methacrylic acid-co-poly(ethylene oxide) methyl ether methacrylate) Microspheres and

- Microgels Prepared by Precipitation Polymerization: A Morphology Study. *Macromolecules.* **2002**, *35*, 9983–9989.
- 23) Sinjari, S.; Freitag, J. S.; Herold, C.; Otto, O.; Smith, D. M.; Stöver, H. D. H. Tunable polymer microgel particles and their study using microscopy and real-time deformability cytometry. *J. Polym. Sci.* **2020**, *58*, 2317–2326
- 24) Arbós, P.; Wirth, M.; Arangoa, M. A.; Gabor, F.; Irache, J. M. Gantrez® AN as a new polymer for the preparation of ligand–nanoparticle conjugates. *J. Control. Release.* **2002**, *83*, 321–330
- 25) Moreno, E.; Schwartz, J.; Larrañeta, E.; Nguewa, P. A.; Sanmartín, C.; Agüeros, M.; Irache, J. M.; Espuelas, S. Thermosensitive hydrogels of poly(methyl vinyl ether-co-maleic anhydride) Pluronic® F127 copolymers for controlled protein release. *Int. J. Pharm.* 2014, 459, 1–9
- 26) Gardner, C.M.; Burke, N.A.D.; Chu, T.; Shen, F.; Potter, M.A.; Stöver, H.D.H. Poly(methyl vinyl ether-alt-maleic acid) Polymers for Cell Encapsulation. *J. Biomater. Sci., Polym. Ed.* 2011, 22, 2127–2145.
- 27) Stewart, S.A.; Backholm, M.; Burke, N.A.D.; Stover, H.D.H. Cross-Linked Hydrogels Formed through Diels–Alder Coupling of Furan- and Maleimide-Modified Poly(methyl vinyl ether-alt-maleic acid). *Langmuir*. **2016**, *32*, 1863–1870
- 28) Aoyagi, J.; Shinohara, I. Esterification of styrene–maleic anhydride copolymer by mixed alcohols. *J. Appl. Polym. Sci.* **1972**, *16*, 449–460.

- 29) Gu, L.M.; Zhu, S.P.; Hrymak, A.N.; Pelton, R.H. The Nature of Crosslinking in N-Vinylformamide Free-Radical Polymerization. *Macromol. Rapid Commun.* 2001, 22, 212–214
- 30) Gao, J.; Frisken, B. J. Cross-Linker-Free N-Isopropylacrylamide gel nanospheres. *Langmuir.* **2003**, *19*, 5212–5216.
- 31) Welsch, N.; Lyon, L. A. Oligo(ethylene glycol)-sidechain microgels prepared in absence of cross-linking agent: Polymerization, characterization and variation of particle deformability. *PLoS one.* **2017**, *12*, e0181369
- 32) Shostakovsky, M. F.; Gershtein, N. A.; Volkova, Z. S. Reactions of vinyl ethers Communication VIII. Reactions of acetals derived from ethylene glycol. *Bull. Acad. Sci. USSR Div. Chem. Sci.* **1953**, *2*, 89–95.
- 33) Zhang, H.; Ruckenstein, E. Self-Polyaddition of Hydroxyalkyl Vinyl Ethers. *J. Polym. Sci., Part A: Polym. Chem.* **2000**, *38*, 3751–3760.
- 34) Hashimoto, T.; Ishizuka, K.; Umehara, A.; Kodaira, T. Synthesis of Polyacetals with Various Main-Chain Structures by the Self-Polyaddition of Vinyl Ethers with a Hydroxy Function. *J. Polym. Sci., Part A: Polym. Chem.* **2002**, 40, 4053–4064.
- 35) Boucher, D.; Laviéville, S.; Ladmiral, V.; Negrell, C.; Leclerc, E. Hemiacetal esters: synthesis, properties, and applications of a versatile functional group. *Macromolecules.* **2024**, 57, 810–829
- 36) Otsuka, H.; Endo, T. Poly(hemiacetal ester)s: New Class of Polymers with Thermally Dissociative Units in the Main Chain. *Macromolecules*. **1999**, *32*, 9059–9061

- 37) Boucher, D.; Madsen, J.; Caussé, N.; Pébère, N.; Ladmiral, V.; Negrell, C. Hemiacetal ester exchanges, study of reaction conditions and mechanistic pathway. *Reactions*. **2020**, *1*, 89–101
- 38) Sugihara, S.; Kawamoto, Y.; Maeda, Y. Direct Radical Polymerization of Vinyl Ethers: Reversible Addition–Fragmentation Chain Transfer Polymerization of Hydroxy-Functional Vinyl Ethers. *Macromolecules*. **2016**, *49*, 1563–1574

## 4.7. APPENDIX

mol% BDVE		% Isolated yield 4% monomer loading
0	$4.0 \pm 1$	40
0.25	$4.1 \pm 1$	34
0.5	$4.3 \pm 1$	37
1	$5.0 \pm 1$	34
1.5	$5.0 \pm 1$	35
2	$5.3 \pm 1$	40
2.5	$9.7 \pm 1$	51
5	$7.0 \pm 2$	33
7.5	$8.0 \pm 2$	30
10	7.9	32

**Table A4.1**. poly(HEVE-co-MAn) particle diameters and isolated yields. Polymerizations were carried out in neat MEK at 4 wt% total monomer loading and varying mol% BDVE. Microgels were swollen in water at pH 9 and imaged on a Nikon LV100 upright microscope in transmission mode to obtain diameters using NIS elements software, with n = 700-2000 measurements taken across 3 or more representative optical images per sample.

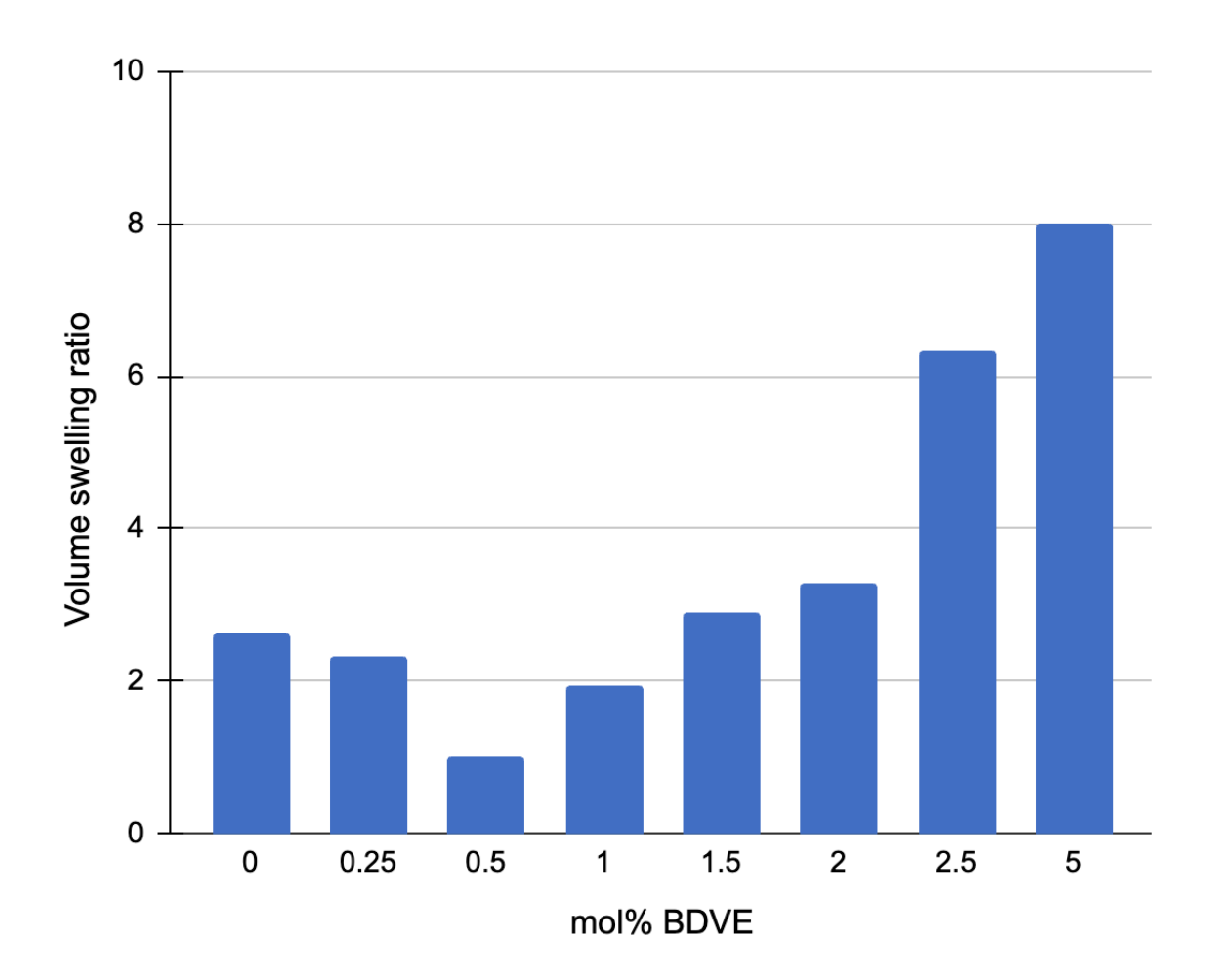


**Figure A4.1.** Volume swelling as a function of mol% BDVE for microgels polymerized in neat MEK at 4% monomer loading. The microgels were hydrolyzed and swelling ratios were calculated as microgel diameter at pH 7 / diameter at pH 2, assuming a fully collapsed microgel state at pH = 2.

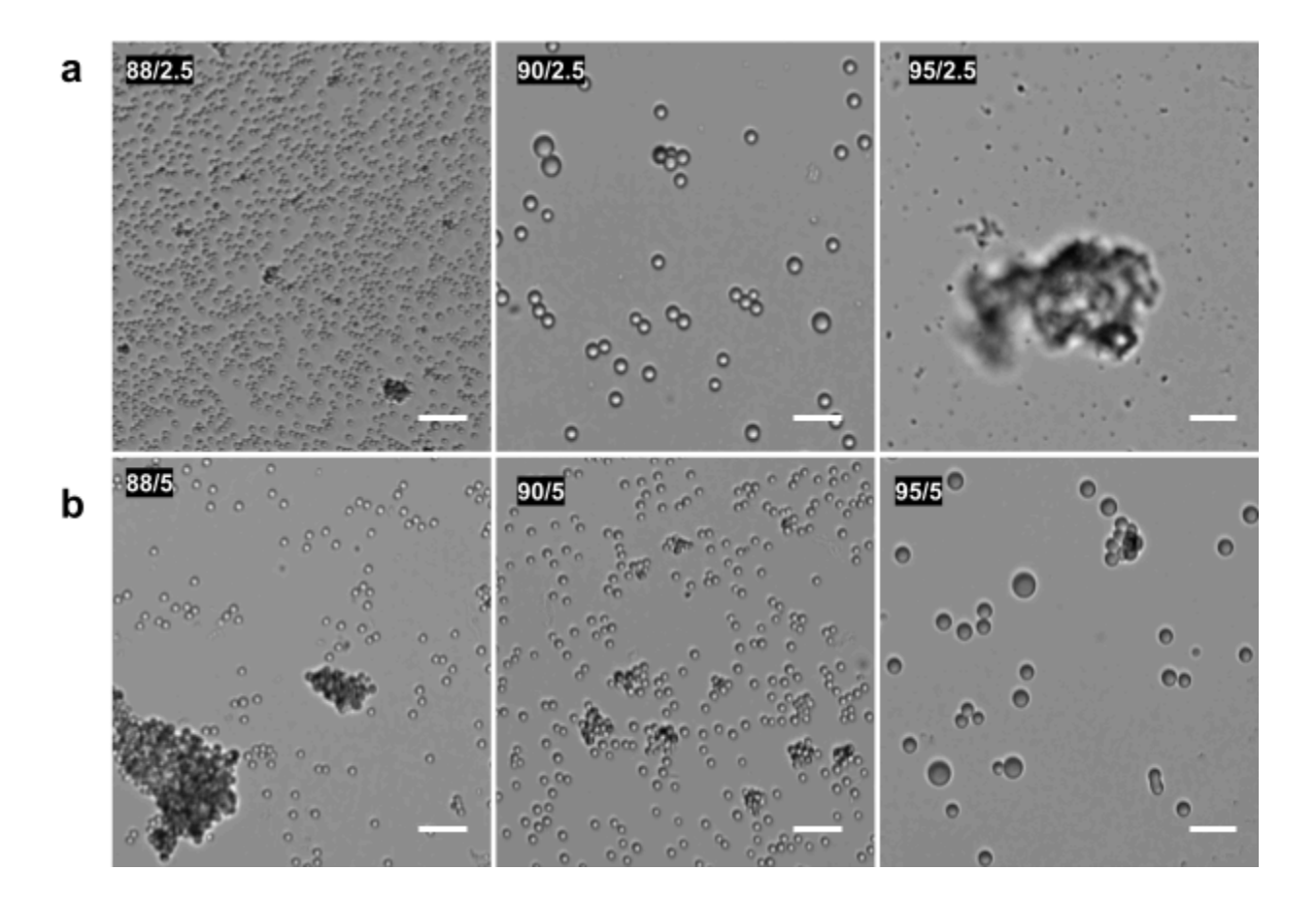


**Figure A4.2.** Representative transmission images of poly(DEVE-*co*-MAn-*co*-BDVE) microgels suspended THF. Microgels were synthesized with 2.5 mol% (top row) or 5 mol% (bottom row) BDVE, with different MEK vol% in the polymerization solvent, represented by the first number in the inset (*e.g.* 88/2.5 corresponds to microgels formed in 88 vol% MEK in the MEK/heptane mixture). Hydrolysis of the anhydride groups lead to complete (88/2.5, 88/5) or partial dissolution (90/2.5, 90/5, 95/2.5, 95/5) of the particles. All scale bars = 25 μm.

# Chapter 5: Properties of Disulfide Crosslinked microgels formed by precipitation polymerization

**Contributions:** This research was designed by SS and HDHS. Experiments were planned by SS. Microgel syntheses and characterizations were carried out by SS, with assistance from AR and HS. <sup>31</sup>P NMR experiments were carried out by SS, with assistance from NB. Degradation experiments were designed and carried out by SS. NB and HDHS provided guidance and editing feedback for the writing of this chapter.

#### 5.1. ABSTRACT

The synthesis of disulfide crosslinked microgels prepared by free-radical precipitation copolymerization of maleic anhydride (MAn), 4-methylstyrene (4MS) and bis(2-acryloyl)oxyethyl disulfide (BAOD), in methyl ethyl ketone (MEK) and heptane cosolvent mixtures is reported. Discrete particles are formed when mol% crosslinker (BAOD) was between 5 and 15%, and volume fraction of MEK in the polymerization solvent was 60 to 70%. Microgel diameters were dependent on MEK volume fraction and crosslinker loading, ranging from 1 to 10µm when swollen in good organic solvents in their anhydride-form. Backbone anhydride groups could be hydrolyzed with 1N NaOH to produce aqueous microgels. Degradation of these microgels in presence of reducing agents, tris(2-carboxyethyl)phosphine hydrochloride (TCEP) and tris(hydroxypropyl)phosphine (THPP), was studied by optical microscopy, showing that an excess of THPP can facilitate complete particle degradation in less than one second.

### **5.2. INTRODUCTION**

Microgels that degrade in response to external stimuli (e.g. pH, temperature, light, chemical environment), have emerged as candidates in drug delivery because their injectable nature, high surface area, and rapid de-swelling response offer significant advantages over analogous bulk gels.<sup>1-6</sup>

Degradability can be introduced by incorporating labile groups including esters, lactones, or disulfides, into the polymer backbone or as crosslinks. Disulfide bonds are particularly interesting as they are stable over a broad pH range but cleave under reducing conditions. Many groups have used disulfide-containing crosslinkers such as N,N'-bis(acryloyl)cystamine (BAC) to make materials that degrade in response to biological reducing agents. For instance, Bian et al. demonstrated the triggered release of anticancer drug doxorubicin (DOX) from hydrogel capsules in the presence of glutathione (GSH). The capsules, formed by crosslinking vinylcaprolactam and methacrylic acid onto sacrificial emulsion droplets using BAC, were stable under physiological conditions and displayed rapid DOX release in 10 mM GSH solutions. Other groups have similarly synthesized BAC-crosslinked micro- or nanogels, and demonstrated their de-crosslinking in response to dithiothreitol (DTT).

Our group and others have previously reported the synthesis of microspheres by precipitation copolymerization of (meth)acrylic esters, maleic anhydride (MAn), divinylbenzene (DVB), and styrenic monomers in marginal, near-theta organic solvents and solvent mixtures, giving access to narrow-disperse microspheres and microgels in the

low micrometre diameter range, without need for surfactants or added steric stabilizers. 10-16

Precipitation copolymerization of DVB-55, 4-methylstyrene, and MAn in MEK/heptane mixtures yields particles that range from hard spheres to swellable microgels, depending on mol% crosslinker or MEK volume fraction. Incorporation of crosslinkers that can be degraded by, *e.g.*, mild reducing agents, would further expand potential applications of this family of microgels. Here, we study the effects of incorporating the disulfide crosslinker, bis(2-acryloyl)oxyethyl disulfide (BAOD), in the precipitation copolymerization of 4MS and MAn. The influence of mol% BAOD and vol% MEK on particle morphology is explored and microgel degradation with phosphine reducing agents is presented.

### **5.3. EXPERIMENTAL**

## 5.3.1. Materials

5-(and-6-)-((N-(5-Aminopentyl)amino)carbonyl)tetramethylrhodamine

(TAMRA-cadaverine) was purchased from AnaSpec. 2,2'-Azobis(2-methylpropionitrile) (AIBN, 99.9%) was purchased from Dupont. Methyl ethyl ketone (MEK, >99%) was purchased from Caledon. bis(2-hydroxyethyl disulfide) (BHEDS, >85%), acryloyl chloride ( $\geq$ 99%), 4-methylstyrene (4MS, >95.5%), maleic anhydride (MAn, >98.5%), CDCl<sup>3</sup> ( $\geq$ 99.8%D atom), D<sub>2</sub>O ( $\geq$ 99.9% D atom), tris(2-carboxyethyl)phosphine hydrochloride (TCEP,  $\geq$ 98%), triethylamine ( $\geq$ 99.5%), tetrahydrofuran (THF,  $\geq$ 99.0%),

dichloromethane (DCM,  $\geq$ 99.5%), potassium carbonate, and *n*-heptane (>98.5%) were purchased from Sigma-Aldrich. Tris(hydroxypropyl) phosphine (THPP,  $\geq$  85%) was kindly supplied by Prof. Jim McNulty. All materials were used as received unless otherwise stated.

# 5.3.2. Synthesis of Bis(2-acryloyl)oxyethyl disulfide (BAOD)

Bis(2-hydroxyethyl)disulfide (4.0g, 26 mmol) and triethylamine (7.3g, 73 mmol, 2.8 equiv) were dissolved in 100mL of DCM in a two-neck round-bottom flask equipped with a stir bar and thermometer. The solution was cooled to 0°C followed by dropwise addition of acryloyl chloride (6.0g, 66 mmol,2.5 equiv.) After 30 minutes, the solution was warmed to room temperature and stirred for 2-24 hours. The crude product was washed with 0.10M K<sub>2</sub>CO<sub>3</sub>, dried over anhydrous sodium sulfate and the solvent removed under reduced pressure. The concentrated product was isolated a viscous orange-brown liquid (4.87g, 72% yield).

### **5.3.3.** Microgel Syntheses

BAOD-cross linked microgels were synthesized using a method previously reported. A synthesis of 50/5 microspheres (using 5 mol% BAOD and 50:50 v/v% MEK:heptane mixtures) is given as an example: Stock solutions of 0.161g of AIBN dissolved in 10.0g of methyl ethyl ketone and 1.0g of BAOD dissolved in 10.0g of methyl ethyl ketone were prepared and stored at -18°C. 0.148g of maleic anhydride, 176μL of 4-methylstyrene, 0.228g of BAOD solution and 0.399g of AIBN solution were weighed into an 8mL

screw-cap vial followed by the addition of 2.600g MEK and 2.736g of heptane. After monomer dissolution, the vial was placed in an insulated commercial hotdog roller and rolled at a rate of 4 rpm for 24 hours at 70°C. After 24 hours, the vial was removed from the reactor and allowed to cool to room temperature. The contents of the vial were emptied into a 50mL polypropylene centrifuge tube and the vial was rinsed three times with 8mL of THF to remove particles adhering to the vial wall. Particles were then pelleted by centrifugation at 3200rcf for 10 minutes. The supernatant was decanted and particles were resuspended to a total volume of 40 mL in THF and centrifuged again. This washing process was repeated for a total of five times. After the final wash, particles were re-suspended to a total volume of 25mL with THF and stored at -18°C.

### 5.3.4. Fluorescent labeling

As-formed microgels were suspended in THF, and combined with a solution of TAMRA-cadaverine dissolved in THF for a targeted degree of labelling of 0.1 mol% relative to anhydride groups. After 12 hours of reaction, the suspension of labelled microgels was combined with a two-fold molar excess of 1N NaOH for 24 hours at room temperature to hydrolyze remaining succinic anhydride groups. The resulting microgels were washed three times by centrifugation, and resuspensed to a total volume of 10mL, in deionized water (DIW). Aliquots of 1 mL of DIW-suspended microgels were adjusted to pH 7 and 150mM NaCl, respectively.

# 5.3.4 Microgel Degradation with tris(2-carboxyethyl phosphine) (TCEP)

Microgel degradation with tris(carboxyethyl phosphine) hydrochloride (TCEP) was monitored by fluorescence microscopy on a Nikon Eclipse LV100ND optical microscope equipped Andor Zyla 4.2 sCMOS camera, running NIS-Elements Imaging Software. A suspension of 70/10 microgels was adjusted to pH 7 and 150mM NaCl, prior to addition of TCEP solution (pH 7.4). In a typical degradation experiment, 92 μL of 70/10 microgels (0.5μmol disulfides) was pipetted into a 4mL screw-cap glass vial, followed by addition of 118μL of TCEP solution (50 μmol, 100 eq'v). The vial was inverted twice to facilitate mixing, and approx. 20μL of microgel/TCEP suspension was pipetted onto a microscope slide and covered with a glass coverslip. Images were taken at 1-10 minute intervals to track changes in particle diameter/swelling, until diameters could no longer be reliably measured (e.g. circularity < 0.7).

### 5.3.5. Microgel degradation with tris(hydroxypropyl phosphine) (THPP)

Particle degradation with THPP was carried out in a similar fashion to TCEP degradation:  $92.4\mu$ L (0.5  $\mu$ mol) of TMR-cadaverine labelled 70/10 microgels suspended in DIW (pH =7.8, [NaCl] = 150 mM) and reacted with a 0.1:1 or 100:1 mole ratio of THPP to disulfide content.

### **5.4. DISCUSSION**

### 5.4.1. Microgel synthesis and characterization

A series of microgels were prepared with varying BAOD crosslinker loading in a range of MEK/heptane cosolvent mixtures to probe effects of polymerization conditions on final particle morphology. At BAOD contents of 10 and 15 mol% relative to total monomer, narrow-disperse particles with diameters ranging from sub-micron to 11 μm were formed between 60 and 70 vol% MEK in the polymerization solvent (Fig. 5.1). MEK levels above 70 vol% or below 60 vol% yielded macrogels or small but irregular aggregates, respectively.

Higher MEK levels and lower BAOD levels correspond to larger microgel diameters. This observed solvency window needed for formation of well-defined, narrow-disperse microgels aligns well with previously reported data for a system crosslinked with 1,4-butanediol diacrylate (Chapter 3). Microgels made in this regime are spherical and narrow-disperse, with only a minor tendency for secondary particle nucleation, observed predominantly at higher BAOD and MEK levels.

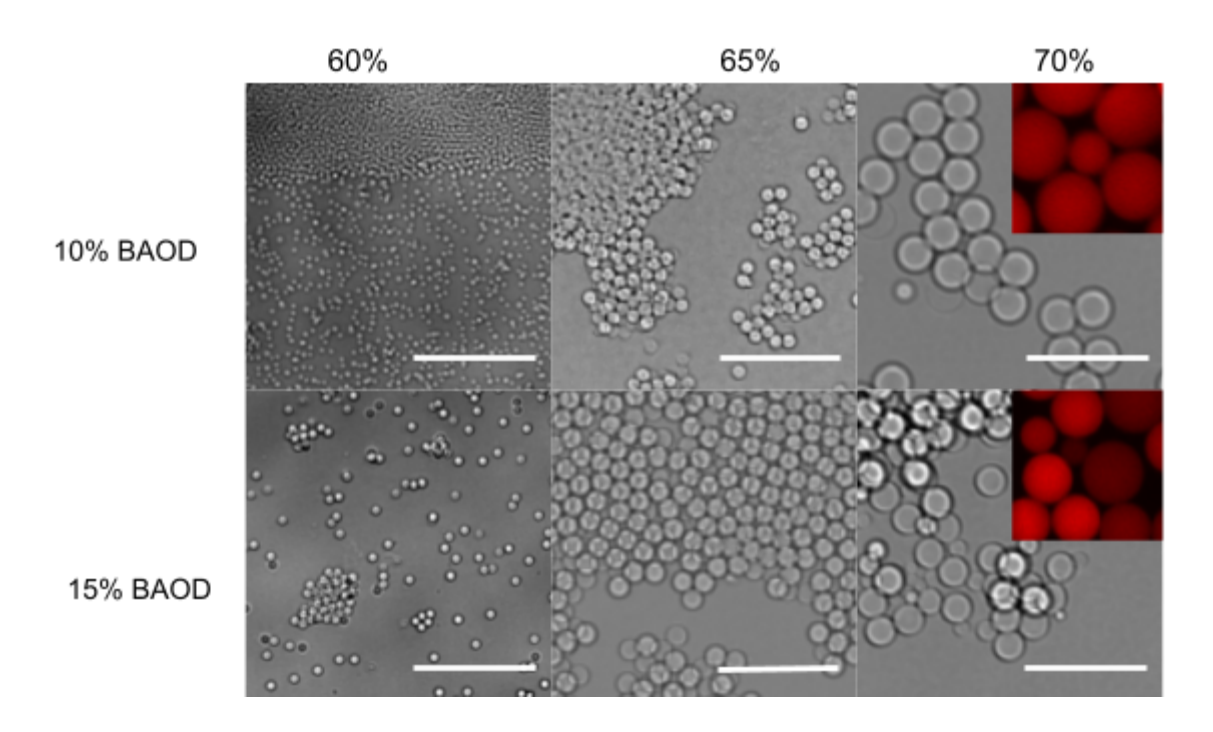


**Figure 5.1.** Transmission optical microscope images of as-formed microgels suspended in THF, showing changes in particle diameter and morphology with varying vol% MEK in the polymerization solvent and mol% BAOD. Insets are representative fluorescence images of microgels suspended in water (pH 7.8) following rhodamine labeling and subsequent succinic anhydride hydrolysis. All scale bars are 50 μm.

# 5.4.2. Microgel degradation with tris(2-carboxyethyl phosphine) hydrochloride (TCEP)

Particle degradation was facilitated with tris(2-carboxyethyl phosphine) hydrochloride (TCEP), a common disulfide reducing agent, to a suspension of fluorescently labelled 70/10 microgels, and the change in microgel morphology/diameter tracked using fluorescence microscopy (Fig. 5.2).

Figure 5.2 shows partial degradation of 70/10 microgels in the presence of 100-fold molar excess of TCEP over 30 minutes.

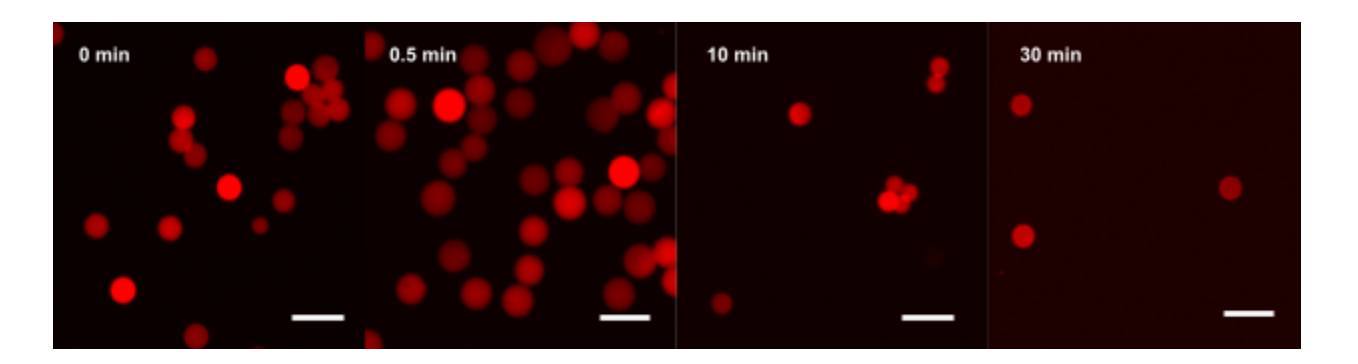
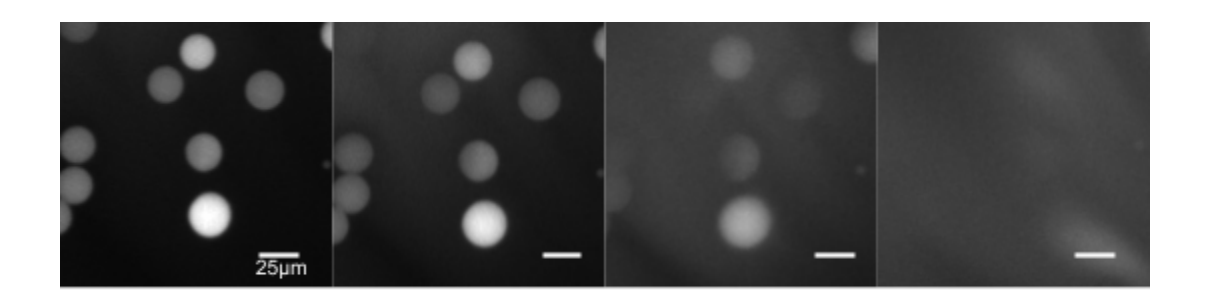


**Figure 5.2.** Fluorescence images of 70/10 microgels at t=0, 0.5, 10, and 30 min, following TCEP addition. [TCEP]:[disulfide] is estimated to be  $\sim$ 100:1 (Table A5.1 and Figure A5.5). Scale bars are 50  $\mu$ m.

The need for such a large excess of TCEP is attributed in part to its rapid conversion to phosphine oxide in solutions of pH  $\geq$  7, and its net negative charge, which may limit diffusion into partially anionic microgel cores. To probe whether incomplete degradation following TCEP treatment was a result of oxidation or electrostatic exclusion, the same microgel suspension was exposed to tris(hydroxypropyl phosphine) (THPP), a strong, air-stable charge-neutral reducing agent that has < 1 mol% conversion to its phosphine oxide in alkaline solutions.

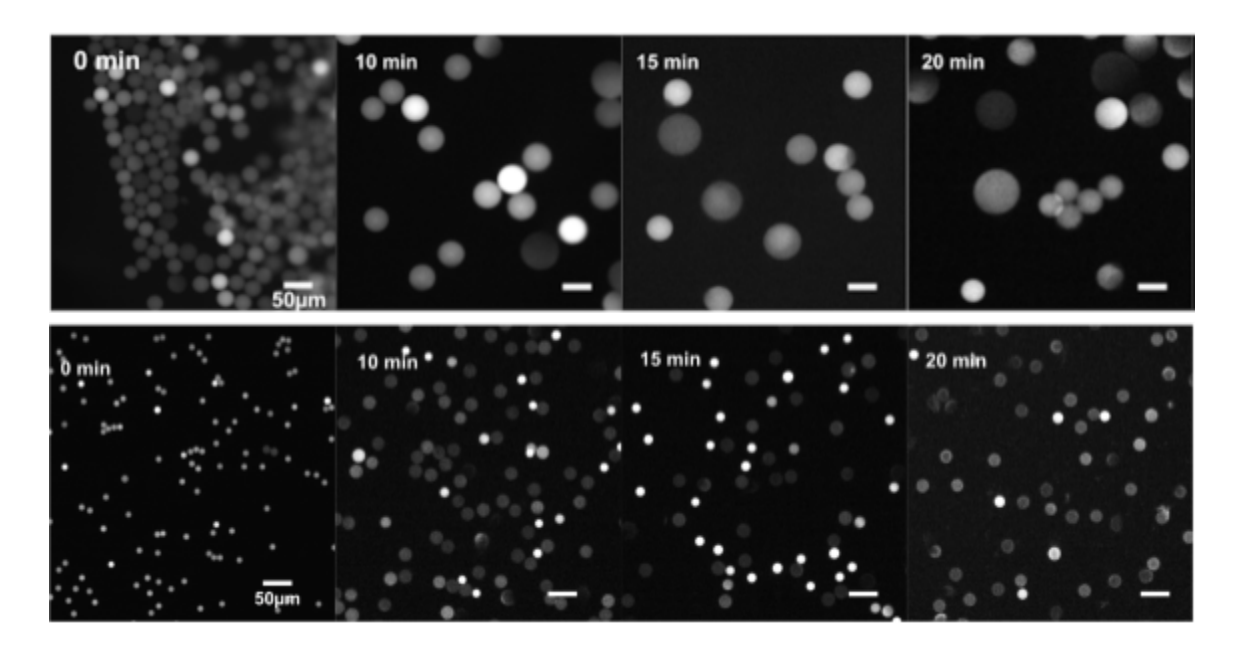
# 5.4.3. Reduction with tris(hydroxypropyl phosphine) (THPP)

Figure 5.3 shows the rapid degradation of 70/10 microgels in presence of 100 fold excess of THPP at near-neutral pH in saline. Complete degradation of 70/10 microgels is observed within 300ms once they encounter the high concentration THPP front.



**Figure 5.3.** 70/10 microgels before (first image) and 0.3s after (last image) exposure to 100-fold excess THPP. Imaged using a fluorescence microscope equipped with Andor Zyla 4.2 sCMOS camera operating at 100fps. Scale bars =  $25 \mu m$ .

Reacting microgels with THPP in a < 1:1 mole ratio allows for the measurement of swelling over time (Fig. 5.4). For the same 70/10 microgel suspension, maximum particle diameters are reached within 15 mins following mixing of microgels with THPP.



**Figure 5.4.** Fluorescence images depicting changes in 70/10 (TOP) and 65/10 (BOTTOM) BAOD microgel diameters with time following mixing with 0.1 eq'v of THPP. Scale bars =  $50 \mu m$ .

## **5.5. CONCLUSIONS**

Degradable microgels containing disulfide crosslinks were prepared by precipitation copolymerization of 4MS, MAn, and BAOD in MEK/heptane cosolvent mixtures and their physical properties studied by microscopy. At a constant crosslinker loading of 10 mol% BAOD, an increase in MEK volume fraction from 60 to 70% corresponds to approximately a four-fold increase in particle diameter, demonstrating the effects of solvency on particle nucleation and growth. At the same time, decreasing BAOD crosslinker levels from 15 to 10 mol% results in a significant increase in particle diameter, in agreement with prior findings. Both TCEP and THPP are shown to degrade disulfide crosslinks, with THPP enabling faster particle degradation and complete dissolution.

## **5.6. REFERENCES**

- 1. Wu, Y., Wang, L., Guo, B., Ma, P. X. J. Mater. Chem. B., 2014, 2, 3674-3685
- Mealy, J. E., Chung, J. J., Jeong, H.-H., Issadore, D., Lee, D., Atluri, P., Burdick,
   J. A. Adv. Mater. 2018, 30, 1705912
- Muir, V. G., Qazi, T. H., Weintraub, S., Torres, B. O., Arratia, P. E., Burdick, J. A. Small. 2022, 18, 2201115
- Coronel, M. M., Martin, K. E., Hunckler, M. D., Kalelkar, P., Shah, R. M., García,
   A. J. Small, 2022, 2106896
- Murthy, N., Thng, Y.X., Schuck, S., Xu, M.C., Fretchet, J.M. J. Am. Chem. Soc.
   2002, 124, 12398–12399
- Foster, G. A., Headen, D. M., González-García, C., Salmerón-Sánchez, M.,
   Shirwan, H., García, A. J. Biomaterials, 2017, 113, 170–175
- 7. Gaulding, J. et al. *Macromolecules*. **2012**, *45*, 39–45
- 8. Bian, S.; Zheng, J.; Tang, X.; Yi, D.; Wang, Y.; Yang, W. *Chem. Mater.* **2015**, *27*, 1262–1268.
- 9. Plunkett, K. N., Kraft, M. L., Yu, Q., Moore, J. S. *Macromolecules*. **2003**, *36*, 3960–3966
- 10. Goh, E. C. C.; Stöver, H. D. H. Macromolecules. 2002, 35, 9983–9989.
- 11. Li, W.H.; Stöver, H.D.H. J. Polym. Sci., Part A: Polym. Chem. 1999, 37, 2899
- 12. Li, K.; Stöver, H. D. H. *J. Polym. Sci., Part A:Polym. Chem.* **1993**, *31*, 3257–3263.

- 13. Downey, J. S.; McIsaac, G.; Frank, R. S.; Stöver, H. D. H. *Macromolecules*. **2001**, *34*, 4534–4541.
- 14. Frank, R. S.; Downey, J. S.; Yu, K.; Stöver, H. D. H. *Macromolecules*. **2002**, *35*, 2728–2735.
- 15. Bai, F.; Yang, X.; Huang, W. S. Macromolecules. 2004, 37, 9746–9752.
- 16. Limé, F.; Irgum, K. Macromolecules. 2007, 40, 1962–1968.

# 5.7. APPENDIX

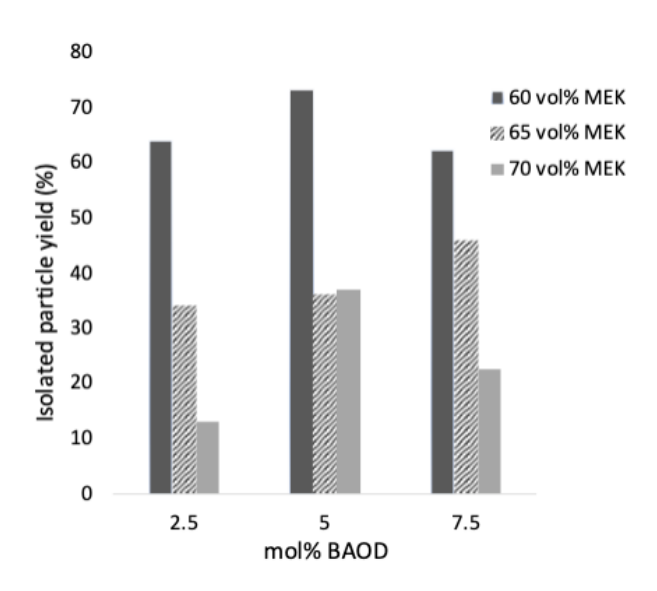


**Figure A5.1.** Isolated particle yields for BAOD-crosslinked microgels at different mol% BAOD loading, made in 60, 65 or 75 vol% MEK in polymerization mixture.

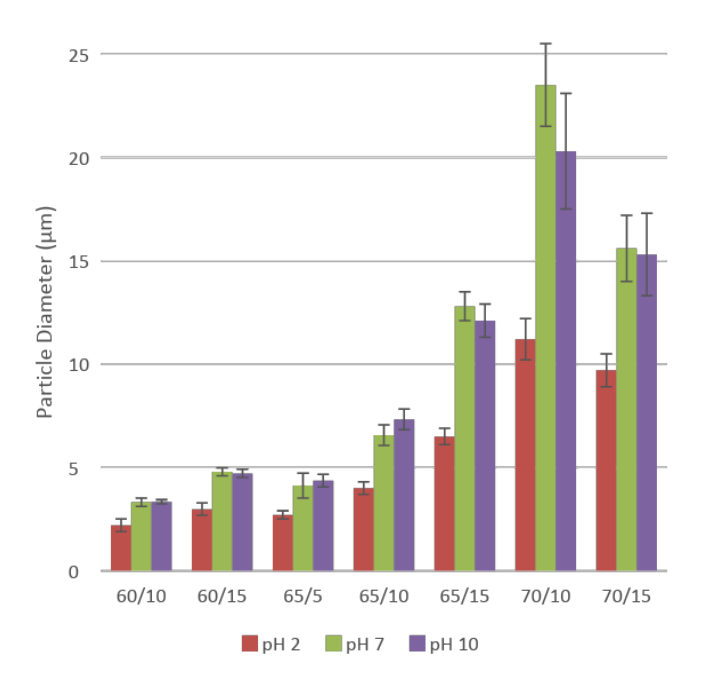


**Figure A5.2.** Microgel diameters as a function of pH. Scale bars are standard deviations of particle diameter taken from an average of > 1000 particle diameter measurements using NIS elements software.

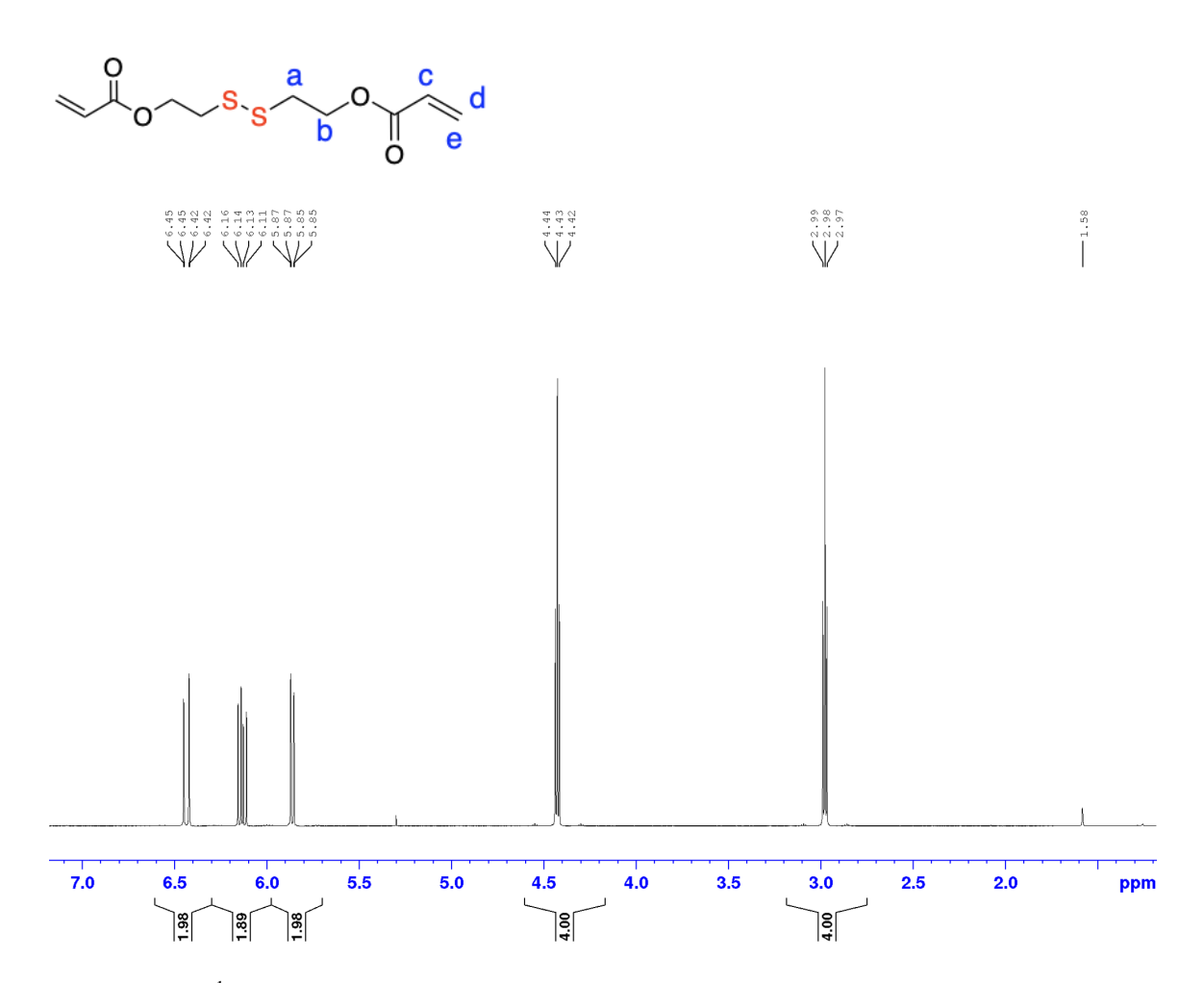


Figure A5.3. <sup>1</sup>H NMR of BAOD in CDCl<sub>3</sub>. ca. 93% yield

# Estimation of microgel disulfide content from quantitative {1H}31P NMR

Spin-lattice relaxation times (T1) for THPP and THPPO were first determined by inverse recovery on a Bruker AV600 spectrometer, using a mixture of THPP and BAOD microgels suspended in  $D_2O$ , with an estimated mole ratio of THPP to disulfide bonds as 4:1. T1 values for THPP and its phosphine oxide (THPPO) were determined to be 2.4s and 0.6s, respectively.

Integration/ microgel	standard	60/5	60/10	60/15	65/5	65/10	65/15	70/10
THPP (-30.251ppm)	33.17	15.692	16.835	8.289	12.465	14.972	8.646	14.73
THPPO (+60.411pmm)	1.00	1.00	1.00	1.00	1.00	1.00	1.00	1.00
mol ratio THPPO: THPP	0.0293	0.0599	0.0561	0.1077	0.0743	0.0626	0.1037	0.0636
Calculated mol % disulfide		1.08	2.04	5.42	1.36	2.25	5.39	2.33

**Table A.5.1.** Estimated mol% disulfide in microgels from {<sup>1</sup>H}<sup>31</sup>P NMR.

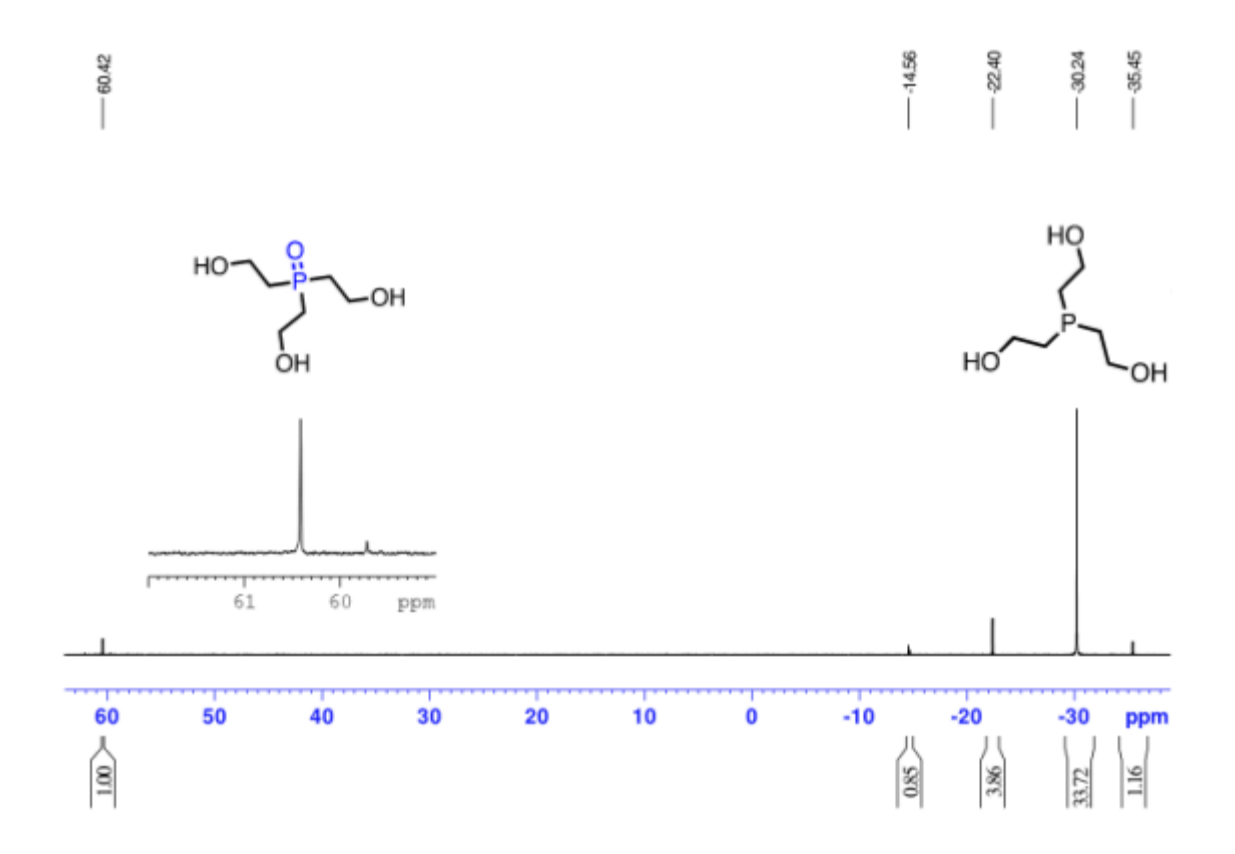


**Figure A5.4.**  $^{31}$ P NMR of THPP standard in D<sub>2</sub>O. THPPO = 60.42 ppm , THPP = -30.24

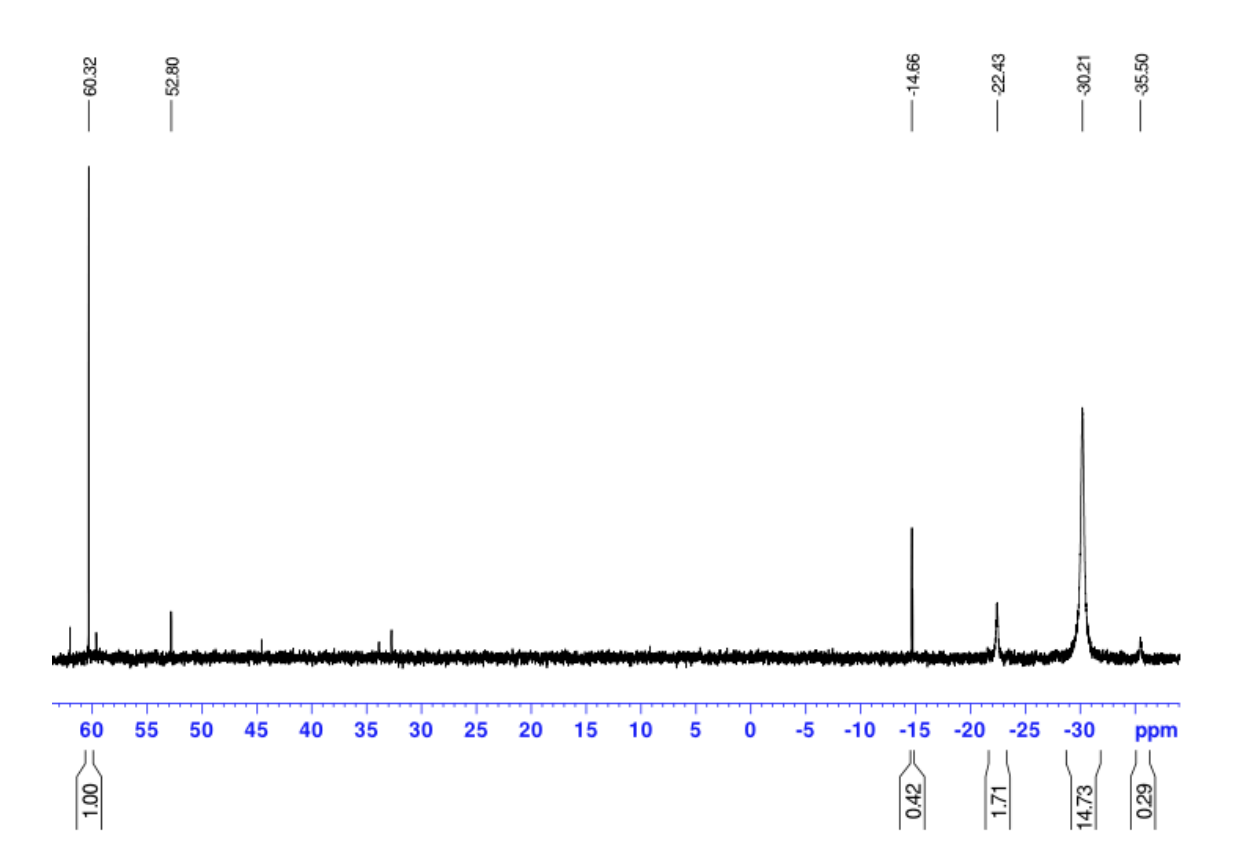
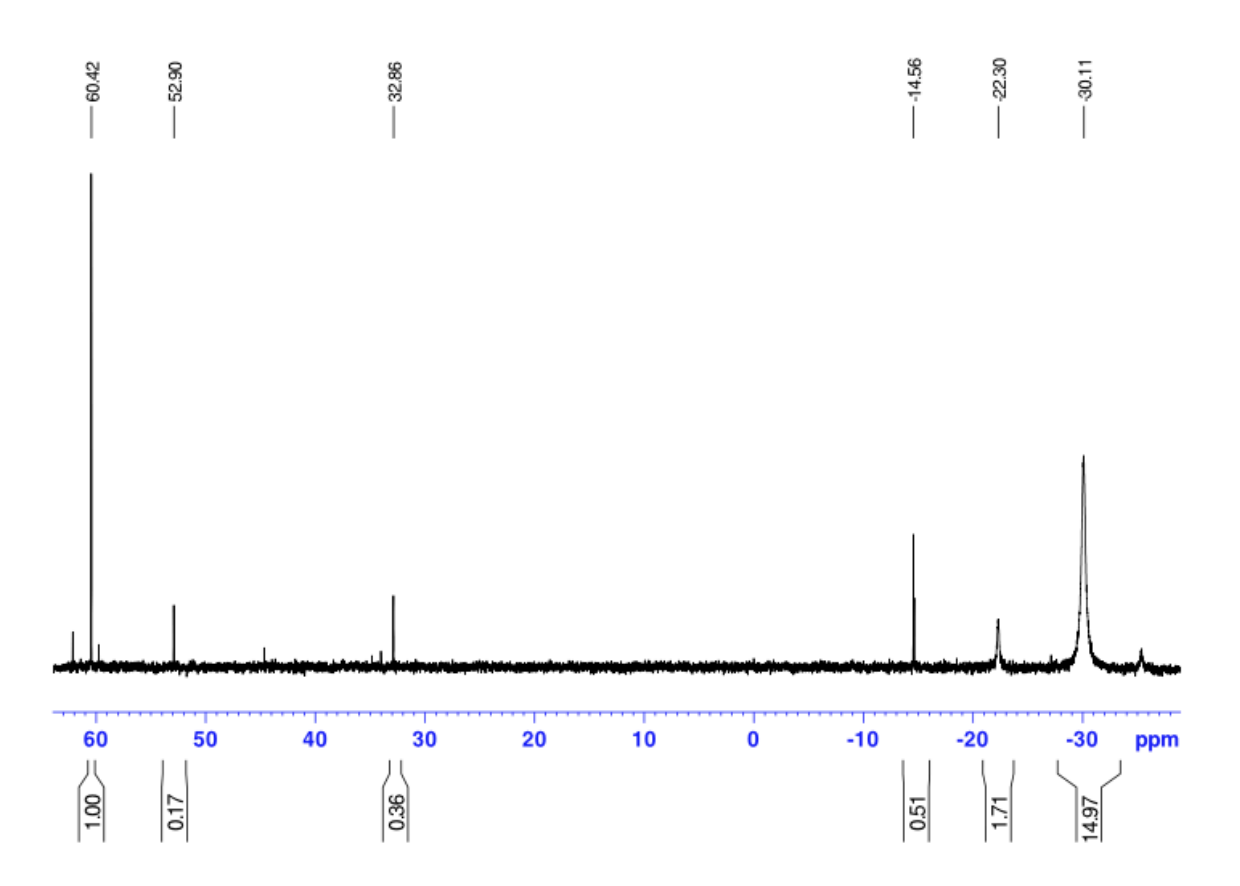
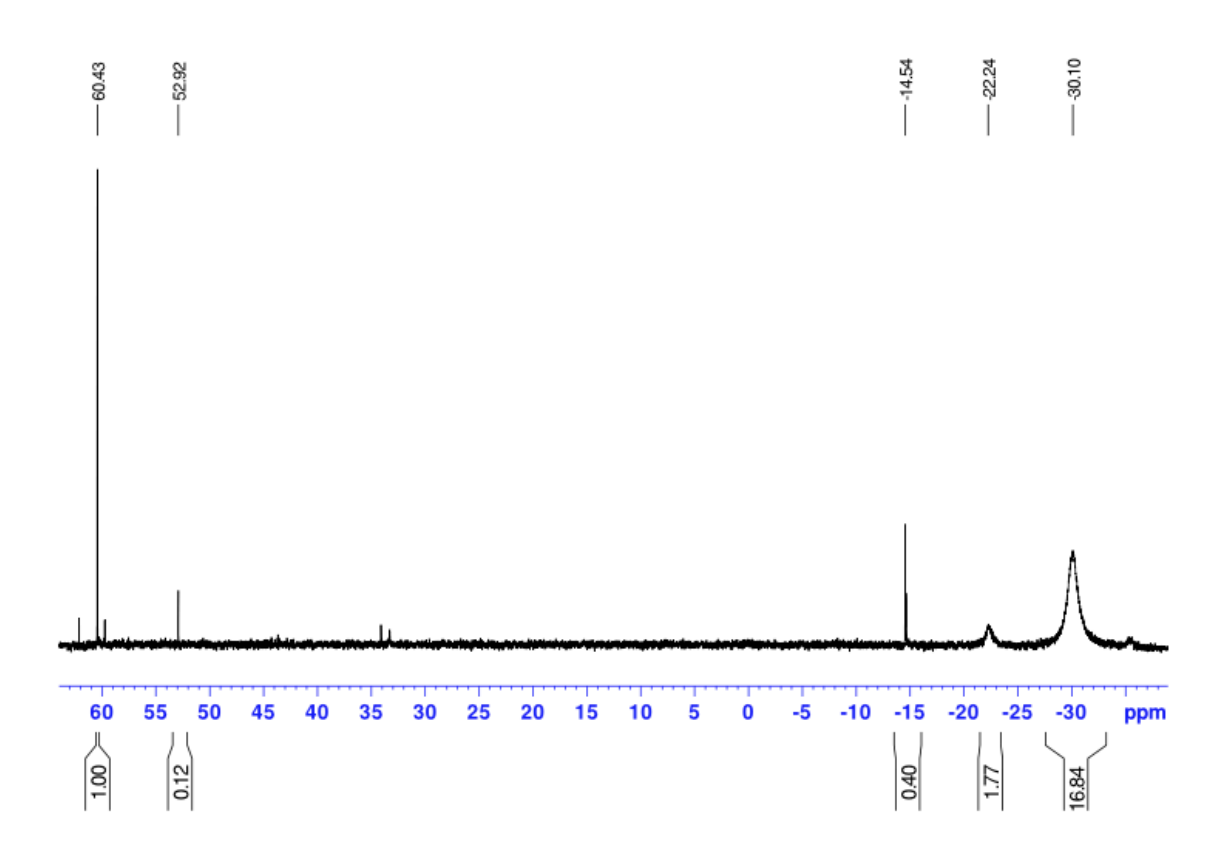


Figure A5.5. <sup>31</sup>P NMR of 70/10 microgels and THPP in  $D_2O$ . Calculated %BAOD = 2.33



**Figure A5.6.**  $^{31}$ P NMR of 65/10 microgels and THPP in D<sub>2</sub>O. Calculated % BAOD = 2.25%



**Figure A5.7.** <sup>31</sup>P NMR of 60/10 microgels and THPP in D<sub>2</sub>O. Calculated %BAOD = 2.04

# Chapter 6. Conclusions, Summary and Recommendations for Future Work

### **6.1.** Thesis Conclusions

The work presented in this thesis demonstrates the utility of precipitation polymerization for the stabilizer-free synthesis of micron-sized polymer microgels with tunable size, morphology and mechanical properties. Maleic anhydride was copolymerized with electron-rich monomers such as styrenics, acrylics and vinyl ethers in marginal solvent mixtures, yielding particles in the  $3-20 \mu m$  range, with narrow size distributions. Careful adjustment of reaction solvent composition, comonomer selection, and crosslinker loading afforded control over particle diameters and elasticity. The application of real-time deformability cytometry (RT-DC) enabled the first high-throughput mechanical characterization of individual polymer microgels, revealing the influence of polymerization parameters like solvency and crosslinker loading on microgel Young's modulus. Copolymerizing maleic anhydride with hydroxy ethyl vinyl ether introduced a new method of crosslinking that eliminated the need for added divinyl monomer, while also affording degradability at neutral or basic pH and elevated temperatures. Collectively, these findings expand the scope of precipitation polymerization for the development of functional microgels, highlighting their potential use in biomedical and soft material applications.

### 6.2. Chapter 2

The properties of a series of microgels formed by precipitation polymerization of 4-methyl styrene (4MS), maleic anhydride (MAn), and divinylbenzene-55 (DVB) in methyl ethyl ketone (MEK) and heptane cosolvent mixtures were investigated using

microscopy and real-time deformability cytometry (RT-DC). Anhydride groups were functionalized with fluorescent labels and/or ring-opened with base to yield aqueous microgels with size and swelling that depended on mol% DVB, vol% MEK, and pH of the suspending medium. Particle morphologies and polymer network distribution were assessed using a combination of fluorescence and confocal and transmission electron microscopy, showing that use of low concentrations of DVB and high vol% of MEK in the polymerization solvent gave rise to highly deformable microgels with diameters up to  $20\mu m$  when swollen in pH  $\geq 7$  solutions.

The deformation and Young's moduli of the microgels were measured using RT-DC, a microfluidic technique developed for the high-throughput measurement of single-cell elastic properties. Individual particle Young's moduli (E) ranged from 1kPa to 10kPa, with E-values having a strong inverse dependence on vol% MEK. Microgels also exhibited non-linear elastic behaviour in response to high flow rates, which was attributed to slow interior network desolvation under increasing shear forces. This chapter highlights how reaction solvent composition and crosslinker loading may be leveraged to tune microgel size and moduli to fall within a range that is biologically relevant. In doing so, it also demonstrates the first utility of RT-DC for the continuous assessment of individual microgel mechanics.

Future work for this chapter may involve comparing bulk mechanical properties of concentrated microgel suspensions to the single-particle information obtained from the RT-DC technique. Results from Chapter 3 demonstrate that altering comonomer ratios has a significant effect on particle diameter and swelling, which should also translate to

changes in elastic properties. RT-DC should also be extended to the microgels synthesized in subsequent chapters, *e.g.* vinyl ether (Chapter 4) and disulfide-containing (Chapter 5) microgels.

## 6.3. Chapter 3

This chapter describes lightly crosslinked microgels synthesized by precipitation polymerization of MAn and mixtures of the monovinyl styrenic monomers, 4MS and styrene (sty), with 5-10 mol% DVB or 1,4-butanedioldiacrylate (BDDA). Microgel properties were assessed using optical and scanning electron microscopy (SEM). At constant vol% MEK and mol% DVB, changing the ratio of 4MS:Sty in the styrenic monomer pool (DVB, 4MS and Sty monomers) from 0.1 to 1 resulted in a decrease in nearly order of magnitude. particle diameter by an Diameters for poly(4MS-co-MAn-co-DVB) and poly(Sty-co-MAn-co-DVB) increased significantly at 70 vol\% MEK and 80 vol\% MEK in the reaction medium, respectively. The difference in onset of large particle formation between 4MS and Sty was attributed to comonomer-induced changes in particle nucleation (e.g. onset of colloidal stability) arising from differences in monomer-solvent matching between the two comonomer systems. As-formed particles in both cases were narrow-dispersed, with diameters ranging from 1-10um when swollen in THF. Anhydride-hydrolyzed microgels had diameters reaching 20 µm in basic solutions and pH-dependent swelling behaviour, similar to those described in Chapter 2. Finally, we found replacing DVB with BDDA in the copolymerization of 4MS and MAn yielded particles with similar cross-linker and solvency dependency as their DVB-counterparts. Ultimately, this chapter demonstrates the complementary effects of polymerization solvent, comonomer ratios, and crosslinker composition on the properties of lightly crosslinked microgels formed from precipitation polymerization.

## 6.4. Chapter 4

Chapter 4 describes the preparation of microgels from precipitation copolymerization of vinyl ethers and maleic anhydride (MAn) in neat MEK and mixed MEK solvents, with the aim of extending the monomer repertoire of precipitation polymerization to hydroxy-containing vinyl ether monomers. At low monomer loadings (4 to 6 wt%), precipitation copolymerization of hydroxy ethyl vinyl ether (HEVE), maleic anhydride (MAn), and 0.5 - 7.5 mol% of 1.4-butanediol divinyl ether (BDVE) in high MEK volume fractions (88-100% v/v MEK in MEK/heptane mixtures) yielded narrow-dispersed particles ranging 1 to 8 um in diameter when swollen in good organic solvents (THF, DMF). Changing reaction solvency had similar effects on microgel morphology as those reported in earlier chapters for styrenic microgels, where diameters increased with increasing volume of good solvent (MEK) in the polymerization mixture. Largest microgels were isolated from polymerizations carried out in neat MEK and the lower limit of solvency for discrete particle formation was 88 vol\% MEK and 12 vol\% HEP. At MEK fractions below 88 v/v%, sub-micron particles or aggregates were formed. Increasing BDVE loading to greater than 10 mol% at constant solvency similarly resulted in aggregation and loss of colloidal stability. Copolymerization of MAn and HEVE in

neat MEK without BDVE yielded cross-linked microgels in isolated yields of 35-40%. As-formed microgels were stable in organic solvents but poly(HEVE-co-succinic acid) exhibited swelling and dissolution when heated to 70°C in neutral (pH 7) and basic (pH 12) solutions. Microgels crosslinked 2.5 to 5 mol% BDVE maintained their integrity after heating under similar pH conditions, a result attributed to permanent crosslinking of BDVE. Degradation of poly(HEVE-co-MAn) microgels over this pH range was suggestive of ester crosslinking, which may be possible via reaction of terminal hydroxyl groups of HEVE with anhydride rings on neighbouring polymer chains. 1H NMR scale copolymerization of HEVE and MAn was used to probe the nature of cross-linking, showing a series of HEVE side reactions, including cyclic acetal and ester formation.

A proof-of-concept confocal study exploring binding of FITC-BSA onto vinyl ether and styrenic-based microgels revealed that styrenic polymers bound more protein than vinyl ether particles of similar size. Copolymerization with hydrophilic vinyl ether monomers in mixed MEK cosolvents somewhat maintains the solvent-dependent morphology control observed in previous chapters, while also yielding degradable microgels from self-crosslinking reactions between HEVE and MAn. Ultimately, this work extends crosslinking precipitation polymerization in marginal solvents to (hydroxy) vinyl ether monomers.

There are several suggestions for future work. Vinyl ether microgels crosslinked with BDVE did not exhibit strong cross-linker dependent morphology transitions like those reported in previous chapters. This was attributed to differences in solubility requirements of HEVE and the relatively non-polar butylene divinyl ether crosslinker.

Future work may involve replacing BDVE with a more polar crosslinker, such as diethylene glycol vinyl ether (DEGVE), and exploring whether this results in crosslinker-dependent diameter changes for resulting microgels. For self-crosslinked microgels, we suggest comparing their elastic properties to those crosslinked with BDVE or other crosslinkers, using methods described in Chapter 2. Since differences in reactivity ratios between crosslinker and monomers may give rise to core-shell or heterogeneous crosslinking, self-crosslinked microgels can exhibit different elastic behaviour than those containing divinyl crosslinker despite having similar diameters when swollen in good solvents.

From a more fundamental perspective, future experiments should focus strongly on elucidating the mechanism of self-crosslinking in HEVE/MAn copolymerizations, as it remains unclear from the results presented in Chapter 4. This may involve determining specific conditions (*e.g.* polymerization temperature, monomer loading, and solvency range) under which self-crosslinking occurs. For example, room-temperature, UV-initiated radical polymerizations of HEVE and MAn in neat MEK did not produce microgels, suggesting temperature plays a critical role in self-crosslinking. A detailed study of polymerization temperature versus gel formation over a wide temperature range may help better understand the role of temperature in self-crosslinking events. Additionally, HEVE can undergo a range of side-reactions in the presence of catalytic amounts of acid, <sup>13</sup>C and <sup>1</sup>H-scale polymerizations, ideally in deuterated MEK, will be useful in understanding rate and degree of crosslinking that result from these side-reactions.

Lastly, microgel formation was also observed for DEVE/MAn copolymerizations conducted in 90/10 MEK/ACN solvents, in the absence of added crosslinker. The explored solvency regime for this copolymer system was limited, thus, one may aim to explore the extent to which self-crosslinking occurs with DEVE and MAn in different cosolvent mixtures.

# **6.5.** Chapter 5

Degradable microgels were synthesized by precipitation polymerization of MAn, 4MS, and a disulfide-containing diacrylate (BAOD), in MEK/heptane solvent mixtures. Particle morphologies were assessed using optical microscopy and demonstrated similar dependence on reaction solvency as microgels cross linked with DVB and BDDA (Chapters 2 and 3). Discrete particles were isolated in a low solvency regime of 60 – 70 vol% MEK, where gelation and aggregation increased with increasing vol% MEK and mol% BAOD. Particle degradation was then studied as a function of reducing agent, demonstrating degradation with TCEP and THPP, where THPP degrades microgels orders of magnitude faster than TCEP under similar conditions.

Future work for this chapter should focus on exploring a different solvency regime to determine whether other polar organic solvents (*e.g.* acetonitrile) may afford uniform microgels of larger diameters. Additionally, studying partially de-crosslinked microgels using the RT-DC methods described in Chapter 2 could provide useful information on changes in microgel modulus with degradation time.